Organic anion transporting polypeptide 1c1 structure and function

A DISSERTATION
SUBMITTED TO THE FACULTY OF THE GRADUATE SCHOOL
OF THE UNIVERSITY OF MINNESOTA
BY

Daniel Eric Westholm

IN PARTIAL FULFILLMENT OF THE REQUIREMENTS
FOR THE DEGREE OF
DOCTOR OF PHILOSOPHY

Grant W. Anderson, Adviser

August 2009

Acknowledgements

First I would like to thank my parents, William and Kathy Westholm for allowing me to pursue my interests in the living world. You never discouraged my wanderings along the river, collections of crayfish or late night excursions into the woods; I am eternally grateful for these experiences. I would also like to thank my late grandmother, Louise Westholm, for watching Ben and Alaina through nearly my entire graduate education. There simply is not space here to do justice to what that meant to me and my family. Most of all I would like to thank my wife Danielle and two children, Benjamin and Alaina for supporting me during my education. Dani, I appreciated your patience while I figured out what to do with my life and Ben and Alaina, your warm smiles are always just what I need when I come from work.

Second, I would like to thank my advisor Dr. Grant Anderson for first hiring me as a laboratory technician and then encouraging me to attend graduate school at the University of Minnesota. You have made the scientific process exciting and rewarding, assisting me in the development of my scientific skills while granting me the freedom to pursue my own ideas. Our time together in the lab has seen triumphs and struggles, and your optimism and enthusiasm for our project and science in general has been a buoying influence. I also would like to extend a grateful thank you to Dr. Jon Rumbley who has provided much needed chemical expertise and unique perspectives on our projects. In addition, I would like to Tim Tracy for his assistance with atypical kinetics applications.

I would also like to thank my fellow graduate students, pharmacy students technicians and undergraduates in Dr. Anderson's lab, including Kevin Viken, Thomas Bastien, Jake Marold, Ariel Johnson, Gregg Baldeshwiler, David Salo, David Stenehjem, Joe Schneider, Becky Palermo, Nick Fetter, Alicia Hartung, Jay Christenson and Jeremy Anderson. Without your help pipetting and troubleshooting, none of this would have been possible.

I also would like to thank the members of my graduate committee for their service and input, as well as the University of Minnesota Biochemistry, Molecular Biology and Biophysics graduate program.

Finally I would like to thank the faculty and staff of the College of Pharmacy and School of Medicine for the friendly conversations (both scientific and non-scientific), borrowed reagents and ready technical assistance.

The research presented in this dissertation was supported by a Torske Klubben Fellowship, Grant-in-Aid of Research, Artistry and Scholarship from the University of Minnesota, and a Research Corporation Grant CC6681

Dedication

This dissertation is dedicated to my Grandma Louise Westholm for setting up nearly full-time child care for us late in her life.

Abstract

Organic anion transporting polypeptides (Oatps) are solute carrier family members that exhibit marked evolutionary conservation. Mammalian Oatps exhibit wide tissue expression with an emphasis on expression in barrier cells. In the brain Oatps are expressed in the blood-brain barrier (BBB) endothelial cells and blood-cerebrospinal fluid barrier (BCSFB) epithelial cells. This expression profile serves to illustrate a central role for Oatps in transporting endo- and xenobiotics across brain barrier cells. One such Oatp, Oatp1c1, is a high affinity thyroxine (T4) transporter. Among Oatps, Oatp1c1 possesses a unique expression and substrate preference profile. Outside of specialized cells in the eye and testes, Oatp1c1 is expressed solely in the BBB and BCSFB cells. In addition, Oatp1c1 appears to have a narrower substrate specificity than other Oatps and has the lowest identified K_m for T4 transport of any known thyroid hormone transporter. Despite these characteristics, Oatp1c1 remains relatively uncharacterized. To better establish Oatp1c1 biology and contributions to overall brain homeostasis, my research was comprised of three components: 1) the characterization of Oatp1c1 transport mechanisms/kinetics, 2) the assessment of Oatp1c1 structure-function relationships through modeling and characterization of the role of multiple Oatp1c1 amino acid residues in substrate recognition, and 3) the identification of novel Oatp1c1 substrates and development of an Oatp1c1 pharmacophore model. To further understand Oatp transport mechanism, I began by analyzing the transport of two known Oatp1c1 substrates, T4 and $E_2$17βG. Reports by other labs suggested differential Oatp1c1 recognition of these substrates. Through detailed kinetic measurements in Oatp1c1 transfected cell lines, I found that Oatp1c1

possesses multiple substrate binding sites that recognize T4 and $E_2$17βG with opposite affinities. Next, topology and high resolution 3-dimensional Oatp1c1 structural models were created to evaluate substrate-transporter complimentarity. Through use of the models, we identified multiple Oatp1c1 amino acids to test for involvement in T4 transport through site-directed mutagenesis. The targeted amino acids are highly conserved amongst Oatps, are in the putative transmembrane domains, and face the putative substrate channel. Polar and charged amino acids in helix 2 (D85, E89, N92) were not expressed at the plasma membrane and thus appear required to for proper protein folding and/or trafficking. Mutations at positions R601, P609, W277W278 and G399G409 were all expressed at the plasma membrane and had varying effects on Oatp1c1 transport. Some mutants, such as R601S, diminished transport, but appeared to leave both Oatp1c1 T4 binding sites functioning. Others, such as G399V,G409V appeared to affect the low affinity Oatp1c1 T4 binding site more severely than the high affinity binding site. Next, in an effort to expand the suite of known structures Oatp1c1 interacts with, a range of known T4 transport inhibitors and multiple sterol glucuronides, structural relatives of the Oatp1c1 substrate estradiol 17-β-glucuronide ($E_2$17βG), were surveyed to assess for Oatp1c1-specific inhibition of T4 transport. I found that the fenamate class of non-steroidal anti-inflammatory drugs (NSAIDs) were competitive inhibitors of Oatp1c1 T4 transport. In addition, sterols glucuronidated in the 17 and 21 positions also competitively inhibited Oatp1c1 T4 transport. Finally, a pharmacophore analysis was performed on Oatp1c1 inhibitors identified in Chapters 2 and 4, as well as known Oatp1c1 substrates. The Oatp1c1 pharmacophore was found to possess two distinct hydrophobic planes and a negative charge. This work on Oatp1c1

structure and function will aid the rational design of drugs that can cross the blood-brain and/or blood-tumor barriers and facilitate greatly needed treatment for a variety of neurological and metastatic diseases.

Table of Contents

List of Tables

List of Figures

List of Figures (con't)

Abbreviations

4-MUS	4-methylumbelliferone sulfate
ABC	ATP-binding cassette transporter
AUC	area under the curve
AZT	3′-azido-3′-deoxythymidine
BBB	blood-brain barrier
BCSFB	blood-cerebrospinal fluid barrier
BSP	bromosulfophthalein
CNS	central nervous system
CoMFA	comparative molecular field analysis
COX	cyclooxygenase
CSF	cerebral spinal fluid
D2	type II deiodinase
DHEA	dehydroepiandrosterone 3-glucuronide
$E_1$3βG	estrone-3-β-glucuronide
$E_2$17βG	estradiol-17-β-glucuronide
$E_3$17βG	estriol-17-β-glucuronide
E3S	estrone-3-sulfate
ER	endoplasmic reticulum
GFAP	glial fibrillary acid protein
GlpT	glycerol 3-phosphate transporter
HEK293	human embryonic kidney 293
ICG	indocyanine green
LAT	L-type amino acid transporter
MCT	monocarboxylate transporter
MFS	Major Facilitator Superfamily
MRP	multidrug resistance associated proteins
NSAID	non-steroidal anti-inflammatory drug
OAT	organic anion transporter
Oatp/OATP	Organic anion transporting polypeptide
OCT	organic cation transporter
P21G	prednisolone 21-glucuronide
PFOA	perfluorooctanoic acid
PFOS	perfluorooctylsulfonic acid
PG	prostaglandin
P-gp	P-glycoprotein
rT3	3,3’,5’ triiodothyronine
SNP	single nucleotide polymorphism
T1AM	3-iodothyronamine
T3	3,3’,5 triiodothyronine
T4	thyroxine
T4-acetic acid	3,5,3',5'-tetraiodothyroacetic acid
T4AM	3,5,3',5'-tetraiodothyronamine
TBG	thyroxine-binding globulin

TR	thyroid hormone receptor
TRE	thyroid response element
TTR	transthyretin
vWF	von Willebrand Factor
WT	wild-type

Chapter 1

General introduction and thesis overview

Portions of this introduction were published in:
Westholm DE, Rumbley JN, Salo DR, Rich TP, Anderson GW (2008) *Current Topics in Developmental Biology*;80:135-70.

General Introduction

The contents of the central nervous system (CNS) must be exquisitely regulated in order to maintain proper functioning of this critical system. The brain has a high metabolic demand, and thus requires constant influx of oxygen and nutrients as well as efflux of waste products (Takano et al., 2006). Tight regulation of this homeostasis is accomplished, in part, by the blood-brain barrier (BBB) and blood-cerebral spinal fluid barrier (BCSFB). Transport across these barriers is often a required operation during waste efflux (e.g., glucuronides), nutrient delivery (e.g., glucose), drug delivery (e.g., phenytoin) and hormonal and other biological signaling (e.g. via T4 and prostaglandins) in the brain (Adachi et al., 2003; Borst et al., 2006; Potschka and Loscher, 2001; Smith and Drewes, 2006; Sugiyama et al., 2003). Despite the importance of these transport processes, little is known about the transport mechanisms and transporter/molecular structural determinants for transport activity at the BBB. This dissertation will discuss the role of an important group of transporters at the BBB and BCSFB barrier: the superfamily of organic anion transporting polypeptides (humans: OATPs; rodents and other animals: Oatps). My specific research focus is directed at the kinetics, structure and function, and substrate specificity of the BBB and BCSFB high affinity thyroxine transporter Oatp1c1.

The following introduction will present background material relevant to the subsequent chapters. First, BBB and BCSFB features and biology are discussed to understand the biological context of Oatp1c1 expression. Second, a broad overview of the superfamily of OATPs/Oatps is presented with special attention given to their roles at the BBB and BCSFB. Next, a brief description of T4 biology is presented, as T4 was

used as the model Oatp1c1 substrate in our experiments. In addition, the role of Oatps in metabolism is summarized. Finally, Oatp protein and substrate structural features, as well as characterized human polymorphisms, are reviewed to provide a foundation for the subsequent Oatp1c1 structure-function and pharmacophore chapters. Where appropriate, focus is given to the connection of Oatp1c1 to each of these topics.

Blood Brain Barrier Structure and Function

The BBB exists as a selectively permeable barrier comprised of a vast network of microvascular endothelium (Drewes, 2001)(Figure 1). Brain endothelia are distinguished from peripheral endothelia by minimal pinocytosis, a lack of fenestrations and the presence of tight junctions (Fenstermacher et al., 1988; Kniesel and Wolburg, 2000; Sedlakova et al., 1999). Although cerebral microvasculature endothelia support the features of the BBB, astrocyte foot processes, pericytes and neurons all surround individual endothelial cells of the capillary bed forming the complete neurovascular unit, thus allowing regulated contact and communication between the brain and blood/peripheral tissues. Tight junctions restrict the entry of most solutes into the brain through junctional adhesion molecules such as claudin and occludin (Drewes, 2001). Unlike other tissues where solutes can leave the stroma and enter the parenchyma through spaces between endothelial cells, BBB tight junctions prevent paracellular diffusion. Therefore, solutes or ligands are required to traverse both the luminal and abluminal membranes of polarized BBB endothelial cells, a distance separated by approximately 110-300nm of endothelial cytoplasm (Pardridge, 2003). Currently,

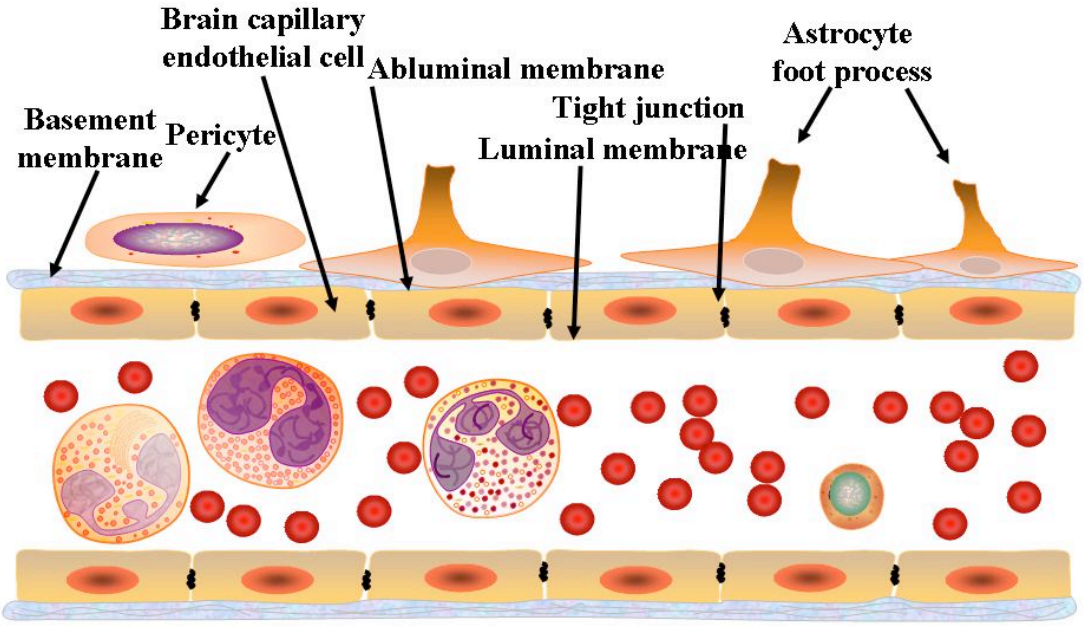

Figure 1. Diagram of BBB anatomy, including capillary endothelial cells sealed with tight junctions, a continuous basement membrane, pericytes, and astrocyte foot processes. Tight junctions limit the paracellular diffusion of solutes from blood into brain parenchyma. Therefore, in order to cross the BBB, solutes must sequentially diffuse or be transported across both endothelial membranes.

it is unknown how ligands traverse the cytoplasmic space between the luminal and abluminal membranes of BBB endothelial cells. Some ligands may passively diffuse, while others may bind carrier molecules that serve as intracellular transporters.

As a result of the limitations imposed by the tight junctions at the BBB, solutes must be transported by transcellular diffusion, carrier mediated transport, or endocytosis (Wolka et al., 2003). Transcellular diffusion across the BBB is limited by the lipophilicity and hydrogen bonding potential of a particular solute. In general, solutes of low molecular weight, polarizability, and hydrogen bonding potential, and high lipophilicity are associated with greater transcellular BBB diffusivity (Habgood et al., 2000). Much less energetic penalty is associated with such molecules crossing the hydrophobic domain of the lipid bilayer than for large polar molecules. Endocytosis plays an important role, albeit reduced and modified compared to other tissues, in the delivery of various compounds to the brain parenchyma (Wolka et al., 2003). Receptor-mediated, adsorptive and fluid phase endocytosis all contribute significantly to the overall endocytosis at the BBB.

Carrier-mediated transport of solutes is facilitated by a specific substrate-transporter interaction and driven by direct energy conversion (e.g. ATP hydrolysis), concentration gradients, cotransport, or combination thereof. BBB transporters have been identified for amino acids, sugars, nucleosides, monocarboxylic acids, peptides, organic cations, and organic anions (Tamai and Tsuji, 2000). Transport families expressed at the BBB include glucose transporters (GLUTs) monocarboxylic acid transporters (MCTs), organic anion transporters (OATs), organic cation transporters (OCTs), amino acid transporters (e.g. LATs) and OATPS/Oatps. In addition, multiple

members of the ATP-binding cassette (ABC) superfamily, including P-glycoprotein (P-gp) and multidrug resistance associated proteins (MRPs) are expressed at the BBB (Girardin, 2006). These efflux transporters serve to export endo- and xenobiotics from the intracellular to extracellular milieu. Xenobiotics are substances that are present, but not synthesized by the organism whereas endobiotics are endogenously synthesized compounds. Both drugs and toxins are classified within the xenobiotic group of compounds. The physical barrier properties of the BBB, combined with the expression of various efflux ABC transporters actively limit the uptake of certain solutes at the BBB. Despite the presence of these efflux transporters, multiple endo- and xenobiotic substrates are transported across the BBB in a vectoral fashion into or away from the brain parenchyma by OATPs, OCTs, OATs, and MCTs or via mechanisms such as endocytosis or diffusion.

BCSFB Structure and Function

The choroid plexuses are leaf-like organs found in the median wall of each lateral ventricle, as well as the roof of the third and fourth ventricles of the brain (Kusuhara and Sugiyama, 2004; Strazielle and Ghersi-Egea, 2000). Epithelial cells of these highly vascularized organs form the BCSFB (Strazielle and Preston, 2003). These cells are polarized, consisting of apical or brush border membranes (CSF facing) and basolateral membranes (blood facing) (Figure 2). Invaginations within the choroid plexus organ combined with brush border membrane provide a very large surface area exposed to the CSF. Since penetrating capillaries in choroid plexuses are fenestrated

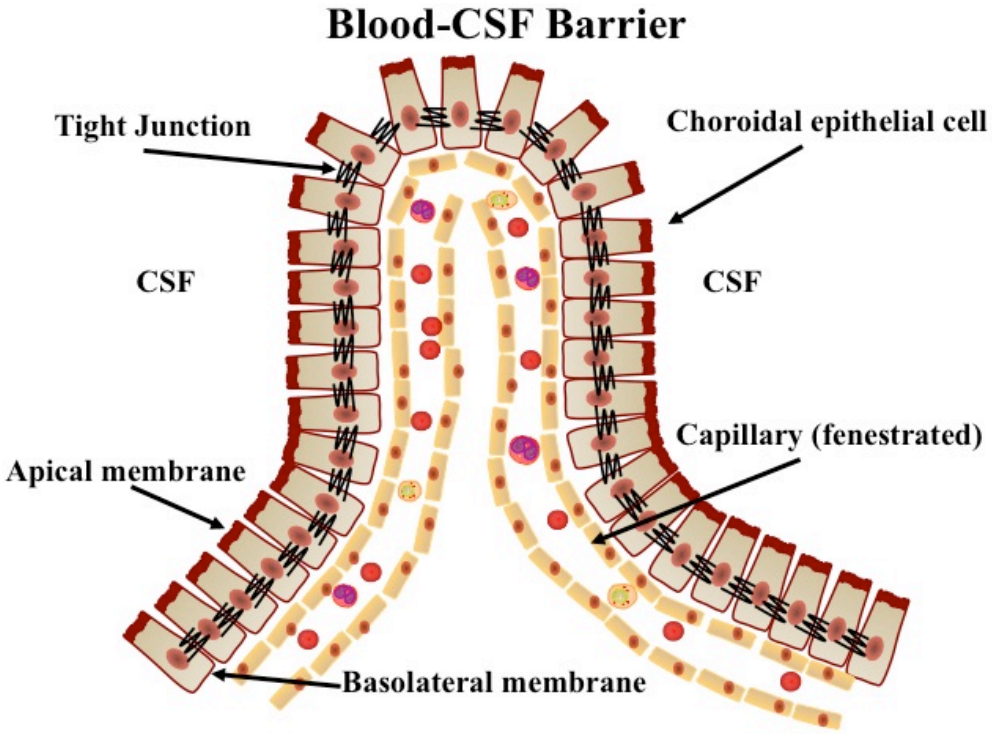

Figure 2. Diagram of BCSFB anatomy consisting of polarized choroidal epithelial cells connected by tight junctions vascularized with a fenestrated capillary bed. The presence of tight junctions between choroidal epithelial cells forces solutes to sequentially cross both the apical (CSF-facing) and basolateral (blood-facing) membranes in order to pass from CSF to blood or vice versa.

(leaky), plasma components have free access to the basolateral membrane. Like the junctions between endothelial cells of the BBB, choroid plexus epithelial cell junctions are tight. Thus, under most circumstances there is no paracellular diffusion from the blood to the CSF. Some compounds are excreted from the CSF to the blood such as drugs and endogenous waste, while other solutes travel from the blood to CSF. In order to accomplish transport in either of these directionalities, these compounds must sequentially cross the apical and basolateral membranes of the choroidal epithelial cell.

The BCSFB forms a dynamic interface between the dense, fenestrated choroidal stroma and the CSF. Choroid plexuses synthesize the majority of CSF, which in turn circulates from the choroid plexuses, into the subarachnoid spaces and then the spinal column. The diverse roles of CSF range from regulation of intracranial volume and buoyancy, to buffering extracranial fluid (Strazielle and Ghersi-Egea, 2000). In addition to synthesizing CSF, choroid plexuses influence the composition of the CSF through the expression of a plethora of transporters. Carrier-mediated transport processes at the BCSFB involve many of the same families of transporters expressed at the BBB. Finally, the choroid plexus plays a major role in the metabolism of endo- and xenobiotics. This topic will be expanded upon in a later section of this dissertation.

Introduction to the OATP/Oatp superfamily

OATPs/Oatps are involved in both influx and efflux across CNS and other cell barriers. OATPS/Oatps form a diverse superfamily of solute carriers expressed throughout the body (Hagenbuch and Meier, 2003b). These transporters, with 12 putative membrane-spanning domains, mediate transmembrane transport of various

amphipathic organic anions including steroid conjugates, thyroid hormones, prostanoids, bile salts, oligopeptides, drugs, toxins and other xenobiotics (Hagenbuch and Meier, 2004; Mikkaichi et al., 2004b). The transport mechanism of OATPs/Oatps is sodium-independent and likely driven through anion exchange. The specific driving force is currently unknown, but intracellular glutathione is a possible candidate, as evidenced by a 1:1 stoichiometry of taurocholoate/glutathione exchange by Oatp1a1 (Jacquemin et al., 1994; Li et al., 1998). However, the use of glutathione as a transport driving force is not universal for all Oatps/OATPS. For example, Oatp1a4 transport appears to be sensitive to intracellular glutathione levels, but does not anti-port glutathione (Li et al., 2000). In addition, OATP1B1 is not susceptible to glutathione levels and may operate simply as a facilitated diffusion transporter (Briz et al., 2006; Mahagita et al., 2007). Oatp/OATP transport has also been shown to have a pH dependent component, with transport stimulation occurring at acidic pH (Leuthold et al., 2009). OATP1C1 transport, however, is not affected by pH, likely due to the absence of a conserved histidine residue in the third transmembrane domain (Leuthold et al., 2009).

Substrate specificity and tissue localization varies widely with different OATP/Oatp members (Cheng et al., 2005; Hagenbuch and Meier, 2004). Some members are expressed ubiquitously and transport numerous substrates, other members are restricted to discrete tissue expression profiles and display a more specialized substrate specificity. Expression of multiple OATPs/Oatps at the BBB and BCSFB puts this superfamily of transporters in a powerful position of influence over the ultimate absorption, diposition and excretion of drugs and endobiotics.

The focus of this thesis, Oatp1c1, is a 716 amino acid protein expressed in the luminal and abluminal membranes of BBB endothelial cells, the basolateral membrane of choroid plexus epithelial cells, human ciliary body epithelial cells and Leydig cells of the testes (Gao et al., 2005; Sugiyama et al., 2003; Tohyama et al., 2004). Human OATP1C1 is also localized to, and highly expressed in the brain (Pizzagalli et al., 2002). A limited sample set of human tissues exhibited variable OATP1C1 expression in BBB endothelial cells in adults, but strong expression in neonates (Roberts et al., 2008). Compared to other Oatps, Oatp1c1 has a relatively narrow range of substrates. However, Oatp1c1 is a high affinity thyroxine transporter and has the lowest reported K_m for T4 of all known transporters (Sugiyama et al., 2003). The physiological role of Oatp1c1 as an important T4 transporter is conserved not only among mammalia, but other vertebrates, including members of class Aves. In support of this, Oatp1c1 isolated from quail was recently shown to transport T4 with a high affinity (K_m=6.8 nM) (Nakao et al., 2006). Other Oatp1c1 substrates include 3,3',5' triiodothyronine (reverse T3), cerivastatin and $E_2$17βG (Sugiyama et al., 2003).

In depth kinetic characterization of Oatps is incomplete. For many known Oatp substrates, kinetic constants (e.g. K_m and V_{max}) are not determined (Sugiyama et al., 2003). However, the knowledge of such parameters is crucial for the determination of what substrate concentrations transporter-substrate interactions might occur. In addition, without determination of kinetic parameters, *in vitro-in vivo* correlations as well as prediction of drug-drug interactions are not possible.

Kinetic parameter determination is usually carried out using the Michaelis-Menten equation which operates under a number of assumptions. First, proper kinetic

characterization requires assurances of linearity with respect to both time and transporter level. In addition, it is assumed nothing is limiting, for example substrate concentration or co-substrate supply. Michaelis-Menten kinetics also assume the presence of a single binding site. However, single Oatps often transport an extremely diverse panel of substrates (Hagenbuch and Gui, 2008). With this consideration, the possibility of a single distinctly shaped binding site accepting the entire compliment of Oatp substrates becomes less likely. Indeed, for other proteins, such as the cytochrome P450 metabolizing enzymes, the existence of multiple binding sites and resultant non-Michaelis-Menten enzyme have been well characterized (Hutzler and Tracy, 2002). For Oatps, the existence of multiple binding sites has begun to be recognized. For example, OATP4C1 transports both T3 and digoxin, but neither substrate significantly cis-inhibits the transport of the other, suggesting the presence of multiple OATP4C1 substrate binding sites (Mikkaichi et al., 2004a). Evidence for multiple binding sites in Oatp1a4, Oatp1c1, OATP1B1, OATP1B3 and OATP2B1 has also been reported and is discussed in more detail in Chapter 2 (Grube et al., 2006; Gui et al., 2008; Sugiyama et al., 2002; Tamai et al., 2001).

OATP/Oatp expression and action at the BBB and BCSFB

Currently, there are over 30 mammalian members of the OATP/Oatp superfamily (Hagenbuch and Meier, 2003b). Of these only a handful are expressed at the BBB and BCSFB. So far, OATP1A2, Oatp1a4, Oatp1a5, Oatp1c1/OATP1C1, Oatp2a1, and possibly Oatp1a1 have been identified at protein level at both the BBB and/or BCSFB (Kusuhara and Sugiyama, 2005). However, definitive localization of

these transporters at the BBB and BCSFB awaits confirmation through protein detection.

These OATP/Oatp members maintain a powerful influence over the CNS disposition and efflux of multiple compounds. Several from this group have high affinities for specific substrates, with significant biological outcomes. For example, Oatp1c1 in its role as high affinity thyroxine transporter appears to account for a significant portion of the T4 that enters the brain (Tohyama et al., 2004). T4 is a prohormone of triiodothyronine (T3), the active thyroid hormone. Most T3 is synthesized through the action of type II 5'-iodothyronine deiodinase (D2) (Anderson et al., 2003). T3 has profound impacts on the timing and initiation of multiple neurological development processes (Anderson, 2001). Oatp1c1-dependent T4 transport accumulates T4 in the CNS at levels higher than would be possible with diffusion alone (Chen et al., 2006). Thus, differential expression of Oatp1c1 and other Oatp T4 transporters may allow an organism to meter CNS T4 concentrations throughout development or during times of T4 fluctuations.

A hallmark of OATP/Oatp expression at the BBB and BCSFB is the asymmetric distribution of different members at the polarized barrier cell membranes. Some members are expressed at both membranes at a certain barrier. For example, Oatp1a4 has been localized to both the luminal and abluminal membranes of the BBB, using immunofluorescence colocalization with von Willebrand factor (vWF) and glial fibrillary acid protein (GFAP) under confocal microscopy (Gao et al., 1999). In contrast, other Oatp/OATPs are expressed only on one membrane. For instance, Oatp1a5 is expressed exclusively at the brush border membrane of choroid plexus

epithelial cells, as evidenced by immunohistochemical analysis (Ohtsuki et al., 2004). Finally, some members display different membrane expression patterns depending on what tissue they are expressed. For example, Oatp1c1 is expressed on both the luminal and abluminal membrane of BBB endothelial cells, but expressed at the basolateral membrane in choroid plexus epithelial cells (Sugiyama et al., 2003; Tohyama et al., 2004). OATP/Oatp trafficking signals may be differentially decoded by various host cells resulting in cell specific membrane localization patterns (Ito et al., 2005; Sugiyama et al., 2003). The precise nature of these signals is unknown, but may include such identifiers as tyrosine motifs for basolateral sorting and N-linked oliogosaccharides for apical sorting (Ito et al., 2005; Mostov et al., 2000).

The specific localization and combined action of different OATPs/Oatps likely have a significant impact on the overall net accumulation of a given substrate in either the plasma or brain parenchyma. Oatp1c1 and Oatp1a4, for example, largely contribute to the efflux of $E_2$17βG from the brain across the BBB (Kusuhara and Sugiyama, 2005; Sugiyama et al., 2001; Sugiyama et al., 2003). $E_2$17βG is a substrate of both Oatp1a4 and Oatp1c1. Glucuronidation is a form of conjugative metabolism crucial to the xenobiotic detoxification systems of the body and will be covered in greater detail later in the introduction. Endogenous compounds are also glucuronidated, allowing directional transport and excretion of lipophilic compounds such as sterols (Sugiyama et al., 2001). Efflux of $E_2$17βG out of the brain across the BBB by luminal and abluminal localized Oatp1a4 and Oatp1c1 helps prevent the accumulation of this metabolized hormone in the CNS.

Under normal physiological conditions, most OATP/Oatp substrates are bound to protein, usually albumin, due to the hydrophobic component of these molecules (Hagenbuch and Meier, 2003b). It is widely assumed that substrates must first dissociate from the protein carrier to the free state before transport (Tanaka and Mizojiri, 1999). Thyroid hormone, a predominant substrate of Oatp1c1, circulates in the CSF bound to transthyretin (TTR), and thyroxine binding globulin (TBG; humans, mice), TTR and albumin in the blood (Schussler, 2000). The free drug/hormone hypothesis states that the amount of drug or hormone available for uptake by intact tissues is equal to the amount of free drug or hormone determined under *in vitro* settings (Koch-Weser and Sellers, 1976; Pardridge and Landaw, 1984). However, Pardridge showed that dissociation of ligands from proteins in the BBB capillary bed is significantly enhanced (Pardridge and Landaw, 1984). As a result, the amount of free hormone available for uptake is possibly much greater than concentration of free hormone under *in vitro* settings. Thus, the microenvironment of the BBB endothelial cell may enhance dissociation of thyroid hormone from TBG or albumin. Interestingly, Oppenheimer proposed that T4 bound to protein in plasma was directly transferred to cellular binding sites (Oppenheimer et al., 1969). He hypothesized that competition between protein binding and cellular binding sites determined the extent of T4 transport into different tissues. Members of the OATP/Oatp superfamily, including Oatp1c1, have large extracelluar domains. More research is needed to explore the possibility of these moieties interacting with protein bound ligand and direct transfer of ligand to transporter. Such a speculative model suggests that the enhanced dissociation of thyroid hormone from its binding protein, as observed by Pardridge, may be explained

by direct interactions with extracellular domains of OATPs/Oatps. One large extracellular domain common to all Oatps is a region with 10 conserved cysteines between transmembrane domains 9 and 10. When these residues were mutated in OATP2B1, both transport and trafficking to the plasma membrane were severely reduced in all cases (Hanggi et al., 2006). It was undetermined whether these residues played a role in any sort of protein docking in the transport process.

OATPs/Oatps also play a significant role in transepithelial T4 transport in the choroid plexuses. Large pools of TTR exist in the CSF. In the brain, TTR is synthesized exclusively by choroid plexus epithelial cells and unidirectionally secreted into the CSF (Cavallaro et al., 1993). The BCSFB is a major site of T4 transfer to the CNS, with Oatp1a4 and Oatp1c1 likely playing important roles in transport from the blood across the basolateral membrane of choroidal epithelial cells (Gao et al., 1999; Tohyama et al., 2004). Transport of T4 into the CSF across the brush border membrane may occur via membrane bound transporters or through TTR binding and concomitant secretion (Southwell et al., 1993). The large pool of TTR in the CSF is then able to bind and increase the concentration of T4 in CSF compared to plasma (Chen et al., 2006). Loss to the blood from CSF is minimal. As a result, concentrating T4 in the CSF may increase CNS retention and permit redistribution of the hormone in the brain and CSF (Chen et al., 2006). However, TTR null mice and human TBG mutations do not have functional effects (Palha et al., 2000).

Recently, an interesting relationship between P-gp and Oatps in the homeostasis of T4 in the CSF was established, perhaps elucidating the mechanism of high CSF T4 concentration maintenance. In 2005, Mitchell et al. first demonstrated that P-gp accepts

iodothyronines (Mitchell et al., 2005). Then, two years later, it was reported that apically expressed P-gp at the BCSFB may play a role in preserving high CSF T4 concentrations through recycling of T4 between the CSF and cytoplasm of BCSFB epithelial cells (Kassem et al., 2007). In addition, based on pharmacologic inhibition studies, the authors hypothesized that basolaterally expressed Oatps, including Oatp1c1, may also deliver T4 into the BCSFB epithelial cell for subsequent energy driven P-gp efflux into the CSF.

Thyroid hormone brain transport

Proper brain function requires thyroid hormone at all developmental stages. It has been over a century since the discovery that the thyroid gland plays an important role in brain development and function (Oppenheimer and Schwartz, 1997). In 1888, members of the Clinical Society of London came to this conclusion after observing that patients with cretinism (a manifestation of iodine deficiency/congenital hypothyroidism) also displayed mental retardation. In the 120 years that have elapsed since this finding, much progress has been made in the understanding of the molecular basis of thyroid hormone action in the brain. As stated earlier in the introduction, thyroid hormone circulates mainly in the form of T4. Once in the cell, the action of type II deiodinase removes a 5' outer ring iodine, forming the active 3,3', 5-triiodo-L-thyronine (T3). Although extranuclear actions of thyroid hormone have been described (Lei et al., 2003), the main mode of thyroid hormone action is the modulation of gene transcription through its role as a ligand for the nuclear transcription factor, thyroid hormone receptor (TR) (Anderson, 2001).

T3 has much greater affinity for TR than T4, and is thus considered the active form of thyroid hormone and primary TR ligand. The T3-TR complex, as a homodimer or heterodimer with RXR, binds specific thyroid response element DNA sequences (TREs) in the promoters of thyroid responsive genes (Anderson et al., 2003). Upon binding the TRE, co-activators with histone acetylase activity are recruited to the liganded TR, resulting in a relaxed chromatin structure conducive to enhanced gene transcription. In the apo-form, TR binds to corepressor complexes that recruit histone deacetylases, thus promoting a heterochromatic state and basal transcription of the target gene. T3 has both direct and indirect gene targets. Direct targets contain TREs, while indirect targets may be a gene, for example, that is regulated by a transcription factor that is a direct target of T3.

Thyroid hormone plays multiple roles in the initiation and timing of brain differentiation and maturation events. Neuronal dendritic arborization, synapse formation and oligodendrocyte proliferation and maturation are influenced, in part, by actions of thyroid hormone (Anderson et al., 2003). Obviously, the first step in the series of events that leads to the critically important action of thyroid hormone in the brain, is the transfer of thyroid hormone from the blood through the brain across the BBB. Thus, identification of the proteins responsible for this transfer is requisite for a complete understanding for both thyroid hormone action and derangements. For years, thyroid hormone was thought to passively diffuse across the plasma membrane. The two aromatic rings (derived from conjugated tyrosines) were thought to lend enough lipophilicity to make thyroid hormone soluble in the plasma membrane. Indeed, early studies showed that T4 bound phospholipid membranes (Hillier, 1970). However,

beginning in the 1970's data began accumulating suggesting thyroid hormone moved across the plasma membrane through carrier mediated processes. First, on a theoretical basis, the pore size between adjacent phospholipids in the plasma membrane was shown to be between 3.5 and 5.5 Å, too small for the 7.2-7.5 Å sized T4 to diffuse through (Stitzer and Jacquez, 1975). Second, thyroid hormone is derived from two amino acids (tyrosines), thus is a charged zwitterion at physiological pH. In addition, thryoid hormone also contains multiple electronegative iodines, significantly increasing mass. Third, thyroid hormone uptake was also shown to be a saturable process, sensitive to both heat (suggestive of a protein-mediated process) and freezing (suggestive of a process occurring at the plasma membrane, not simple intracellular binding) (Rao et al., 1976). Finally, Lai et al. demonstrated that spin-labeled T3 did not flip-flop significantly across phospholipid bilayers (Lai et al., 1985). Together, these data suggested that thyroid hormone crossed plasma membranes through a carrier-mediated process.

With the advent of in vitro molecular biology techniques, the specific proteins responsible for T3 and T4 transport across cellular plasma membranes were identified. Transporters from multiple families of solute carriers are now known to transport thyroid hormones, including monocarboxylate transporters (Mct8 and Mct10), L-type amino acid transporters (Lat-1), sodium taurocholate co-transporting polypeptide (Nctp) and Oatps/OATPs (Friesema et al., 2005).

Numerous Oatps have been shown to transport thyroid hormone, including members of the Oatp1 and Oatp4 families. At the BBB and BCSFB Oatp1a4, Oatp1a5, Oatp1c1 (rodent) and OATP1A2 and OATP1C1 (human) are known to transport T4. In

particular, the role of Oatp1c1 as a thyroxine transporter at the BBB and BCSFB, is likely very important for overall thyroid hormone function in the CNS. Other Oatps that transport thyroid hormones, such as Oatp1a4 and Oatp1a5 transport thyroxine and T3 with roughly equal affinity with K_m's in the μM range. Thus, with a K_m for T4 transport in the low nM range, Oatp1c1 has a T4 transport K_m of at least two orders of magnitude less than all other Oatp thyroxine transporters, suggesting Oatp1c1 maybe the predominant T4 transporter expressed at the BBB and BCSFB. T4 circulates at very low free concentrations (12 pM) and thus will theoretically preferentially engage Oatp1c1 under most circumstances. In support of a strong role for Oatp1c1-mediated BBB T4 transport, *in situ* brain perfusion studies examining pharmacologic inhibition of T4 transport, suggested a significant fraction of BBB T4 transport is mediated by Oatp1c1 (Tohyama et al., 2004). The preference for thyroxine transport of Oatp1c1 may offer another level of control for thyroid hormone in the brain. Instead of delivery of active thyroid hormone directly to the CNS, transport of thyroxine allows T3 level modulation through control of D2 activity.

Oatps in metabolism

One of the primary roles of the BBB and BCSFB is to form a biochemical barrier functioning to protect the brain through detoxification enzymes expressed in brain barrier cells. Endogenous chemicals and environmental toxins added selective pressure on the living systems to evolve oxidative and conjugative metabolic pathways with transporting capabilities to neutralize compounds. In addition to handling many endogenous compounds in their native state, Oatps are known to transport many

endogenous and xenobiotic molecules that have been marked for elimination though one of the many conjugative metabolism reactions. Thus, Oatps along with the multi-drug resistance-associated proteins (Mrps/MRPs) work collectively with metabolic enzymes to protect the organism from harmful compounds and modulate levels of endogenous substrates (e.g. steroid hormones) within target tissues like the brain.

Oatps in the BBB and BCSFB, likely play essential roles in transporting conjugated endo- and xenobiotics across brain barrier cells. Oatps are localized to both membranes of both choroid plexus epithelial and endothelial cells. Therefore, Oatps could theoretically participate to a large extent in efflux of glucuronides such as $E_2$17βG from the brain. Indeed, experiments conducted by Sugiyama et al. implicated Oatps in the efflux of $E_2$17βG from the brain. Using the Brain Efflux Index method, in the presence of different inhibitors, the authors pharmacologically identified the transporters responsible for $E_2$17βG efflux across the BBB (Sugiyama et al., 2001). The authors concluded that Oatps were responsible for at least 40% of the $E_2$17βG efflux across the BBB. Along with Oatps/Oats, data from *Mrp1* knockout mice also suggest this active transporter is involved in $E_2$17βG elimination from the brain (Tohyama et al., 2004). These data have together led to the development of a model for vectoral $E_2$17βG transport across brain barrier cells (Kusuhara and Sugiyama, 2005). Oatps expressed on the apical membrane of the choroid plexus epithelial cell, such as Oatp1a5 transport $E_2$17βG from the CSF into the choroid plexus epithelial cell. Polarized basolateral expression of Oatp1c1 and Oatp1a4, along with *Mrp1* then allows energy driven transport of $E_2$17βG out of the epithelial cell and into the blood. As one

of the transporters (Mrp1) uses energy to drive transport, the movement of substrate becomes vectoral.

Efflux of the conjugated substrates from the brain targets them for elimination in the urine and bile. In addition to the brain, Oatps participate in this elimination process in the liver and kidney, tissues responsible for ultimate elimination of these conjugates (Hagenbuch and Meier, 2003b; Hagenbuch and Meier, 2004). The polarized expression Oatp transporters on the kidney contributes to the directional efflux of metabolites out of the body and through the bile and urine (Chen et al., 2005).

Molecular Architecture of the Oatp Superfamily

Although no high resolution structure is available for any member of the Oatp superfamily, significant structural inferences have been made from sequence analysis and homology modeling. One common feature of the Oatps is the presence of 12 putative transmembrane spanning α-helices. It should be noted that this is not an empirically determined topology and predictions using the human OATP1C1 sequence and several predictive algorithms yields between 10 and 12 transmembrane spans. The assignment of 12 transmembrane spanning helices seems reasonable by analogy and moderate sequence similarity to the major facilitator superfamily (MFS), three of which have known three-dimensional structures (see Chapter 4).

Recently, two groups have used homology modeling to construct three-dimensional structures of Oatps using the known MFS structures. Meier-Abt et. al. reported the first structural models, using human OATP1B3 and OATP2B1 (Meier-Abt et al., 2005). They identified the glycerol-3-phosphate transporter and the lactose

permease as structural homologues to the Oatps. Both MFS structures, containing 12 transmembrane spans and a single proposed substrate binding site, were used in the comparative modeling. Following sequence alignment (two Oatps and two MFS proteins), the aligned amino acids of the OATP1B3 and OATP2B1 were mapped onto the three-dimensional structures using the program MODELLER (Sali and Blundell, 1993). Meier-Abt et. al. used the calculated electrostatic surface potential to evaluate the reliability of the structures returned. This analysis showed the expected positive potential within the putative substrate binding site as well as a lack of electrostatic potential (positive or negative) on the helical surfaces predicted to face the lipid bilayer. Of the 12 transmembrane helices, modeled helices 1, 2, 4, 5, 7, 8, 10, and 11 all appear to make some contribution to the substrate pore. Several polar amino acids, conserved in the OATP1 family, were shown lining the pore. A similar result was obtained with the OATP2 family. They identified the conserved Arg181 (OATP1) and His579 (OATP2) as potential family specific contributors to the substrate binding site (Meier-Abt et al., 2005). A number of other conserved amino acids were proposed to play a more structural role, including the conserved glycines and prolines, which may be important in packing and orienting helices toward the pore. The large hydrophilic domain between helices 9 and 10 was modeled independently based on its sequence similarity to the Kazal-type serine proteases. In this model some of the cysteines, conserved in all Oatps, are proposed to be involved in disulfide bonds. Recently, Hanggi et. al. proposed that all of the cysteines are involved in disulfide bonds using a cysteine labeling reagent (Hanggi et al., 2006). The structural comparison to the MFS was extended to include a similar proposed mechanism, an alternating two state

mechanism of inward and outward facing states referred to as a rocker-switch type of movement (Abramson et al., 2003; Huang et al., 2003).

Oatp Polymorphisms

Polymorphisms have been identified for all human OATPs, but only OATP1B1, OATP1B3, OATP1A2, and OATP1C1 have been investigated biochemically. Most functional characteristics have been carried out with respect to drug transport.

OATP1B1 polymorphisms

OATP1B1 is one of the most highly expressed OATPs in the liver and is localized to the sinusoidal membrane in hepatocytes (Hsiang et al., 1999). In addition to a variety of bile salts, OATP1B1 transports many drugs including pravastatin, rosuvastatin, rifampin, and methotrexate (Marzolini et al., 2004). At least 35 polymorphisms have been identified in both structural and promoter regions of the OATP1B1 gene (Iwai et al., 2004; Kameyama et al., 2005; Konig et al., 2006; Nozawa et al., 2004; Rohrbacher et al., 2006). Allelic frequencies are dependent on ethnicity and have widely ranging values. Some allelic frequencies are strikingly high. For example, OATP1B1*1b (Asn130Asp) has a 74% allelic frequency in African Americans (Konig et al., 2006). In contrast, another study found OATP1B1*2 (Phe73Leu) has a 2% allelic frequency in European Americans and was not detected in African Americans (Tirona et al., 2001). Although not all OATP1B1 polymorphisms have been functional characterized, many have displayed altered transport kinetics (usually higher K_m and lower V_{max}) compared to the reference allele (Niemi et al., 2005a; Niemi et al., 2004; Tirona et al., 2001).

Of particular clinical interest with some OATP1B1 polymorphisms, is their effect on OATP1B1 substrate plasma concentrations. Most studies have focused on the effect OATP1B1 polymorphisms have on plasma concentrations of HMG-CoA-reductase inhibitors including pravastatin and pitavastatin. OATP1B1 transports both pravastatin and pitavastatin with K_m's of 35 μM and 3 μM, respectively (Hsiang et al., 1999). Although the majority of pravastatin is not metabolized in humans, large inter-individual differences in plasma pravastatin levels are reported (Neuvonen et al., 1998). Thus, functional differences resulting from SNPs in pravastatin transporters, such as OATP1B1, are hypothesized to account for inter-individual variations in pravastatin plasma concentrations. This hypothesis has been borne out in the literature. For example, individuals carrying the OATP1B1*15 allele (Asn30Asp, Val174Ala; ↓ pravastatin transport *in vitro*) have 106% higher area under the curve (AUC) the first 12 hours after dosing than individuals carrying the reference allele (Niemi et al., 2004; Nishizato et al., 2003). Significantly, no associations have been found between polymorphisms in the pravastatin transporters OATP2B1, MRP2 or MDR1 with changes in pravastatin pharmacokinetics (Niemi et al., 2004). In these cases, the authors argue the high pravastatin plasma levels result from decreased OATP1B1 transport into the liver. In light of these results, Niemi et al. examined whether the higher pravastatin AUC in individuals carrying polymorphic OATP1B1 alleles results in lower pravastatin efficacy. They found that individuals carrying the OATP1B1*17 allele had significantly reduced pravastatin efficacy as measured by plasma lathosterol concentration and lathosterol:cholesterol ratios (Niemi et al., 2005b).

OATP1B3 polymorphisms

OATP1B3 is highly expressed in the liver (Konig et al., 2000a). In addition, OATP1B3 and OATP1B1 are in the same phylogenetic sub-family and share 80% amino acid identity and much substrate specificity (Konig et al., 2000b; Konig et al., 2006; Marzolini et al., 2004). Polymorphic data, especially functional characterization, is lacking compared to OATP1B1 and OATP1A2. However, some interesting progress has been made. For example, Tsujimoto et al. discovered that the OATP1B3 Ser112Ala and Met233Ile variants are in complete linkage disequilibrium (Tsujimoto et al., 2006). Iida et al. identified multiple OATP1B3 SNPs in the 5' flanking and coding regions (Iida et al., 2001). OATP1B3-S112A and OATP1B3-M233I were subsequently analyzed for function and displayed reference transport and localization characteristics. However, OATP1B3-G522C showed decreased intrinsic clearance in both HEK293 and MDCKII transfected cell lines. The G522C substitution in the OATP1B3 variant is in the predicted 5th extracellular loop, a region of suggested importance in OATP1A1 (Konig et al., 2006).

OATP1B3 is also a known high affinity transporter of paclitaxel (K_m = 7 μM) (Smith et al., 2005). Smith et al. investigated possible pharmacokinetic effects of OATP1B3 polymorphisms in cancer patients treated with paclitaxel. They reported no differences in paclitaxel clearance or any other pharmacokinetic parameter in patients with 334T>G (Ser112Ala), 699G>A (Met233Ile), and 1564G>T (Gly522Cys) OATP1B3 loci compared to patients with the reference locus.

OATP1A2 polymorphisms

OATP1A2 accepts a wide range of substrates, including thyroid hormones, methotrexate, fexofenadine and rocuronium and is expressed in the brain capillaries,

kidney and liver (Kullak-Ublick et al., 1995). High OATP1A2 expression in brain capillaries makes this transporter a critical component of the blood brain barrier (Lee et al., 2005). Several OATP1A2 polymorphisms in both 5' flanking and exonic regions have been identified and characterized *in vitro* (Badagnani et al., 2006; Lee et al., 2005). Allelic frequencies vary according to ethnicity with values ranging from 1-11%. *In vitro* characterization of these polymorphisms has occurred in multiple labs but is not comprehensive. However, multiple transport phenotypes have been reported. Glu172Asp, Asn135Ile and Arg168Cys have reduced uptake capacity for estrone sulfate and methotrexate (Badagnani et al., 2006; Lee et al., 2005). Substrate dependent V_{max} reductions have been observed in Ala185Thr (decreased deltorphin II uptake) and Thr668Ser (decreased estrone sulfate uptake) variants. In addition, a hyperfuntional variant, Ile13Thr, has displayed a 2-fold increase in V_{max} for methotrexate uptake (Badagnani et al., 2006). A non-functional deletion variant, Asn277DEL has also been identified (Badagnani et al., 2006). Expression patterns have been examined for several OATP1A2 variants. A portion of the differences in variant OATP1A2 transport capabilities may be due to alterations in glycosylation state and sub-cellular localization (Glu172Asp, Asn135Ile) (Lee et al., 2005). None of these polymorphisms have been investigated *in vivo* or under clinical settings. However, the magnitude of OATP1A2 contributions to blood-brain barrier transport and to the delivery of toxic drugs (e.g. methotrexate) makes such investigations essential.

OATP1C1 polymorphisms

OATP1C1 polymorphisms are just beginning to be characterized. A recent paper has highlighted a possible association with therapy resistant hypothyroid

symptoms and OATP1C1 polymorphisms (van der Deure et al., 2008). Adult hypothyroidism causes reversible fatigue, depression and neurocognitive deficits. These symptoms arise, in part, from derangements in brain thyroid hormone action. A primary step of thyroid hormone action in the brain is the transport of the main circulating form of thyroid hormone, T4, across the blood-brain barrier. Van der Deure et al. examined whether OATP1C1 polymorphisms are determinants for depression status and neurocognitive activity in hypothyroid patients treated with levothyroxine (van der Deure et al., 2008). The authors found an association between OATP1C1-intron3C>T and OATP1C1-C3035T polymorphisms and low scores on psychological well-being tests in adequately treated hypothyroid patients (van der Deure et al., 2008). No differences between polymorphic OATP1C1-Pro143Thr and the reference allele were detected. Importantly, however, in vitro biochemical assays showed no difference in transport activity between the reference allele and any of the identified polymorphisms.

Oatp/OATP structural and pharmacogenetic conclusions

Based on *in silico*, *in vitro* and clinical findings presented above, general features of Oatp/OATP structure can be inferred. Most models are in agreement that Oatps likely possess 12-transmembrane alpha-helical domains. Transmembrane alpha helices are likely amphipathic, with lipophilic amino acid side chains facing the lipid bilayer and more polar sides lining the pore. In general, polymorphisms in the membrane domains, having effects on transport and retaining protein expression levels, have been shown to be amino acids facing the pore in the proposed structures. In addition, large extracellular domains, such as the large cluster of conserved cysteines,

are critical for Oatp function and trafficking. Within this architecture, the amino acids defining the selectivity of the individual Oatps must exist. As more polymorphisms are characterized, models are built, and differences in the substrate recognition site identified, the rules for Oatp substrate discrimination will be elucidated. This topic is the subject of chapter 4.

Oatp substrate structural features

The disposition of small molecules in the brain that cannot diffuse across lipid bilayers is dependent on the specificity of the membrane transporters expressed at the BBB. The pathway through the transporter that the small molecules (substrates) must traverse necessarily contains a molecular surface complimentary to the substrate surface. This means that in three-dimensional space, an Oatp transporter should contain a counter charge for electrostatic interactions, a hydrogen bond donor or acceptor to compliment an acceptor or donor, respectively, and non-polar amino acids to interact with hydrophobic domains common in many Oatp substrates (Yarim et al., 2005). Although Oatps have wide ranging tissue distributions and somewhat different substrate specificities, there remains considerable substrate overlap between the multiple isoforms. The expectation for a comparison of common substrates is the identification of common rules for substrate discrimination. This will only be elucidated with complimentary mutational analysis and detailed substrate/inhibitor kinetics measurement, including comparative molecular field analysis (CoMFA).

Although the precise molecular determinants of Oatp substrate multi-specificity have not been identified, a few groups have published analyses of Oatp substrate

chemical characteristics (Chang et al., 2005; Gui et al., 2009; Yarim et al., 2005). Yarim et al. performed a 3D-QSAR analysis on a heterogenous training set of 18 substrates of the BBB and BCSFB expressed Oatp1a5 (Yarim et al., 2005). Structures were flexibly aligned using the Genetic Algorithm Similarity Program (GASP) program (Jones et al., 1995). The GASP algorithm created structural superpositions that resulted in a hypothetical pharmacophore model containing a negatively charged group on one end, an extended hydrophobic domain in the central part of the structure, and a hydrogen bond donor at the opposite end. Therefore, as noted by the authors, a substrate containing all three of these properties would be expected to interact more strongly with Oatp1a5 than a substrate containing only 1 or 2 of the features. The aligned structures were then subjected to a comparative molecular field analysis (CoMFA) analysis to generate a QSAR model. The author's CoMFA model had good predictive power when a test set was applied to it. A new set of 5 potential Oatp1a5 substrates was selected based on similarities to the original 18 training set compounds. The CoMFA model predicted K_i values for this test set in agreement with experimentally derived K_i values.

In another study, Chang et. al. created a training set for rat Oatp1a1 that contained 26 molecules with a range of K_m values from 0.015 to 3300 μM (Chang et al., 2005). In general, the results reported by Chang et al. were in agreement with those published by Yarim et al. The pharmacophore generated in this case contained two hydrogen bond acceptors and three hydrophobes. Again, the polar groups (hydrogen bond acceptors) were located on the opposite ends of the molecules. This is consistent with the Yarim et. al. study, showing the importance of the characteristic negative

charge at one end of the substrate and a second polar group at the opposite end. Although, in their study, Yarim et. el. suggest that the second polar group is a hydrogen bond donor (Yarim et al., 2005). The distribution of hydrophobic determinants in the Oatp1a1 pharmacophore model was also consistent with the Oatp1a5 results of Yarim et. al. In fact, there appears to be favorable hydrophobic interactions near one polar end similar to the steric bulk preference near the negative charge for 1a5. These similarities are not surprising considering the extensive substrate overlap of these two Oatp variants reported in the literature (Hagenbuch and Meier, 2003a). Further, although these two proteins have different tissue distributions they share significant sequence homology.

More recently, Gui et al. performed a CoMFA analysis of OATP1B1 inhibitors (Gui et al., 2009). The authors screened 39 known nuclear receptor ligands for inhibition activity of OATP1B1-mediated $E_2$17βG transport. The authors developed a CoMFA model based on a training set of 18 of the newly identified inhibitors, using molecular structures and experimentally determined K_i's. For model validation, the authors selected 4 additional compounds predicted to inhibit OATP1B1, as a test set. The predicted K_i's were in good agreement with the subsequently determined experimental K_i's, with an $R^2 = 0.917$. The authors concluded that an ideal OATP1B1 substrate contains a central hydrophobic region, a flanking negatively charged region, as well as another negatively charged or polar region critical for interacting with OATP1B1 channel surfaces.

The structural features of the common Oatp substrate, T4, fit well with the pharmacophore models proposed for Oatp substrate specificity. For example, T4 possesses a negatively charged carboxyl group on one end of the molecule and a

phenolic hydroxyl group with hydrogen bonding potential on the opposite end. The interior hydrophobic ring structures, originally thought to facilitate passive diffusion, were found to be a critical structural component for recognition by Oatps (Yarim et al., 2005).

To date no CoMFA or QSAR studies have been performed for Oatp1c1. This is important, as Oatp1c1 has a more restricted substrate specificity compared to other Oatps and thus may require different molecular determinants for substrate recognition.

Thesis overview

The chapters following the introduction detail my work on the characterization of the high affinity T4 transporter Oatp1c1. Chapter 2 describes my findings on the kinetic characterization of the Oatp1c1 substrates T4 and $E_2$17βG. The identification of multiple T4 and $E_2$17βG Oatp1c1 binding sites through kinetic analyses are presented along with Oatp1c1 inhibition data mediated by multiple sterol glucuronides. Chapter 3 examines Oatp1c1 structure-function, using T4 as the model substrate. Topology and 3-D Oatp1c1 structural models are presented as well as kinetic characterization and subcellular expression of various Oatp1c1 mutants of conserved amino acids. Chapter 4 presents the identification of novel inhibitors of Oatp1c1-mediated T4 transport, including the fenamate class of NSAIDs. In addition, modeling in the form on electrostatic potential maps and structural overlays are presented to determine common chemical characteristics required for Oatp1c1 interaction. Chapter 5 explores a pharmacophore analysis of competitive Oatp1c1 inhibitors identified in Chapter 2 and 4, in addition to known Oatp1c1 substrates. A general pharmacophore model for

Oatp1c1 substrate recognition is presented based on this analysis. Finally, Chapter 6 outlines my universal conclusions generated from combined chapters 2-5. Comprehensive discussion of my Oatp1c1 data is presented within the framework of the BBB, metabolism, and drug targeting. Future directions are also presented for the investigation of Oatps at the BBB and beyond.

Chapter 2

The blood-brain barrier thyroxine transporter Oatp1c1 displays atypical transport kinetics

Daniel E. Westholm, David R. Salo, Kevin J. Viken, Jon N. Rumbley, Grant W. Anderson

The entirety of this chapter has been accepted for publication in *Endocrinology*.

Abstract

Organic anion transporting polypeptide 1c1 (Oatp1c1) is a high affinity thyroxine transporter expressed in brain barrier cells. Oatp1c1 transports a variety of additional ligands including the conjugated sterol estradiol 17β-glucuronide ($E_2$17βG). Intriguingly, published data suggest that $E_2$17βG inhibition of Oatp1c1-mediated thyroxine transport exhibits characteristics suggestive of atypical transport kinetics. To determine whether Oatp1c1 exhibits atypical transport kinetics we first performed detailed thyroxine and $E_2$17βG uptake assays using Oatp1c1 stably transfected HEK293 cells and a wide range of thyroxine and $E_2$17βG concentrations (100pM-300nM and 27nM-200μM, respectively). Eadie-Hofstee plots derived from these detailed T4 and $E_2$17βG uptake experiments display a biphasic profile consistent with atypical transport kinetics. These data along with thyroxine and $E_2$17βG cis-inhibition dose response measurements revealed shared high and low affinity Oatp1c1 binding sites for T4 and $E_2$17βG. Thyroxine and $E_2$17βG recognized these Oatp1c1 binding sites with opposite preferences. In addition, sterols glucuronidated in the 17 or 21 position, exhibited preferential substrate dependent inhibition of Oatp1c1 transport, inhibiting Oatp1c1-mediated $E_2$17βG transport more strongly than T4 transport. Together these data reveal that Oatp1c1-dependent substrate transport is a complex process involving substrate interaction with multiple binding sites and competition for binding with a variety of other substrates. A thorough understanding of atypical Oatp1c1 transport processes and substrate dependent inhibition will allow better prediction of endo- and xenobiotic interactions with the Oatp transporter.

Introduction

Atypical kinetics are defined as non-Michaelis-Menten type kinetics that often arise from the existence of multiple binding sites in the active site of an enzyme or transporter (Tracy, 2003). Multiple categories of atypical kinetics have been characterized including auto-activation, substrate dependent inhibition, and biphasic kinetics (Hutzler and Tracy, 2002) and have been extensively described for the cytochrome P450 drug metabolizing enzymes (Tracy, 2006; Tracy et al., 2002). In addition, atypical transport mechanisms have also been observed in several transporters including multi-drug active efflux pumps (P-glycoprotein, multi-drug resistance associated proteins, and breast cancer resistance protein), nucleoside transporters, and organic anion transporting polypeptides (Oatps, rodents and other species; OATPs humans) (Clark et al., 2006; Hagenbuch and Gui, 2008; Li et al., 2001; Martin et al., 2000; Noe et al., 2007; Sugiyama et al., 2002; Tamai et al., 2001).

Organic anion transporting polypeptides form a diverse and widely expressed superfamily of membrane bound bidirectional solute transporters (Hagenbuch and Meier, 2003; Hagenbuch and Meier, 2004; Westholm et al., 2008). Although some Oatps/OATPs transport a class of compounds (e.g. the prostaglandin transporter Oatp2A1), most Oatps/OATPs recognize a large range of amphipathic anions including hormones and their conjugates (thyroxine and sterol conjugates), bile salts (taurocholate), nutrients (folate), drugs (statins), and toxins (microcystin) (Westholm et al., 2008).

The transport of such structurally diverse compounds by individual Oatps suggests the presence of either a single promiscuous binding site or multiple substrate

binding sites. In support of a multiple binding site, atypical kinetic Oatp/OATP transport model, Noe et al. observed a biphasic uptake profile for OATP1B1 estrone-3-sulfate transport (Noe et al., 2007). These authors also noted the fibrate drug Gemfibrozil displayed substrate-dependent inhibition of OATP1B1, strongly inhibiting statin transport, while not affecting estrone 3-sulfate transport. In addition, Tamai et al. also reported biphasic uptake kinetics for OATP1B1 estrone-3-sulfate transport, suggesting the presence of both a high and low affinity estrone-3-sulfate binding site (Tamai et al., 2001).

Oatp1c1/OATP1C1 is a high affinity thyroxine transporter expressed predominantly in brain endothelial cells in both humans and rodents (Sugiyama et al., 2003). As a result, Oatp1c1 may play a significant role in regulating T4 flux into and out of the brain. *In vitro* data suggest that the rodent and human Oatp1c1 orthologs transport the same cohort of substrates including T4, however, the *in vivo* functional role of Oatp1c1 is still unclear. Interestingly, recent reports indicate polymorphisms in human OATP1C1 may be linked to fatigue and depression in hypothyroid patients (van der Deure et al., 2008).

Reported Oatp1c1 K_m measurements for T4 transport have varied widely (90-340 nM) (Pizzagalli et al., 2002; Sugiyama et al., 2003; Tohyama et al., 2004). In addition, K_i values for cis-inhibition studies with the two Oatp1c1 substrates T4 and $E_2$17βG have not equaled the K_m values for Oatp1c1-mediated T4 and $E_2$17βG transport (Chu et al., 2008; Tohyama et al., 2004). These discrepancies suggest the presence of multiple asymmetrical Oatp1c1 substrate binding sites. In the present study, we fully characterized Oatp1c1-dependent atypical T4 and $E_2$17βG transport kinetics. We performed detailed

Oatp1c1 T4 and $E_2$17βG uptake experiments using a wide range of substrate concentrations to fully assess substrate concentration-dependent contributions of the putative multiple substrate binding sites. In addition, we examined the nature of cis-inhibition of Oatp1c1 T4 and $E_2$17βG transport by multiple sterol glucuronides to assess substrate-dependent differences in Oatp1c1 transport inhibition. We found that Oatp1c1 T4 and $E_2$17βG transport exhibited biphasic uptake curves, suggesting the presence of multiple substrate binding sites. The two substrates did not cis-inhibit as strongly as the measured K_m values would predict, suggesting T4 and $E_2$17βG recognize Oatp1c1 binding sites differently. Sterol glucuronides, structurally similar to $E_2$17βG, inhibited Oatp1c1-mediated $E_2$17βG transport more strongly than T4 transport. Furthermore, sterol glucuronide inhibition of Oatp1c1-dependent transport revealed a stereospecific effect, with 17' and 21' sterol glucuronides inhibiting more strongly than 3' position glucuronides. Combined, these data indicate that Oatp1c1 carries multiple T4 and $E_2$17βG binding sites and exhibits biphasic transport kinetics.

Materials and Methods

Cloning of Oatp1c1 and stable transfection of Oatp1c1-pEF-DEST51 and empty vector pEF-DEST51 in HEK293 cells

Rat Oatp1c1 was cloned into pEF-DEST 51 expression vector (Invitrogen) as previously described (Westholm et al., 2009). HEK293 cell lines were created carrying either Oatp1c1-pEF-DEST51 or empty vector pEF-DEST51.

General Transport Assay

Cell-culture transport assays were carried out using a method published by Sugiyama et al (Sugiyama et al., 2003). $1.5x10^5$ cells/well were plated in four-well plates (Nunc; Rochester, NY) in standard culture medium. 24 h before the assay, media was changed and supplemented with 10mM sodium butyrate, and 10% stripped serum (T4 removed, prepared as previously described) (Westholm et al., 2009). To perform the assay, cells were washed and incubated with Krebs-Henseleit buffer (142 mM NaCl, 23.8 mM $NaHCO_3$, 12.5 mM HEPES, 5 mM glucose, 4.83 mM KCl, 1.53 mM $CaCl_2$, 1.2 mM $MgSO_4$, and 0.96 mM KH_2PO_4, pH 7.4). Uptake was commenced with the addition of 200 μl of Krebs-Henseleit containing 1nM ^{125}I-T4 (specific activity 1080-1320uCi μCi/μg, Perkin Elmer; Wellesley, MA) or 55nM ^{3}H-$E_2$17βG (specific activity 30-60Ci/mmol, Perkin Elmer; Waltham, MA) and ended at specific timepoints with three washes of Krebs-Henseleit without radio-labeled ligand. Cells were then lysed with 0.5% TritonX100 (Sigma; St. Louis, MO) and the associated radioactivity measured. Protein concentrations were determined with a BCA Protein Assay kit (Pierce). Uptake was calculated from the proportion of radioactivity associated with the cell lysate as compared to total radioactivity associated with the isotopic Krebs-Henseleit buffer and expressed in

units of pmol/min/mg protein. The uptake units were expressed as a cell-to-medium ratio of associated radioactivity derived from the following equality: counts in isotopic standard/volume of standard = counts in lysate sample/"volume" taken up by cells in lysate sample. The volume units were then converted to molar units by equating sample uptake volume to the standard volume which had a known T4 concentration. In most experiments, labeled substrates were kept at a fixed concentration (^{125}I-T4 = 1nM, ^{3}H-$E_2$17βG = 55nM) and supplemented with unlabeled substrate to achieve higher total substrate concentrations when needed. All unlabeled compounds used in transport assays were purchased from Sigma (St. Louis, MO).

Dose response, velocity vs. substrate, and Lineweaver-Burk assays and determination of kinetic parameters

Procedurally, time courses, dose response, velocity vs. substrate, and Lineweaver-Burk assays were carried out as described above. Dose response, uptake, and Eadie-Hofstee curves were fitted using non-linear regression with Graph Pad Prism Version 4 and 5 (San Diego, CA). Lineweaver-Burk plots were fitted using linear regression with Graph Pad Prism Version 4.

Time course

Uptake of 1nM ^{125}I-T4 or 55nM ^{3}H-$E_2$17βG at 37^{o}C was examined at a variety of time points. ^{125}I-T4 uptake was monitored from 30 sec-20 min and ^{3}H-$E_2$17βG from 30 sec-30 min. Background radioactivity associated with the zero minute was subtracted from all samples. Zero time points were performed as follows. Following equilibration in Krebs-Henseleit buffer, the buffer was aspirated from cells and 200 μl of isotopic media was overlaid on confluent HEK293 cells and immediately removed. Cells were then

rapidly washed with fresh Krebs-Henseleit buffer. The ^{125}I-T4 associated counts at zero min account for approximately 10% and 30% of uptake at 2 min in Oatp1c1-transfected cells for ^{125}I-T4 and ^{3}H-$E_2$17βG, respectively.

Kinetic measurements

In velocity vs. substrate T4 kinetic studies, uptake of 0.1-1nM ^{125}I-T4 supplemented with unlabeled T4 (total T4 concentration = 100pM-300nM), was monitored at 2 min time points. In the mirror assays examining ^{3}H-$E_2$17βG uptake, uptake of 27-55nM ^{3}H-$E_2$17βG alone and in the presence of various concentrations of unlabeled $E_2$17βG (total $E_2$17βG concentrations = 27nM-250μM), was examined at 2 min. In both experiments, empty vector contributions at equivalent time points and substrate concentrations were subtracted from Oatp1c1 uptake. Experiments were repeated 3 times. Velocity vs. substrate uptake curves were generated using the biphasic uptake equation: $v = ((V_{max1}*[S])+(Cl_{int2}*[S]^2))/(K_{m1}+[S])$, where S equals the substrate concentration, V_{max1} equals the maximum transport velocity of site 1, K_{m1} equals the K_m of site 1, and Cl_{int2} equals the slope of the line after site 1 saturation (slope=0.004198); multi-site Michaelis-Menten equation: $v= V_{max1}*[S]/[S]+K_{m1} + V_{max2}*[S]/[S]+K_{m2}$; or Michaelis-Menten equation: $v = V_{max}*[S]/[S]+K_m$ with Graph Pad Prism Version 4 and 5. Eadie-Hofstee plots were fitted with segmental linear regression using the equation: $Y_1 = intercept_1 + slope_1*X$; Y at $X_0 = slope1*X_0 + intercept_1$; Y_2 = Y at $X_0 + slope_2*(X - X_0)$ using Graph Pad Prism Version 5.

Dose response

In the multiple sterol glucuronide dose response experiments, uptake of 1 nM ^{125}I-T4 or 55nM ^{3}H-$E_2$17βG in the presence of various concentrations of inhibitors was measured

after 2 min of incubation. Empty vector uptake at equivalent time points was subtracted from Oatp1c1 uptake. Substrate-inhibitor cocktails were kept in the dark and mixed before overlay on the cells. Dose-response curves followed the "four-parametric logistic equation" of the form: Response=Bottom+(Top-Bottom)/[1+$10^{(LogIC_{50}-[Drug])}$].

Lineweaver-Burk

In Lineweaver-Burk assays, uptake of 1 nM ^{125}I-T4 supplemented with cold T4 to achieve the 5 concentrations of total T4 (27-540nM) ± 2 concentrations of inhibitor, was examined after 2 min incubations. Empty vector transfected cell uptake at equivalent T4 concentrations at zero time point was subtracted from Oatp1c1 transfected cell uptake. Linear regression of the form Y = mx+b was generated using Graph Pad Prism Version 4.

Substrate molecular modeling

Thyroxine, $E_2$17βG and $E_2$3βG structures were generated as described previously (Westholm et al., 2009). Structures were minimized with MOPAC using the PM3 semi-empirical method within the Sybyl 8.0 (Tripos, Inc.) software environment. Structural space was sampled as before using simulated annealing and dihedral angle energies of rotatable bonds were calculated with the dihedral driver algorithm in ChemBio3D Ultra 11.0 (CambridgeSoft Corp.) (Westholm et al., 2009). Multifit was used to generate the initial molecular overlays followed by manual adjustment; including bond rotation. Partial atomic point charges for electrostatic surface generation were calculated by Mulliken population analysis in MOPAC. The MOLCAD module in Sybyl 8.0 was used for the electrostatic surface calculation.

Results

Oatp1c1-dependent T4 and $E_2$17βG transport

Cells stably transfected with Oatp1c1-pEF-DEST 51 transported known Oatp1c1 substrates T4 and $E_2$17βG in a time dependent manner (Figure 1A, 1B). Uptake of both substrates initially increased linearly, with T4 uptake reaching equilibrium at 10 min and $E_2$17βG reaching equilibrium at 7.5 min.

Assessment of Oatp1c1 T4 and $E_2$17βG transport kinetics

In order to test the hypothesis that Oatp1c1 displays atypical kinetics, Oatp1c1-mediated T4 transport was tested with a wide range of substrate concentrations. Uptake was examined at 2 min time points using a total of 15 T4 concentrations (0.1-300 nM). Total T4 concentrations were achieved through supplementation of 1nM ^{125}I-T4 with various concentrations of unlabeled T4. Biphasic kinetics exhibit a characteristic two-phase Eadie-Hofstee profile. Eadie-Hofstee plot analysis of Oatp1c1-mediated T4 transport (Figure 2A) displayed such a biphasic profile suggestive of multiple Oatp1c1 T4 binding sites. The observed Oatp1c1 T4 transport kinetics were best fit (R^2=0.94) with a multi-site, non-asymptotic biphasic non-linear regression model ($v = ((V_{max1}*[S])+(Cl_{int2}*[S]^2))/(K_{m1}+[S])$, see methods; Figure 2B), in contrast to the traditional Michaelis-Menten fit (R^2=0.91). At low T4 concentrations, Oatp1c1 T4 transport initial velocities increased rapidly in a linear fashion (Figure 2B). As T4 concentrations continued to increase, initial velocities began to level off. Oatp1c1-mediated transport did not rapidly saturate however, suggesting the presence of a second low affinity T4 binding site(s). The high affinity site exhibited a transport K_{m1} of 10.3 nM (Table 1). As continued contributions from the saturated high affinity site obscure the

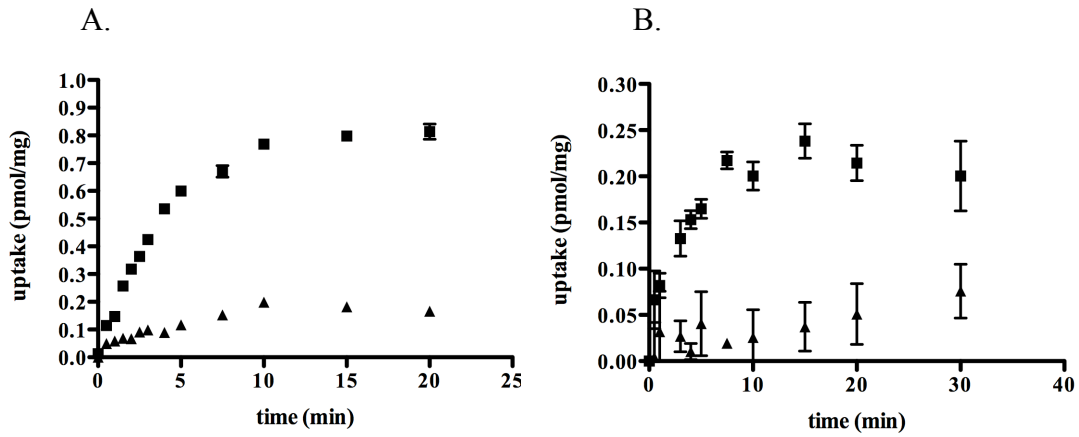

Figure 1. Thyroxine and $E_2$17βG are both transported in a time dependent manner by Oatp1c1 transfected HEK293 cells. Uptake of 1 nM ^{125}I-T4 (A) and 55 nM ^{3}H-$E_2$17βG (B) was examined at different timepoints in cells stably transfected with either Oatp1c1-pEF-DEST 51 (square) or empty pEF-DEST 51 vector (triangle) at 37^{o}C. Each point represents the mean uptake ± standard error (n=3).

sole contributions from the second site(s), a pure K_m for the low affinity site cannot be calculated. Therefore, an intrinsic clearance rate (Cl_{int2}) for the low affinity site(s) was calculated instead (Cl_{int2}=4.2 μl/min/mg protein; see Table 1). Since contributions of the saturated high affinity site remain constant, the Cl_{int2} is a measure of the clearance mediated solely by the low affinity site. However, a non-arbitrary segmental linear regression fit of the Eadie-Hofstee plot yielded two slopes resulting in calculated K_m's for each putative T4 binding site of 9.6 nM and 85.1 nM (Figure 2A inset and Table 1).

Likewise, Oatp1c1-mediated $E_2$17βG transport appeared to exhibit multi-site biphasic kinetics. The dynamic range of the Oatp1c1-mediated $E_2$17βG uptake was not as large as Oatp1c1 T4 uptake, but a sufficient number of data points permitted multiple methods of uptake analysis. Eadie-Hofstee plots of $E_2$17βG uptake displayed a distinct biphasic profile, also suggestive of multi-site Oatp1c1 $E_2$17βG binding (Figure 2C). Although goodness of fit for velocity vs. substrate plots was in the acceptable range with a single site Michaelis-Menten fit (R^2=0.93), Oatp1c1-mediated $E_2$17βG uptake was fit best with a multi-site biphasic non-linear regression model (Figure 2D R^2=0.95), yielding a K_{m1} of 22.0 μM and a C_{lint2} of 0.47 μl/min/mg protein. Segmental linear regression of the Eadie-Hofstee plot resulted in calculated K_m's of 1.3 μM and 175.7 μM. Since the K_{m1} values derived from the biphasic fit of the velocity vs. substrate plot and segmental linear regression of the Eadie-Hofstee plot were inconsistent, we refit the velocity vs. substrate data with a multi-site Michaelis Menten equation (data not shown, R^2=0.95). This resulted in a K_{m1} of 6.7 μM, suggesting the lower value K_{m1} measurements (1.3 μM and 6.7 μM) are more accurate.

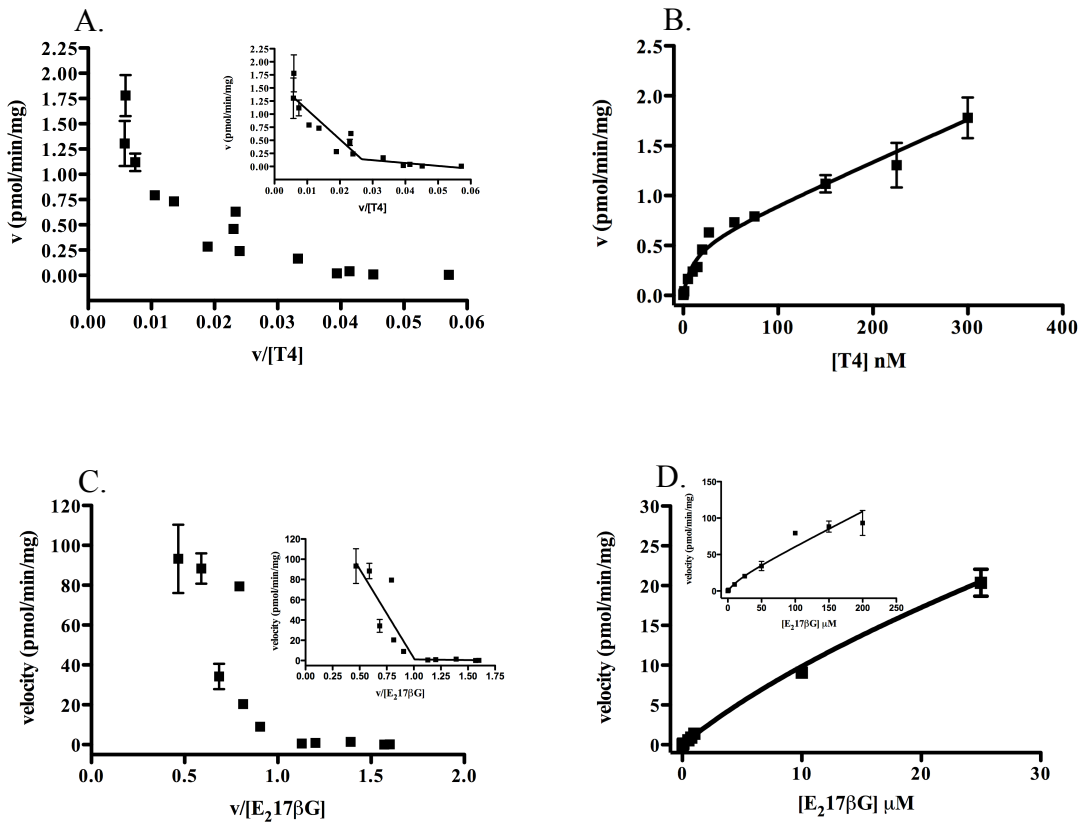

Figure 2. Oatp1c1-dependent T4 and $E_2$17βG transport exhibits atypical transport kinetics. Uptake of varying concentrations of T4 (A) and $E_2$17βG (C) was examined at 2 min at 37°C and plotted in an Eadie-Hofstee analysis. Inset of T4 and $E_2$17βG Eadie-Hofstee plots show segmental linear regression fit. Data was replotted as velocity vs. substrate concentration for both T4 (B) and $E_2$17βG (D and inset) transport. Larger Fig 2D plot shows lower range of $E_2$17βG concentrations tested, while Fig 2D inset shows full range of $E_2$17βG concentrations tested. Uptake curves were fitted using non-linear regression (Graph Pad Prism). Each point represents the mean Oatp1c1 uptake minus empty vector contributions at equivalent time points and substrate concentrations ± standard error (n=3).

	Biphasic		Eadie-Hofstee		Transport inhibition kinetics	
Substrate	K_{m1}	Cl_{int2}	K_{m1}	K_{m2}	T4 K_i	$E_2 17\beta$ G K_i
T4	10.3 nM	4.2 µl/min/mg	9.6 nM	85.1 nM	24 nM	81 µM
$E_2 17\beta$ G	22.0 µM	0.47 µl/min/mg	1.3 µM	175.7 µM	93 nM	5.7 µM

Table 1. Kinetic constants for Oatp1c1-mediated T4 and $E_2$17βG transport

Oatp1c1 T4 and $E_2$17βG self and reciprocal cis-inhibition

In order to detect whether T4 and $E_2$17βG interacted with the same binding sites, Oatp1c1 T4 and $E_2$17βG self and reciprocal cis-inhibition studies were performed. If both substrates recognized the same binding sites without preference, the K_i for unlabeled T4 and $E_2$17βG inhibition of ^{125}I-T4 transport should equal the K_i for unlabeled T4 and $E_2$17βG inhibition of ^{3}H-$E_2$17βG transport. Oatp1c1-mediated ^{125}I-T4 and ^{3}H-$E_2$17βG transport was examined in the presence of multiple concentrations of unlabeled T4 and $E_2$17βG. T4 self-inhibition yielded a K_i of 24nM (Figure 3A; Table 1). $E_2$17βG self-inhibition of Oatp1c1-mediated transport yielded a K_i of 5.7μM (Figure 3C; Table 1). In both cases, Oatp1c1-mediated T4 and $E_2$17βG self-inhibition revealed a K_i near the respective K_{m1} for Oatp1c1 T4 and $E_2$17βG transport (Table 1). $E_2$17βG inhibition of Oatp1c1 ^{125}I-T4 transport resulted in a K_i of 81μM (Figure 3B). T4 inhibition of Oatp1c1 ^{3}H-$E_2$17βG transport resulted in a K_i of 93nM (Figure 3D). The non-equivalence of self vs. reciprocal inhibition suggests T4 and $E_2$17βG recognize Oatp1c1 binding sites differently.

Sterol glucuronide inhibition of T4 and $E_2$17βG transport

In order to detect substrate-dependent inhibition and the universality of Oatp1c1-sterol glucuronide interactions, cis-inhibition of Oatp1c1-mediated ^{125}I-T4 and ^{3}H-$E_2$17βG transport by multiple glucuronidated sterols was tested. Sterols glucuronidated in the 17' and 21' positions inhibited Oatp1c1 T4 transport with an IC_{50} of approximately 100 μM, while sterols glucuronidated in the 3' position inhibited T4 transport with an IC_{50} of approximately 1000 μM (Figure 4A). In contrast, the 17' position sterol $E_3$17βG

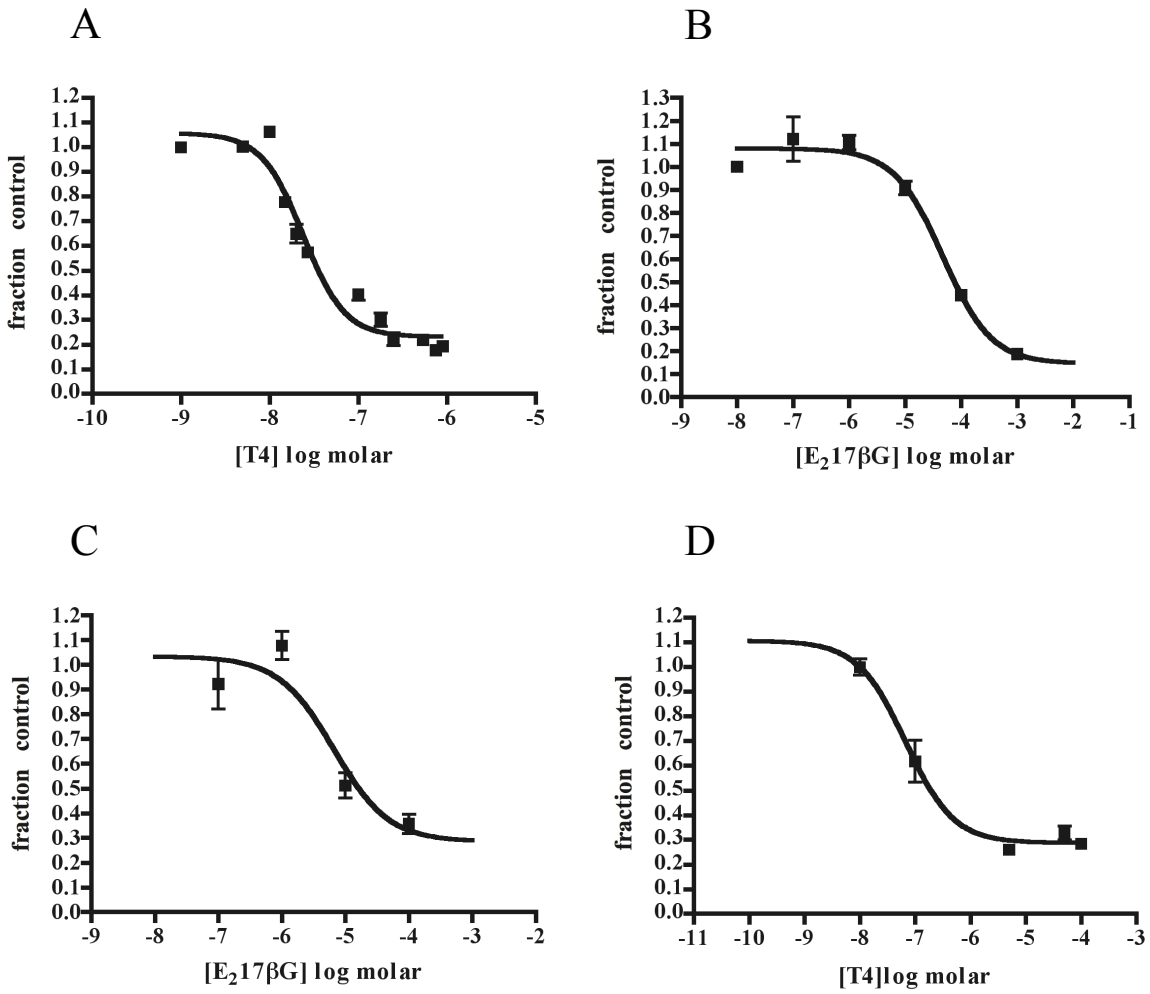

Figure 3. Oatp1c1-dependent ^{125}I-T4 and ^{3}H-$E_2$17βG transport is inhibited by both unlabeled T4 and $E_2$17βG. Uptake of 1 nM ^{125}I-T4 was examined in the presence of increasing concentrations of unlabeled T4 (A) and $E_2$17βG (B). Conversely, uptake of 55 nM ^{3}H-$E_2$17βG was examined in the presence of increasing concentrations of unlabeled $E_2$17βG (C) and T4 (D). Dose response curves and IC_{50}s were calculated for each competing substrate using non-linear regression (Graph Pad Prism). Each point represents the mean uptake ± standard error (n=3-6).

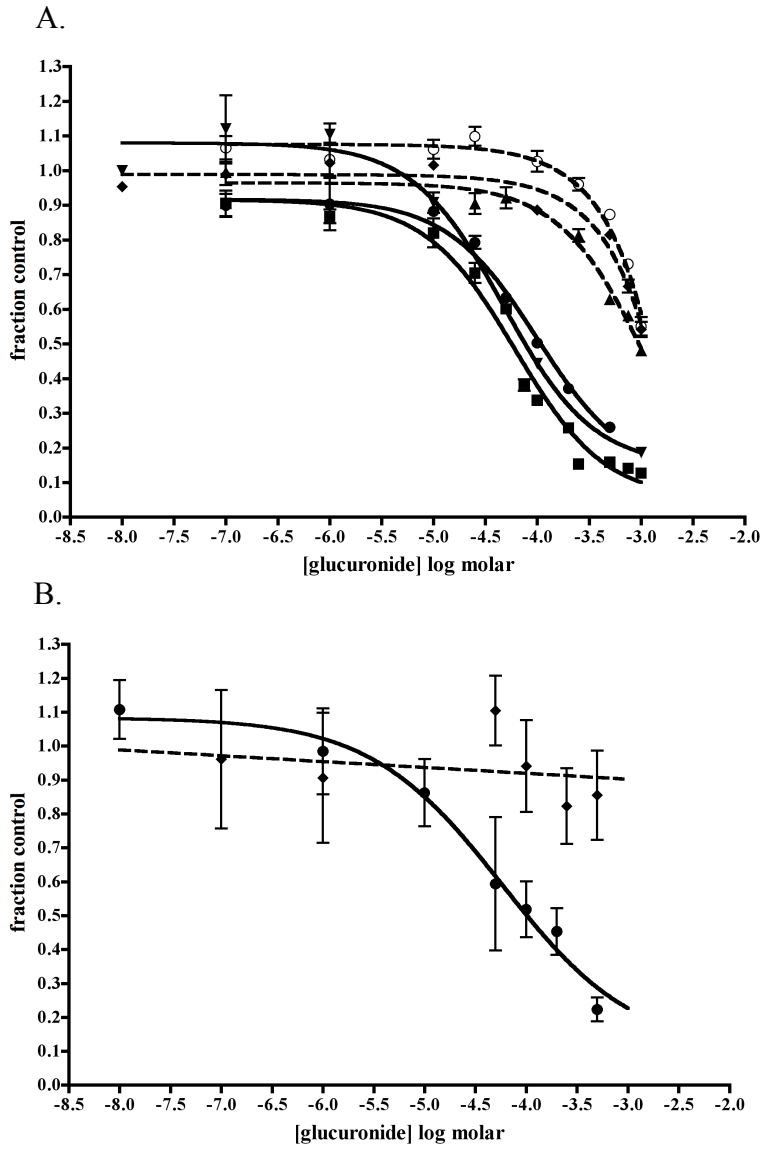

Figure 4. Multiple sterol glucuronides inhibit Oatp1c1-dependent T4 and $E_2$17βG transport. Uptake of 1 nM ^{125}I-T4 (A) and 55 nM ^{3}H-$E_2$17βG (B) was monitored in the presence of sterol glucuronides (closed inverted triangle $E_2$17βG, closed circle $E_3$17βG, closed square P21G, closed diamond $E_2$3βG, open circle $E_1$3βG, closed triangle DHEA3G; dashed lines correspond to sterols glucuronidated in the 3' position whereas solid lines represent sterols glucuronidated in the 17' or 21' positions. Each point represents the mean uptake ± standard error (n=3-6).

inhibited Oatp1c1 $E_2$17βG uptake with an IC_{50} of 22μM (Figure 4B), lower than the corresponding IC_{50} for Oatp1c1 T4 transport and closer to Oatp1c1 K_m for the structurally similar $E_2$17βG (Table 1). The 3' position glucuronide $E_2$3βG did not inhibit Oatp1c1 $E_2$17βG transport (Figure 4B).

Finally, Lineweaver-Burk plots were used to determine the type of inhibition the glucuronidated sterols exhibited on Oatp1c1-dependent transport. In Lineweaver-Burk plots, linear regressions of substrate uptake ± inhibitor that intersect on the y-axis indicate competitive inhibition (same V_{max} achieved), while linear regressions that intersect on the x-axis indicate non-competitive inhibition (same apparent K_m achieved). As seen in Figures 5A-C, sterols glucuronidated in the 17' and 21' positions inhibited Oatp1c1 T4 transport competitively (y-axis intersection), whereas in Figures 5D-E, sterols glucuronidated in the 3' position inhibited non-competitively (x-axis intersection). Together with the dose response data (Figure 4A), these data suggest a regioselectivity for Oatp1c1 glucuronidated sterol recognition.

The weak to non-inhibitory action of sterols glucuronidated in the 3' position for both T4 and $E_2$17βG Oatp1c1 transport (Figures 4A and B, and Figures 5D and E) suggest a strong steric effect on Oatp1c1 sterol glucuronide binding. Although chemically identical to some of the 17' sterol glucuronides tested (for example, $E_2$17βG and $E_2$3βG), the 3' glucuronides apparently interact very weakly with Oatp1c1 and suggest a important positional role for the glucuronide moiety in Oatp1c1 sterol glucuronide binding. Figure 6A shows an optimized overlay of thyroxine, $E_2$17βG and $E_2$3βG following conformational and dihedral sampling. Although multiple orientations

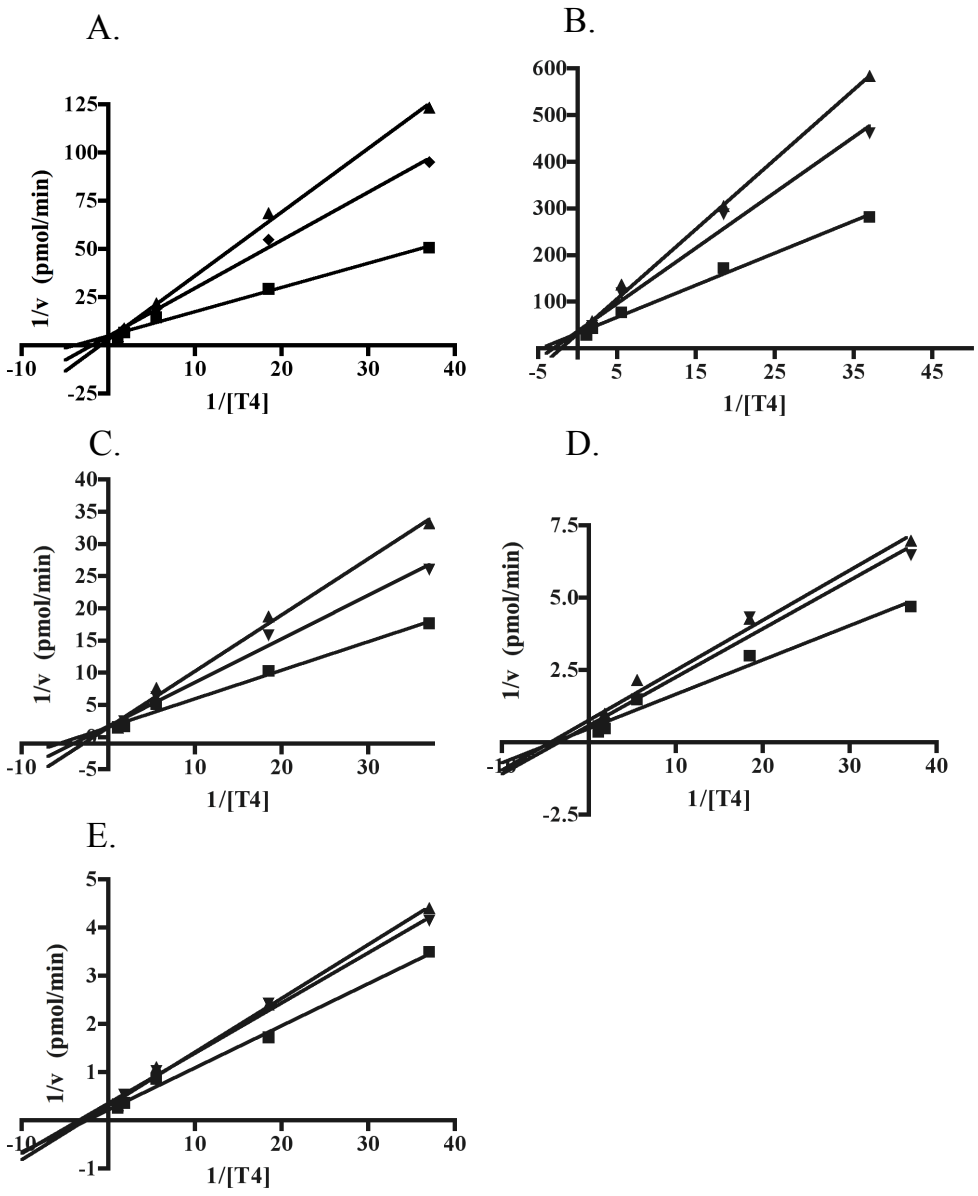

Figure 5. Sterols glucuronidated in the 17 and 21, but not the 3 position competitively inhibit Oatp1c1-mediated thyroxine transport. Uptake of varying concentrations of T4 was examined in the presence of $E_2$17βG (A), $E_3$17βG (B), P21G (C), DHEA3βG (D), and $E_1$3βG (E). Sterol glucuronide inhibitor concentrations were 50 and 100 μM (A-C) and 250 and 500 μM (D and E). Lineweaver-Burk plots were graphed as the reciprocal of velocity versus the reciprocal of T4 concentration. Each point represents the mean velocity (n=3).

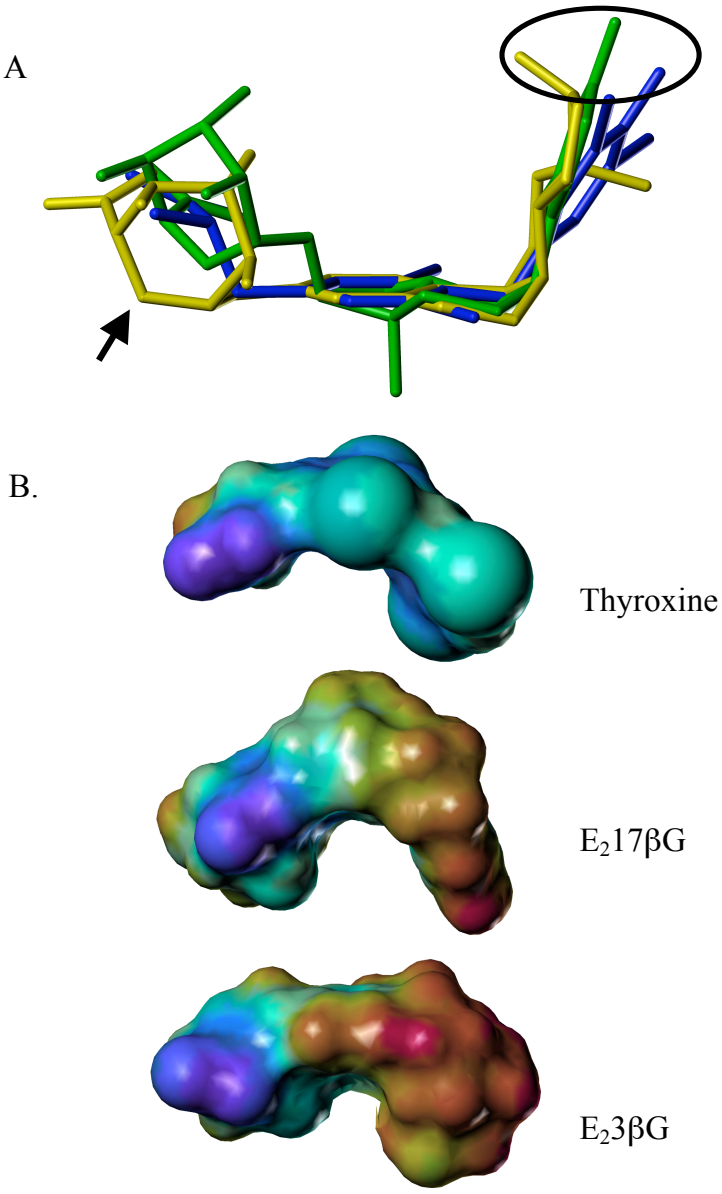

Figure 6. Structural superposition and electrostatic surface mapping of thyroxine, $E_2$17βG and $E_2$3βG. Structural overlays (A) of thyroxine (blue), $E_2$17βG (green) and $E_2$3βG (yellow) following conformation and dihedral angle sampling were calculated in Sybyl 8.0 using multifit with manual adjustment. The arrow shows one point of steric divergence in $E_2$3βG, circled is a hydroxyl group present in all three compounds. Connolly accessible electrostatic surface (B), calculated in Molcad, shows the location of significant partial positive (red) and partial negative (blue) atomic point charges contributing to binding characteristics.

of the glucuronides and peptide group of thyroxine are possible (left-hand domains of the structures), no suitable low energy structure of $E_2$3βG allows the requisite juxtaposition of its carboxyl group with that of the other two compounds. Further, when higher energy conformations are allowed in $E_2$3βG to orient the carboxyl group, significant steric differences remain. At the opposite end of the structures, planarity of the conjugated rings of thyroxine and $E_2$17βG may be significant as well as the orientation of the hydroxyl group, a potential hydrogen bond donor or acceptor. Similarities and differences are also shown in the Connolly electrostatic potential surfaces (Figure 6B). Overall shape and position of the carboxyl group (blue) are quite similar for thyroxine and $E_2$17βG. The presence of a hydrogen bond donor behind this group is also consistent with their ability to occupy similar binding sites.

Discussion

Together, our data reveal biphasic, atypical Oatp1c1-mediated T4 and $E_2$17βG transport kinetics. Such biphasic transport kinetics is characteristic of a transport model incorporating multiple substrate binding sites. In our assays, T4 and $E_2$17βG appeared to share, in a reciprocal manner, high and low affinity Oatp1c1 binding sites. Earlier studies characterizing Oatp1c1 T4 transport concluded uptake followed typical Michaelis-Menten kinetics or did not fully characterize the transport kinetics (Chu et al., 2008; Sugiyama et al., 2003; Tohyama et al., 2004). Importantly, the presence of atypical kinetics is easily missed if an insufficient number of data points are assessed. In addition, very low concentrations of substrate must be included in the assay or the high affinity site may be saturated and obscured at all other tested concentrations. In contrast, our study examined a wide range of T4 concentrations (100 pM to 300 nM) that fully spanned the substrate concentrations necessary to reveal both the high and low affinity binding sites (Figure 2B). Thus a complete uptake curve was defined that best fit a biphasic kinetics regression (see Methods). The Oatp1c1 T4 biphasic uptake curve reveals the presence of Oatp1c1 high and low affinity binding sites. In Figure 2B, the initial rapid linear uptake portion of the Oatp1c1 T4 uptake curve corresponds to T4 binding at the high affinity Oatp1c1 site. As T4 concentrations increase, T4 begins to occupy the low affinity site(s), causing the initial linear portion of the line to break but not show saturation. This biphasic pattern is also represented in the Oatp1c1-T4 Eadie-Hofstee plot (Figure 2A) where two distinct populations of data points are observed. Each population of data points contributes a unique trajectory and when combined, results in a two unique slopes (K_m's). The mode of Oatp1c1-mediated $E_2$17βG transport also appeared to exhibit

biphasic kinetic patterns similar to Oatp1c1 T4 transport. Velocity vs. [substrate] plots for Oatp1c1 $E_2$17βG transport fit both Michaelis-Menten and biphasic kinetics. However, Eadie-Hofstee analysis for Oatp1c1-mediated $E_2$17βG transport shows a clear biphasic profile (Figure 2C). Thus, it appears likely that $E_2$17βG also binds high and low affinity Oatp1c1 sites.

As T4 and $E_2$17βG each competitively inhibit the transport of the other, they likely share binding sites. However, the substrates do not appear to interact with the binding sites with the same hierarchical preference. Dose response experiments (Figure 3) show that the high affinity Oatp1c1 T4 and $E_2$17βG binding sites are not mutual. In a cis-inhibition kinetics assay using two substrates of the same transporter, the K_i should equal K_m. However, both T4 and $E_2$17βG inhibited each other's transport with a K_i higher than would be predicted based on the measured K_m (Table 1). Self inhibition assays, carried out as a positive control, showed that the K_i for T4 and $E_2$17βG Oatp1c1 self inhibition was near the K_m for both Oatp1c1-mediated T4 and $E_2$17βG transport (Figure 3 and Table 1). These results confirm data described by Tohyama et al. in mouse Oatp1c1 and Chu et al. in rat Oatp1c1 (Chu et al., 2008; Tohyama et al., 2004). Both groups reported K_i for $E_2$17βG inhibition of Oatp1c1 T4 transport higher than the K_m for Oatp1c1 $E_2$17βG transport and suggested the presence of asymmetric T4 and $E_2$17βG binding sites, but did not fully characterize the binding mode.

In order to assess the generality and nature of glucuronide conjugate interaction with Oatp1c1, multiple sterol glucuronides were tested in Oatp1c1 T4 and $E_2$17βG uptake assays. As seen in Figure 4A, sterols glucuronidated in the 17' and 21' positions ($E_2$17βG, $E_3$17βG and P21G) inhibited Oatp1c1 T4 uptake with a K_i of approximately

100 μM. Sterols glucuronidated in the 3' position only weakly inhibited Oatp1c1 T4 uptake with a K_i of approximately 1000 μM. Next, similar sterol glucuronide dose response experiments were performed to assess inhibition of Oatp1c1-mediated $E_2$17βG transport. In contrast to Oatp1c1-mediated T4 transport, the 17' position sterol glucuronide $E_3$17βG inhibited Oatp1c1 $E_2$17βG transport with a K_i of approximately 22 μM (Figure 4B); similar in magnitude to the $E_2$17βG K_m and self-inhibition K_i (Table 1). A sterol glucuronidated in the 3' position did not inhibit Oatp1c1 $E_2$17βG transport (Figure 4C).

During the sterol glucuronide dose response assays, T4 concentrations were held at 1 nM. Under these conditions, T4 occupies the high affinity Oatp1c1 site. As $E_3$17βG and P21G inhibition of Oatp1c1 T4 transport is nearly identical to $E_2$17βG inhibition of T4 transport (Figure 4A), these sterol glucuronides all appear to preferentially bind Oatp1c1 at same low affinity binding site. In addition, $E_3$17βG is a stronger inhibitor of Oatp1c1 $E_2$17βG transport than Oatp1c1 T4 transport in dose response assays (Figures 4A and 4B). As ^{3}H-$E_2$17βG concentrations were low (55nM) in the dose response assays causing $E_2$17βG to occupy its high affinity site, these data suggest that the 17' position sterol glucuronide $E_3$17βG recognizes the $E_2$17βG Oatp1c1 high affinity binding site more strongly than the T4 Oatp1c1 high affinity site.

Interestingly, sterols glucuronidated in the 17' and 21' position, including $E_2$17βG, inhibited Oatp1c1 T4 uptake in a competitive manner in diagnostic inhibition assays (Figures 5A-C) despite the weaker than predicted inhibition in the dose response for T4 uptake. Under assay conditions, T4 concentrations ranged from 27-540 nM and

sterol glucuronide concentrations ranged from 50-100 μM. At such concentrations, both high and low affinity T4 and $E_2$17βG Oatp1c1 binding sites are predicted to be occupied, with dynamic binding occurring at the low affinity site and saturation at the high affinity site. Since the inhibition under these conditions was competitive, T4 and $E_2$17βG may share the same low affinity Oatp1c1 binding sites. However, weak reciprocal inhibition by both substrates was observed in dose response assays where measured substrate concentrations drive binding in the high affinity site. Inhibition did not occur until high concentrations of inhibitor were present. In addition, the K_{m2} for T4 uptake was similar to the K_i for T4 inhibition of Eadie-Hofstee $E_2$17βG inhibition, suggesting at high concentrations T4 binds the high affinity $E_2$17βG binding site. Together, weak dose response inhibition combined with competitive inhibition between T4 and $E_2$17βG, suggest these substrates share the same binding sites, but the relative affinity to each site is reversed.

Binding preference may arise from steric constraints about the carboxyl group, significantly greater positive potential displayed on the opposite end of $E_2$17βG and rigidity of the closed rings of the sterol (Fig. 6). Differences are exacerbated in $E_2$3βG where similar carbonyl orientations are not energetically possible, a hydrogen bond donor behind the carboxyl does not occupy a similar space, more dramatic electrostatic differences appear, and lower steric compatibility appears on the opposite end.

Other groups studying Oatps have shown drastically different transporter affinities for structurally similar substrates (Hagenbuch and Gui, 2008). For example, Sugiyama et al. reported the presence of multiple binding sites in rat Oatp1a4 while studying the transport of structurally related substrates $E_2$17βG, taurocholate, and digoxin

(Sugiyama et al., 2002). They found that increasing concentrations of unlabeled $E_2$17βG had a stimulatory effect on Oatp1a4 ^{3}H-taurocholate uptake, but a weaker than expected (based on $E_2$17βG Oatp1a4 K_m) inhibitory effect on ^{3}H-digoxin transport. Thus, the authors concluded that these three structurally similar compounds interacted with Oatp1a4 at different sites (Sugiyama et al., 2002). This data supports our finding that compounds with highly similar structures can interact very differently with binding sites within the same transporter.

Although this is the first report of detailed analysis of atypical biphasic kinetics in Oatp1c1, Sugiyama et al. observed a classic biphasic Eadie Hofstee plot for Oatp1c1-mediated cerivastatin uptake (Sugiyama et al., 2003). In addition, as previously noted, Tohyama et al., observed weaker than predicted cis-inhibition between T4 and $E_2$17βG in mouse Oatp1c1 uptake assays and a similar finding was reported by Chu et al. in rat Oatp1c1 (Chu et al., 2008; Tohyama et al., 2004). In addition, as described in the introduction, OATP1B1 is known to display biphasic uptake profiles of estrone 3-sulfate. Other enzymes, known to accept a wide range of substrate structures, including various cytochrome P450's, exhibit multiple forms of atypical kinetics and are extensively reviewed elsewhere (Atkins, 2005; Houston and Kenworthy, 2000; Shou et al., 2001).

Our data does not allow us to speculate on the precise mechanism of the observed atypical Oatp1c1 kinetics. However, the mere presence of biphasic kinetics and multiple binding sites suggests that two or more substrates may occupy the Oatp1c1 pore simultaneously. For example, if only one T4 molecule could bind Oatp1c1 at a time, the high affinity site would almost always be bound instead of the low affinity site. Conversely, if two or more sites could be occupied simultaneously, at high concentrations

of T4 the high affinity site would become saturated exposing the low affinity site to substrate binding. Certain transporters, such as the serotonin transporter, adopt intricate multiple transmembrane binding sites after formation of homodimers (Kilic and Rudnick, 2000; Tate et al., 2001). Although no data yet exists to support multimeric structure in Oatps/OATPs, this possibility should be considered as knowledge of 3-dimensional Oatp/OATP structure advances. Recently, the x-ray structure was determined for the active efflux transporter, P-glycoprotein (P-gp) (Aller et al., 2009). P-gp x-ray structures determined in the presence of substrates revealed distinct binding sites dependent on interactions with hydrophobic and aromatic P-gp residues. This data supports the concept of distinct substrate binding regions within a transporter. Future studies will need to physically map binding sites through mutational analysis and photoaffinity labeling of Oatps.

The presence of multiple binding sites on transporters have potential clinical and physiological implications (Tracy, 2003). First, in the presence of multiple binding sites, drug-drug and drug-hormone interactions may be more or less likely to occur at therapeutic and physiological concentrations. In addition to endogenous roles, T4 is a commonly prescribed drug. A full understanding of the nature and potential of drug-hormone interactions is necessary to predict and prevent adverse interactions. This is especially true in the hypothyroid condition when the thyroid cannot respond to changing tissue T4 demands. It is not enough to assume that two substrates (drugs/hormones) of the same transporter will inhibit each other's transport if administered simultaneously, thus creating a drug-drug interaction. Cis-inhibition studies are needed to characterize the nature of the type of interaction. Free plasma T4 concentrations are approximately 12

pM. Thus, at physiological T4 concentrations, free T4 will only be bound to the high affinity site. Only under conditions where high concentrations of a high affinity site inhibitor are present, will T4 be forced into the low affinity Oatp1c1 binding site. Second, Oatp1c1 has been previously shown to play a role in the BBB transport of T4, a hormone initiating multiple developmental processes in brain (Anderson et al., 2003; Tohyama et al., 2004). Under physiological conditions T4 uptake into the brain would be driven through the high affinity T4 Oatp1c1 binding site due to low free T4 plasma concentrations. In addition, Oatp1c1 has a lower K_m for T4 transport than other BBB T4 transporters, such as Oatp1a4, monocarboxylate transporter 8 (Mct8), and large neutral amino acid transporter-1 (Lat-1). We would thus predict that *in vivo* T4 brain uptake would be primarily driven through Oatp1c1 and reveal a transport K_m in the low nM range. This transport hierarchy may be rodent specific however, as mutations in human MCT8 result in Allan-Herndon-Dudley Syndrome, while Mct8 knock-out mice lack a similar gross neurological phenotype (Dumitrescu et al., 2006; Schwartz et al., 2005). However, even in the rodent it is likely that Mct8 plays an important role in T3 transport across the BBB (Ceballos et al., 2009); the role of Mct8 in T4 transport across the BBB is less clear. Finally, our data suggests Oatp1c1 may also be involved in the transport and metabolism of multiple sterols. Estrogens including estradiol, estriol, and estrone are known to exert action in the prefrontal cortex and hippocampus, thalamus, and brainstem (Morrison et al., 2006). Through glucuronidation, estrogens are inactivated, made water soluble and targeted for transporters. Removal of glucuronidated estrogens from the brain through transport serves to modulate brain estrogen activity (Kusuhara and Sugiyama, 2005; Westholm et al., 2008). The dose response data in Figures 4A-C

suggest multiple 17' and 21' sterol glucuronides interact with and are possibly transported by Oatp1c1, thus further implicating this transporter in brain sterol metabolism, previously suggested by Sugiyama et al. (Sugiyama et al., 2001).

In summary, these data reveal that Oatp1c1 possesses multiple T4 and $E_2$17βG binding sites. Oatp1c1 contains high and low affinity T4 binding sites. Oatp1c1 also displays substrate dependent and regioselective inhibition by glucuronidated sterols. Further studies are needed to characterize the detailed kinetics of other Oatp1c1 substrates as well as carefully assess the presence of atypical kinetics in other thyroid hormone transporters.

Chapter 3

Structure-function analysis of organic anion transporting polypeptide 1c1

Daniel E. Westholm, Jacob D. Marold, Kevin J. Viken, Alicia M. Hartung, Grant W. Anderson, Jon N. Rumbley

Abstract

Organic anion transporting polypeptide 1c1 (Oatp1c1) is a high affinity thyroxine (T4) transporter expressed in brain barrier cells. In the present study we sought to identify Oatp1c1 amino acid residues critical for T4 transport. 2-dimesional topology was predicted and 3-dimensional Oatp1c1 structures were produced using SWISS-model with glycerol 3-phosphate, lactose permease, and the multidrug resistance protein EmrD Major Facilitator Superfamily transporters as templates. A total of nine amino acid mutations were generated using site-directed mutagenesis methods. The rationale used for generating the mutants was based on amino acid conservation across all rat Oatps, localization in putative transmembrane domains, and side chain character. Mutant constructs were transiently transfected into HEK293 cells and assessed for plasma membrane localization by confocal microscopy, and the capacity to transport the Oatp1c1 substrate ^{125}I-T4. Wild-type Oatp1c1 was expressed at the plasma membrane and displayed biphasic T4 transport kinetics suggestive of two substrate binding sites. Proteins mutated at polar and charged amino acids in transmembrane domain 2 (D85A, E89A, N92A) were not expressed at the plasma membrane and thus likely contribute to proper protein folding or trafficking. Proteins mutated at R601, P609, W277W278 and G399G409 were all expressed at the plasma membrane. The conservative W277F, W278F mutation retained transport activity similar to WT. However, the more severe W277A, W278A mutation abolished Oatp1c1 T4 transport. G399A,G409A and G399V, G409V mutants displayed near WT activity in an initial screen, but exhibited diminished T4 transport activity at high substrate concentrations. Finally, transmembrane domain 11 Arg601S and Pro609Ala mutants displayed partial T4 transport activity. These data

provide the experimental foundation for mapping Oatp1c1 substrate binding sites, and will contribute towards prediction of novel Oatp1c1 substrates.

Introduction

Organic anion transporting polypeptides (Oatps/OATPs, rodents/humans) are a superfamily of multi-specific organic anion membrane transporters (Hagenbuch and Meier, 2003; Mikkaichi et al., 2004b). Oatps/OATPs are expressed primarily in cell types that form biological barriers, including those in the liver bile duct, kidney, intestinal epithelia, the choroid plexus, and brain endothelia (Hagenbuch and Meier, 2004; Ito et al., 2005). Oatps/OATPs serve as bidirectional transporters for a broad panel of substrates including hormones, steroids, bile salts, toxins and drugs that exhibit a variety of chemical structures (Westholm et al., 2008). The high affinity thyroxine (T4) transporter Oatp1c1/OATP1C1 is expressed in brain barrier cells, including blood-brain barrier (BBB) endothelial cells and choroid plexus epithelial cells comprising the blood-cerebral spinal fluid barrier (BCSFB) (Roberts et al., 2008; Sugiyama et al., 2003; Tohyama et al., 2004). Although numerous Oatps/OATPs are known to transport T4, Oatp1c1/OATP1C1 transports T4 with an affinity more than 2 orders of magnitude greater than other Oatps/OATPs (Hagenbuch, 2007). This suggests that the substrate channel has been selectively-tuned to facilitate T4 transport. As such, Oatp1c1 provides an appealing target for understanding the precise Oatp protein structures that are involved in substrate transport.

Despite over a decade of research since the recognition of Oatps/OATPs as a distinct group of transporters, little is known about Oatp/OATP structure and what protein sequences and motifs are required for Oatp/OATP substrate recognition. Most work to date has focused on substrate identification for this diverse solute carrier family.

An iterative, incremental approach to the identification of important residues in Oatp transport has received more limited attention. Nevertheless, some data is beginning to be published regarding the Oatp/OATP structural characteristics. Meier-Abt et al performed comparative modeling between OATP1B3 and OATP2B1 and two members of the Major Facilitator Superfamily (MFS) of transport proteins (Meier-Abt et al., 2005). Based on similarities to the MFS transporters, the authors proposed a common rocker-switch mechanism with alternating inward and outward facing active site conformations (Abramson et al., 2003; Huang et al., 2003; Meier-Abt et al., 2005). In addition, some Oatps of the same family possess differential affinities for canonical Oatp/OATP substrates, yielding potentially useful structure-function data. For example OATP1B1 and OATP1B3 recognize estradiol-17β-D-glucuronide ($E_2$17βG) with similar affinities, but estrone 3-sulfate is preferentially accepted by OATP1B1. Miyagawa et al generated chimeric OATP1B1 constructs containing transmembrane domain 8 and 9 substitutions from OATP1B3. The authors found that OATP1B1 transmemebrane domain 8 was critical for $E_2$17βG and estrone 3-sulfate transport, but transmembrane domain 9 was interchangeable with that of OATP1B3 for $E_2$17βG transport, but not estrone 3-sulfate transport (Miyagawa et al., 2009). Also, Gui and Hagenbuch identified three amino acid residues in OATP1B3 transmembrane domain 10 (Y537, S545, and T550) important for transport of the peptide hormone cholecystokinin (Gui and Hagenbuch, 2008). A recent study by Leuthold et al showed that a highly conserved histidine residue in transmembrane domain 3 of multiple Oatps/OATPs was responsible for pH-gradient driven transport (Leuthold et al., 2009). Interestingly, OATP1C1, which lacks this conserved histidine, did not display pH-sensitive transport. Finally, a number of OATP

polymorphisms have been identified that effect substrate transport (Konig et al., 2006; Tirona and Kim, 2002).

Oatps/OATPs accept a variety of substrates with diverse chemical structure characteristics. Therefore, a single Oatp/OATP transporter must have a flexible substrate binding site to accept such varying chemical structures. Thus, it is not surprising that numerous Oatps/OATPs have displayed atypical kinetic properties, suggestive of the presence of multiple substrate binding sites (Hagenbuch and Gui, 2008). For example, two groups have reported multiple substrate binding sites in OATP1B1 for estrone-3-sulfate, resulting in biphasic transport kinetics for this substrate (Noe et al., 2007; Tamai et al., 2001). Iodothyronines are also known to interact with multiple binding sites within Oatps/OATPs. For example, OATP4C1 is a transporter of digoxin and 3,3',5 triiodothyronine (T3) and is expressed in the liver. However, digoxin and T3 do not cis-inhibit OATP4C1-mediated transport of each other, suggesting the two substrates recognize different binding sites (Mikkaichi et al., 2004a). In addition, there are reports of multiple binding sites in Oatp1c1. Both Tohyama et al. and Chu et al. reported weaker than predicted cis-inhibition for two Oatp1c1 substrates, T4 and β-estradiol 17-β-D-glucuronide ($E_2$17βG) (Chu et al., 2008; Tohyama et al., 2004). Moreover, data from our lab has shown Oatp1c1 displays biphasic transport kinetics with these two substrates (see Chapter 2). This transport characteristic must be an inherent property of Oatp/OATP structure. Through the identification and biochemical characterization of amino acids predicted to line the Oatp/OATP substrate channel, the individual amino acids that comprise the different substrate binding sites may also be defined.

An Oatp/OATP crystal structure has not yet been obtained, though most *in silico* work has agreed that Oatps/OATPs possess 12 transmembrane domains with cytoplasmic N and C termini (Hagenbuch and Gui, 2008). High resolution structures have been generated for three proteins containing 12 transmembrane domains in the MFS transporters including lactose permease, multidrug resistance protein EmrD, and glycerol 3-phosphate transporter (GlpT) (Abramson et al., 2003; Huang et al., 2003; Yin et al., 2006). In the present study, utilizing homology modeling to GlpT, lactose permease and EmrD, we generated a 3-dimensional rat Oatp1c1 structure. Assessing this structure in the context of topology maps and evolutionary conservation among rat Oatps, allowed us to identify a series of amino acids predicted to line the substrate channel and play a role in Oatp1c1 T4 transport. Through site-directed mutagenesis, we mutated 9 amino acids in Oatp1c1 putative transmembrane domains 2, 6, 8, and 11. Utilizing transient expression of mutated Oatp1c1 constructs in HEK293 cells, we identified several amino acids critical for Oatp1c1-mediated T4 transport. Conserved polar amino acids D85, E89, and N92 in transmembrane domain 2 are absolutely required for plasma membrane localization and subsequent T4 transport. In transmembrane domain 6, W277 and W278 could be conservatively replaced by phenylalanines, but mutation to alanines abolished activity. In addition, mutation of two fully conserved glycines in transmembrane domain 8, G399 and G409, resulted in little change of T4 transport at low concentrations, but showed decreased transport activity at higher T4 concentrations. Finally, conserved amino acids in transmembrane domain 11, R601 and P609, were required for full Oatp1c1 transport activity. For mutations that showed partial or full transport activity, a full kinetic analysis over a wide range of T4 concentrations was performed to assess for

contributions the targeted amino acids may have at the individual Oatp1c1 substrate binding sites. In addition, Eadie-Hofstee plots were generated to determine the type of kinetics displayed by the Oatp1c1 mutants.

Materials and Methods

Cloning Oatp1c1

Rat Oatp1c1 was cloned as previously described (see Chapter 4). Briefly, total RNA was extracted and cDNA transcribed from postnatal day 15 rat brain. PCR was then performed against Oatp1c1 using att-flanked primers. Resulting att-flanked Oatp1c1 PCR products were cloned into pDONR221 (Invitrogen) and subcloned into the expression vector pEF-DEST51 carrying a C-terminal V5 epitope tag (Invitrogen) and sequence verified.

Oatp1c1 mutagenesis

Site-directed mutagenesis was perfomed on Oatp1c1-pEF-DEST51 using a Stratagene Quik-Change XL Site-directed mutagenesis kit according to the manufacturer's instructions (Stratagene). Resulting mutagenized constructs were isolated using Qiagen Mini- and Midi-prep kits and sequence verified. Forward sequences for complementary primers generating specific Oatp1c1 amino acid changes (highlighted in bold underline) were as follows:

D85A 5'cccttcctctctggtgggaataatt**gcc**ggcagtttcgaaattgggaatctcc3'

E89A 5'gggaataattgatggtagtttc**gcg**atcgggaatctcctggtcataacattcg3'

N92A 5'gggaataattgatggtagtttcgaaattgga**gcg**ctcctggtcataacattcg3'

W277A,W278A 5'gatccccagtgggtcggggcc**gctgct**cttggttacctaatagca3'

W277F,W278F 5'tccccagtgggtcggggcc**tttttt**cttggttacctaatagcag3'

G399A, G409A 5'gtcatt**gct**ctcatcaatattcctgcaagtggcccttt**gct**atattc3'

G399V, G409A 5'gtcatt**ggt**ctcatcaatattcctgcagtggcccttt**gga**atattc3'

R601S 5'ggcatctacaccttagcagta**agt**gttcttgcaggaatcccagcc3'

P609A 5'gcagtaagagttcttgcaggaatcccagct**gcc**gtgtactttggtggtttaatcg3'

Cell culture and transfection

All cell-based studies were carried out in HEK293 cells. HEK293 cells were cultured at 37^{o}C in 5% CO2 with Minimal Essential Media supplemented to contain 10% FBS, 1 mM sodium pyruvate and non-essential amino acids. Mutant function and expression studies were assessed through transient transfection of HEK293 cells using Lipofectamine 2000 according to the manufacturer's instructions (Invitrogen; Carlsbad, CA). One day before transfection, 2x10^{5} cells/well were plated in a four-well plate (1.9 cm^{2}/well; Nunc; Rochester, NY) in media without antibiotics. The following day, DNA:Lipofectamine 2000 complexes were applied to HEK293 cells at a ratio of 1:3 (0.8 μg DNA:2.5μl Lipofectamine 2000). Media was replaced after cells were in contact with DNA:Lipofectamine 2000 complexes for 5 hours. Oatp1c1 function and expression was assessed 24 hours after transfection. In all studies, plates and coverslips were coated with rat-tail collagen (Sigma; St. Louis, MO and Gibco; Carlsbad, CA).

General Transport Assays

Cells were plated and transfected as described above. Five hours before the transport assay, culture medium was changed to MEM supplemented with 10% thyroid hormone stripped FBS and 10 mM sodium butyrate. Transport assays were performed as described previously (Westholm et al., 2009). Briefly, cells were washed and then preincubated with Krebs-Henseleit buffer (142 mM NaCl, 23.8 mM $NaHCO_3$, 12.5 mM HEPES, 5 mM glucose, 4.83 mM KCl, 1.53 mM $CaCl_2$, 1.2 mM $MgSO_4$, and 0.96 mM KH_2PO_4, pH 7.4) for 10 min in a CO_2 incubator. Following the preincubation, buffer was aspirated and cells were incubated with 1 nM ^{125}I-T4 (specific activity 1080-1320uCi

μCi/μg, Perkin Elmer; Wellesley, MA) suspended in Krebs-Henseleit buffer for various periods of time. Following incubation, cells were washed twice with fresh Krebs-Henseleit buffer and then lysed using 0.5% TritonX100. Radioactivity associated with the cell lysate was measured using a WIZARD^2 Automatic Gamma Counter (Perkin Elmer). Uptake was corrected for protein content which was assessed with a BCA assay (Pierce; Rockford IL). Specific assays in the form of time courses and kinetic measurements were performed and analyzed as previously described (Chapter 2). Non-linear regression and statistics were performed using Graph Pad Prism version 4.0 (Graph Pad Software; San Diego, CA) as described in Chapter 2.

Immunocytochemistry

Cells were plated on glass coverslips and transfected as described above. Immunocytochemistry was performed as previously described (Westholm et al., 2009). Briefly, transfected cells were fixed in cold 100% methanol for at least 30 min. Fixed cells were then permeabilized with 3 three washes with PBSA (PBS, 1% BSA, 0.1% TritonX100), and probed with primary anti-V5 antibodies and secondary rabbit anti-mouse-FITC antibodies (Jackson ImmunoResearch; West Grove, PA). Coverslips were then mounted on glass slides using Prolong Antifade Reagent (Invitrogen). Images were captured with a Nikon D-Eclipse laser scanning confocal unit attached to a Nikon TE2000-U inverted microscope using depth of field slices ranging from 30-60 μM (Nikon Instruments; Melville, NY). Images were converted to readable format using ImageJ software (http://rsbweb.nih.gov/ij/; National Institutes of Health; Bethesda, Maryland).

Generation of structural models

Rat Oatp sequence alignments

Sequence comparisons were performed between rat Oatp1c1 and all known rat Oatps. Rat Oatp sequences were derived from a BLAST search against the rat genome on NCBI using rat Oatp1c1 as query (http://blast.ncbi.nlm.nih.gov/Blast.cgi). In order to compile amino acid conservation data, a multiple sequence alignment was performed between rat Oatp1c1 and other rat Oatps using the PROMALS multiple sequence alignment server (http://prodata.swmed.edu/promals/promals.php). Amino acid conservation is indicated with respect to membrane topology in Figure 2.

Generating rat Oatp1c1 consensus membrane topology maps

Oatp1c1 transmembrane spanning domains were first predicted based on a consensus between eight predictive algorithm programs including DAS, BPROMPT, Split4.0, Memstat, HMMTOP2, HMM-TM, Phobius, and PolyPhobius. Multiple algorithms were used because each one has individual biases, thus combining predictions from all eight algorithms gives a more accurate membrane topology consensus. The final topology map was then created with TeXtopo (Beitz, 2000) using input from the eight predictive algorithms and sequence conservation information previously determined with PROMALS. Transmembrane predictions for rat Oatp1c1 were validated by sequence comparison to consensus topology predictions with human, chicken and zebrafish Oatp1c1 (data not shown). This was done by evaluating the coincidence of the transmembrane spans in a multiple sequence alignment between rat, human, chicken, and zebrafish Oatp1c1.

Alignments between Oatp1c1 and three Major Facilitator Superfamily transporters and generation of 3-dimensional Oatp1c1 structure

Before any Oatp1c1-specific modeling was done, structural alignments for the three MFS transporters (GlpT, lactose permease and EmrD) were performed using the SAlign feature of MODELLER (http://www.salilab.org/modeller/) in order to produce structural superpositions of the three transporters. In addition, a MFS sequence alignment was performed using PROMALS3D (http://prodata.swmed.edu/promals3d/promals3d.php). The PROMALS3D alignment was compared to the sequence alignment derived from the structural alignments of the three MFS transporters to evaluate the ability of PROMALS3D to align transmembrane domains of proteins with different sequences.

Using MODELLER, rat Oatp1c1 structure was built into the existing MFS structural alignment (see above) resulting in an initial rat Oatp1c1 model. This model had a number of polar amino acid residues facing the lipid bilayer, indicating a poorly predicted model. Thus, a second homology model was generated. To produce the second model, a rat Oatp1c1 sequence alignment to the three MFS transporters was produced using PROMALS3D. Rat Oatp1c1 sequences from 1-30, 136-187, and 451-551 were removed during the alignment as they contained very low homology and removal resulted in sequence of more similar length to the MFS transporters. Output from the PROMALS3D alignment of all four transporters was then submitted to MODELLER to generate a second rat Oatp1c1 homology model. This approach produced a 3-dimensional rat Oatp1c1 with few polar and no charged amino acids facing the lipid bilayer. Two poorly predicted transmembrane domains (8 and 12) in the second

homology model were adjusted with a PROMALS based alignment of rat, mouse, human Oatp1c1 and GlpT to remove gaps at these positions. Energy minimization and molecular dynamic simulations were performed to relieve strain within the rat Oatp1c1 model. This was accomplished by setting bond lengths to their canonical distances, correcting steric overlap, and relieving charge-charge repulsive forces. Final 3-dimensional figures were produced using Chimera (http://www.cgl.ucsf.edu/chimera/; Resource for Biocomputing, Visualization, and Informatics; University of California, SF).

Results

In the current study we sought to identify Oatp1c1 amino acids employed in substrate recognition and maintenance of structural integrity. Individual Oatp1c1 amino acids were targeted for mutagenesis based on conservation amongst all rat Oatps, localization within the putative transmembrane domains, orientation towards the substrate pore, and side chain character. Based on these characteristics, we hypothesized that D85, E89, N92, W277,W278, G399,G409, R601, and P609 played critical roles in Oatp1c1 structure and function. We hypothesized polar and charged amino acids D85, E89, N92 formed electrostatic surfaces and hydrogen bonding potentially important for substrate contact, W277,W278 localized at the interface of extracellular and transmembrane domains plays either a structural or functional role, G399,G409 provides a void volume allowing steric freedom during substrate binding or contributes to helical orientation for competent substrate binding, R601 provides a positively charged residue to attract anionic substrates, and P609 forms a helical constraint important in the structural organization of the Oatp1c1 pore.

Oatp1c1 homology models

The conservation, localization and orientation of the targeted Oatp1c1 amino acids were identified through computer modeling. Based on sequence alignment of all rat Oatps and use of eight predictive algorithms, topology modeling predicted 12 transmembrane domains within rat Oatp1c1 (Figs 1 and 2, respectively). Of the 716 amino acids in Oatp1c1, 25 were invariable (100% conservation amongst rat Oatps), 149 conserved (over 50% identity), and 13 were similar (similar position and side chain character). Of the 25 invariable amino acids identified, 7 were in the transmembrane

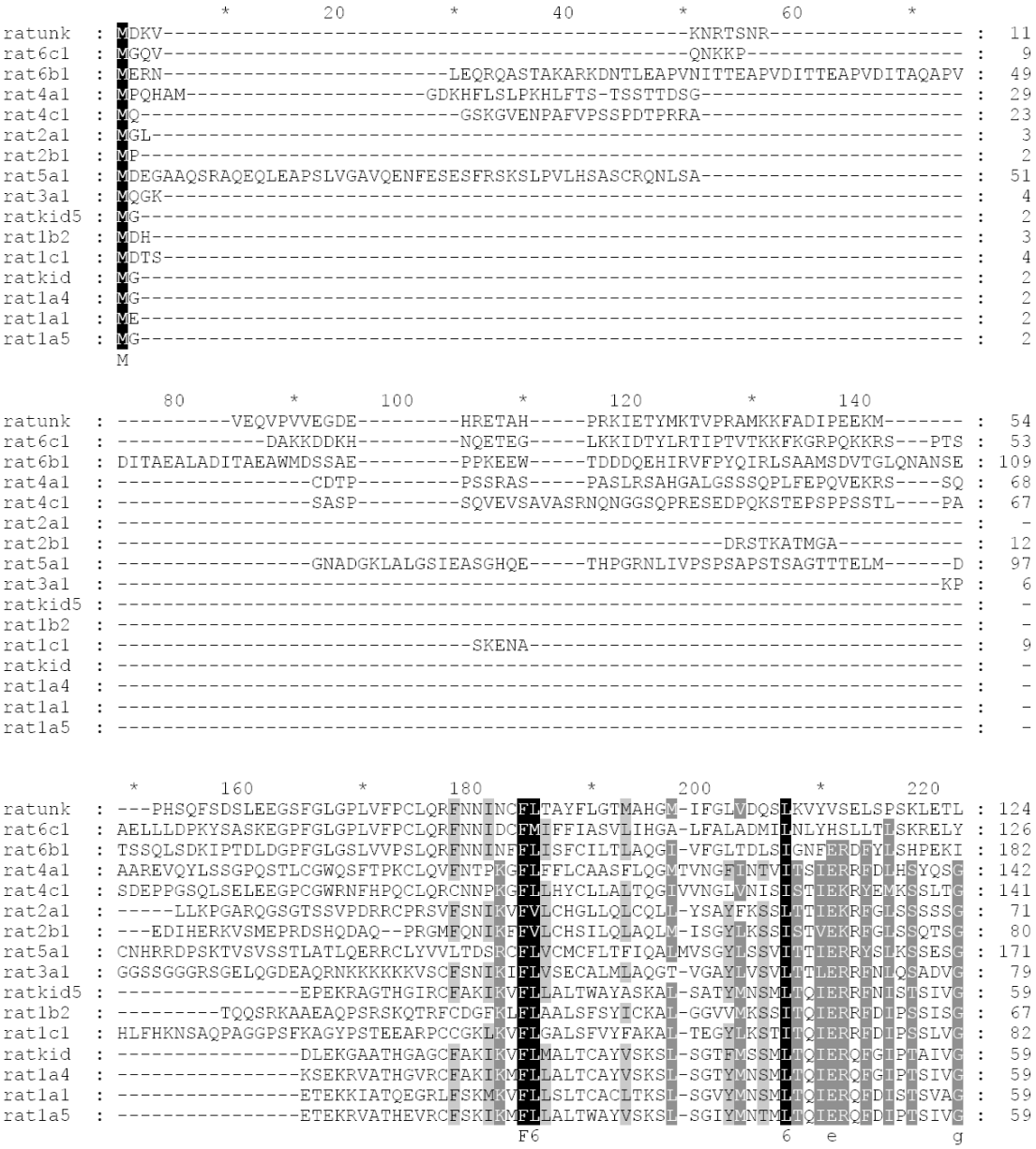

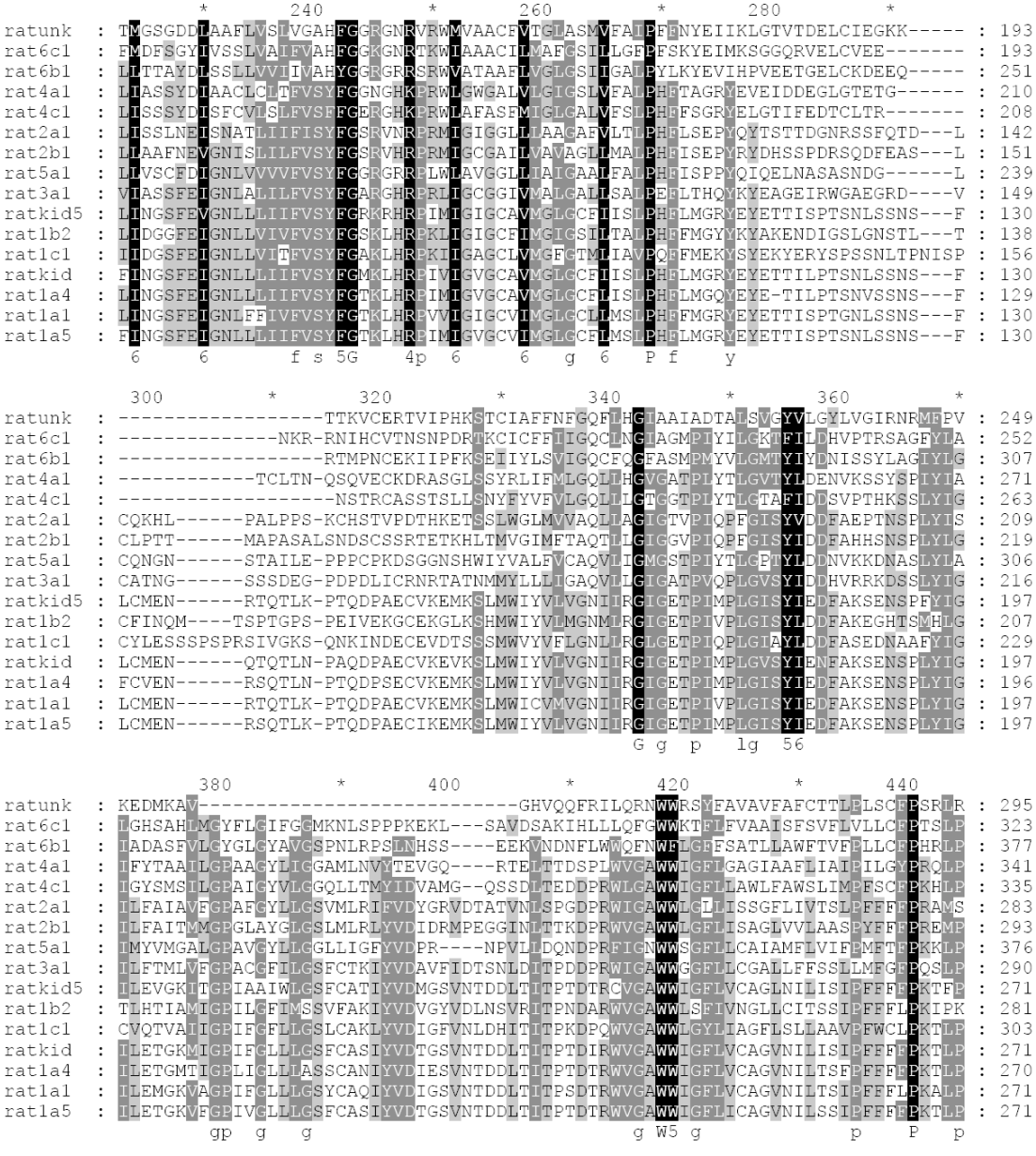

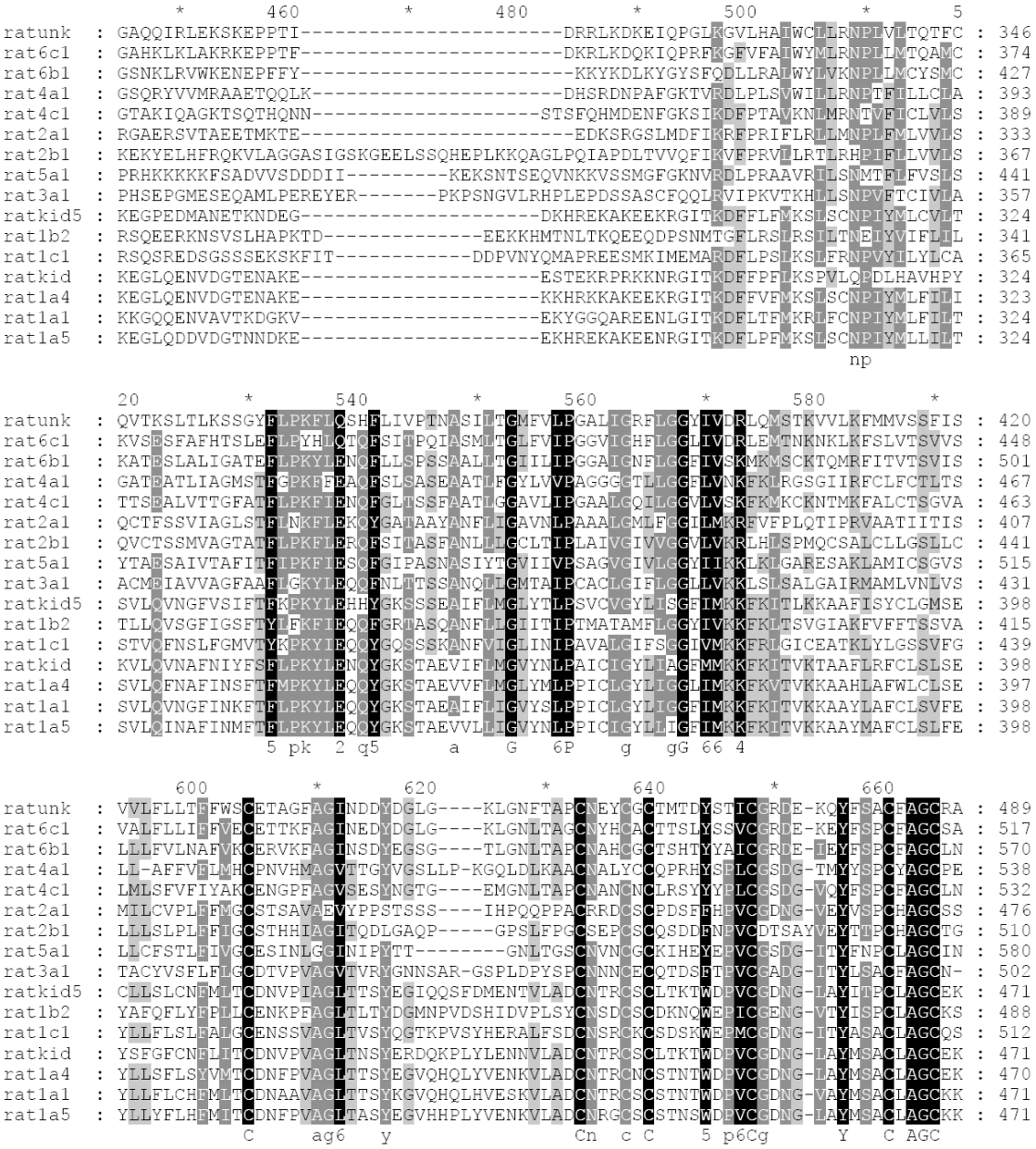

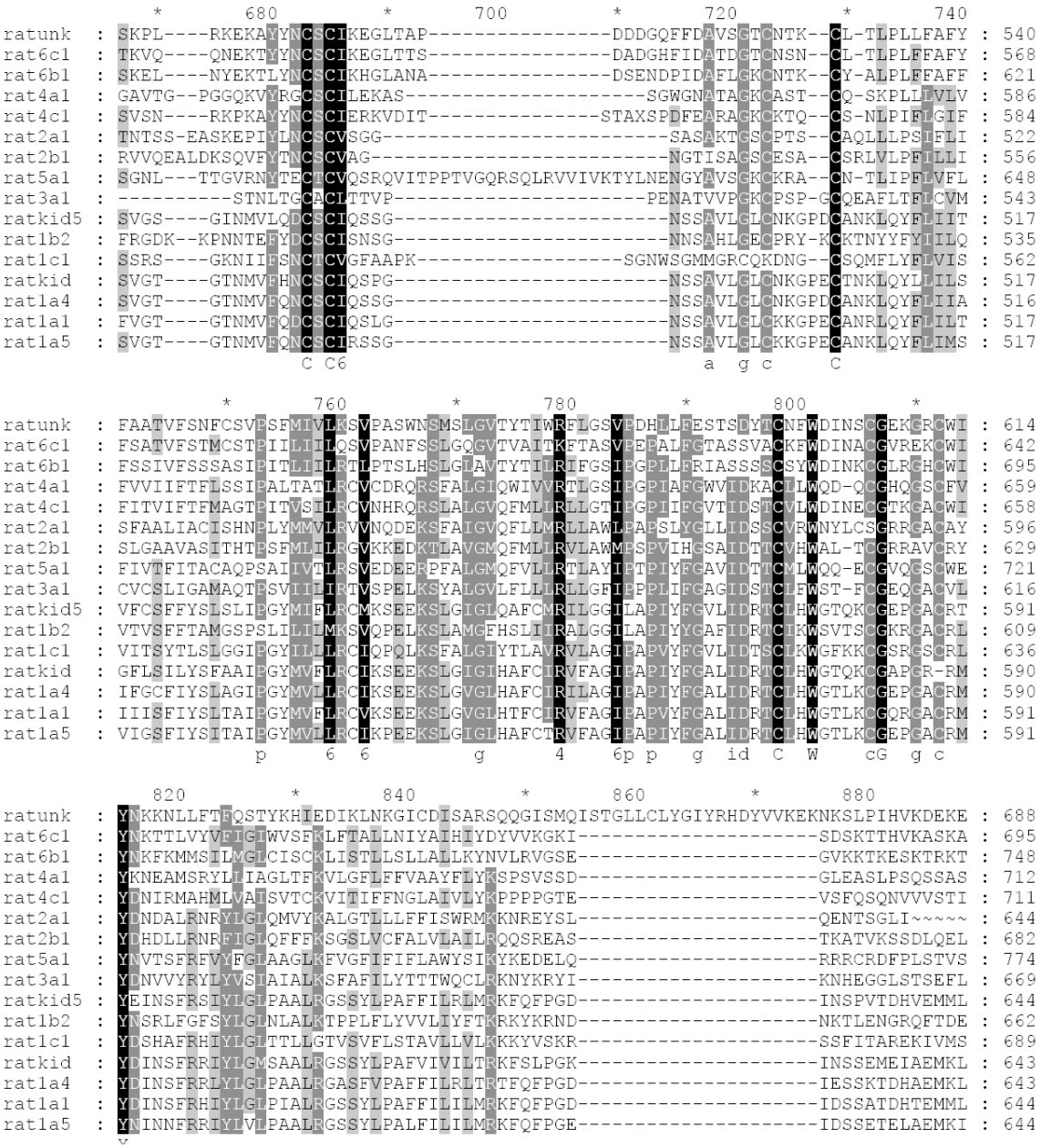

```
            *        900         *        920         *        940         *        960
ratunk  : -KEKK-----------------------SLISN~~~~~~~~~~~~~~~~~~~~~~~~~~~~~~~~~~~~~~~~~ : 697
rat6c1  : QKERRA~~~~~~~~~~~~~~~~~~~~~~~~~~~~~~~~~~~~~~~~~~~~~~~~~~~~~~~~~~~~~~~~~~~~ : 701
rat6b1  : ~~~~~~~~~~~~~~~~~~~~~~~~~~~~~~~~~~~~~~~~~~~~~~~~~~~~~~~~~~~~~~~~~~~~~~~~~~ :   -
rat4a1  : DSPTE----------------QLQSNV~~~~~~~~~~~~~~~~~~~~~~~~~~~~~~~~~~~~~~~~~~~~~~~ : 723
rat4c1  : TV-------------------EEDLN--KIENEG~~~~~~~~~~~~~~~~~~~~~~~~~~~~~~~~~~~~~~~~ : 724
rat2a1  : ~~~~~~~~~~~~~~~~~~~~~~~~~~~~~~~~~~~~~~~~~~~~~~~~~~~~~~~~~~~~~~~~~~~~~~~~~~ :   -
rat2b1  : ~~~~~~~~~~~~~~~~~~~~~~~~~~~~~~~~~~~~~~~~~~~~~~~~~~~~~~~~~~~~~~~~~~~~~~~~~~ :   -
rat5a1  : EHVG-------RPSKAEKYSRTTSCP--AFSTQGESHEETALQKGFPGTTLTYPGPFSEAESSSADRGLDESLD : 839
rat3a1  : ASTLTLDNLGRDPVP------AHQTHRTKFIYNLEDHE------------------------------WCENME : 707
ratkid5 : TEKES------EHTD------VHRSP--QVENDGE-------------------------------------LK : 667
rat1b2  : GNPDS------VNKN------GYYC---VPYDEQS-------------------------------------NE : 684
rat1c1  : SSVKK------ETCA-----ARDHGL--QPKYWPG-------------------------------------KE : 713
ratkid  : TEKES------QCTD------VHRNP--KFKNDGE-------------------------------------LK : 666
rat1a4  : TLKES------ECTE------VLRSK--VTED~~~~~~~~~~~~~~~~~~~~~~~~~~~~~~~~~~~~~~~~~~ : 661
rat1a1  : GEKES------EHTD------VHGSP--QVENDGE-------------------------------------LK : 667
rat1a5  : TVKKS------ECTD------VHGSP--QVENDGE-------------------------------------LK : 667


ratunk  : ~~~ :   -
rat6c1  : ~~~ :   -
rat6b1  : ~~~ :   -
rat4a1  : ~~~ :   -
rat4c1  : ~~~ :   -
rat2a1  : ~~~ :   -
rat2b1  : ~~~ :   -
rat5a1  : AAL : 842
rat3a1  : SVL : 710
ratkid5 : TKL : 670
rat1b2  : TPL : 687
rat1c1  : TRL : 716
ratkid  : TKL : 669
rat1a4  : ~~~ :   -
rat1a1  : TKL : 670
rat1a5  : TRL : 670
```

Figure 1. Rat Oatp polypeptide sequence comparison. Rat Oatp protein sequences were compiled using BLAST (NCBI) against rat Oatp1c1 and then aligned using PROMALS. In addition to Oatp1c1, retrieved rat Oatp sequences included Oatp1a1, 1a4, 1a5, 1a6, 1b2, 2a1, 2b1, 3a1, 4a1, 4c1, 5a1, 6b1, 6c1, 6d1 and an unassigned 1a subfamily member. Moving from light gray, to dark gray to black indicates increasing levels of sequence homology.

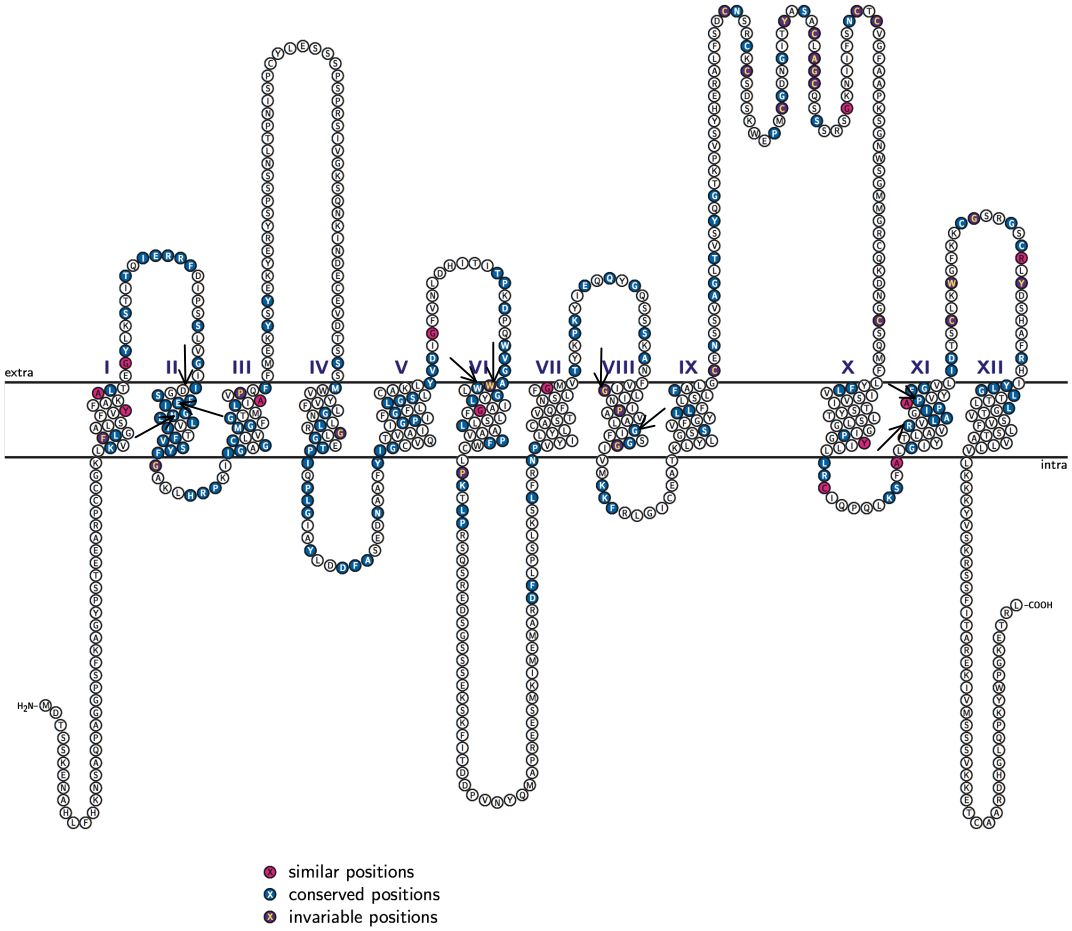

Figure 2. Rat Oatp1c1 membrane topology. Oatp1c1 consensus membrane topology as predicted by rat Oatp protein sequence alignment and the eight predictive algorithms DAS, BPROMPT, Split4.0, Memstat, HMMTOP2, HMM-TM, Phobius, and PolyPhobias. The 12 predicted transmembrane domains are located between the two solid lines and numbered with Roman numerals (I-XII). Amino acid conservation amongst all rat Oatps is mapped onto the Oatp1c1 topology. Red shaded residues denote similar positions (similar side chain character), blue shaded residues denote conserved positions (>50% identity), and purple shaded residues denote invariable positions (100% conservation).

domains, 16 in the extracellular domains, and 2 in the intracellular domains. Of the 149 conserved amino acids, 73 were in the transmembrane domains, 49 in the extracellular domains, and 27 in the intracellular domains. Finally, for the 13 similar amino acids, 7 were found in the transmembrane domains, 4 in the extracellular domains and 2 in the intracellular domains. Amino acids targeted for site-directed mutagenesis are identified in the topology map with arrows (Fig 2).

Sequence alignments between rat Oatp1c1 and MFS transporters (Fig 3) were used to generate 3-dimensional homology models (Fig 4A). As would be predicted for membrane proteins, polar and charged amino acids were oriented towards the substrate pore (Figure 4B). Helices 8 and 12 were poorly predicted resulting in large intra-helical gaps. Thus, helices 8 and 12 were aligned only with GlpT along with human, chicken, and zebrafish Oatp1c1 to remove gaps. Low identity in the extra- and intra-cellular domains did not allow modeling of the loops between transmembrane domains. Modeled rat Oatp1c1 3-dimensional structure aligned well with the known structures of GlpT, lactose permease and EmrD (Figure 4C).

Subcellular localization of Oatp1c1 mutants

As a first step in assessing the structural and functional consequences of mutations to the targeted Oatp1c1 amino acid residues, we used confocal microscopy to analyze the subcellular localization of Oatp1c1 mutants. HEK293 cells were transiently transfected, methanol fixed and probed with primary anti-V5 antibodies and FITC-conjugated secondary antibodies. When viewed laterally (x-y) using confocal microscopy, WT Oatp1c1 predominantly localized to the plasma membrane, with a small amount of intracellular expression (Fig 5A). Only background staining was detected in

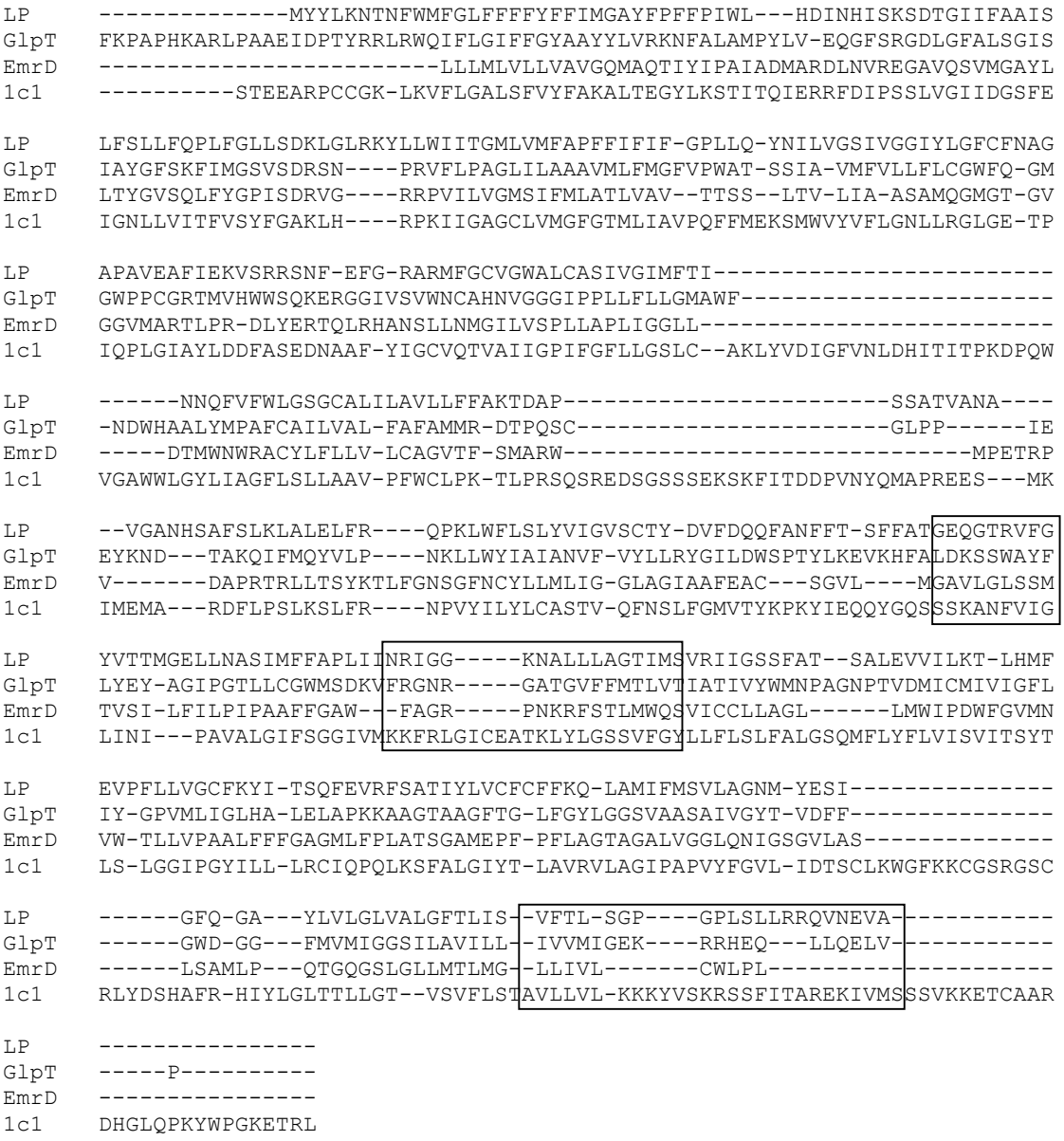

Figure 3. Alignment between rat Oatp1c1 and members of the Major Facilitator Superfamily of transporters. The polypeptide sequences of the crystallized MFS transporters were aligned with the rat Oatp1c1 polypeptide sequence. Areas with considerable alignment and no gaps were predicted to be transmembrane domains. The boxed regions represent helices 8 and 12 that were aligned with only Glpt and human, chicken and zebrafish Oatp1c1 in the 3-dimensional Oatp1c1 strucutre.

4A.

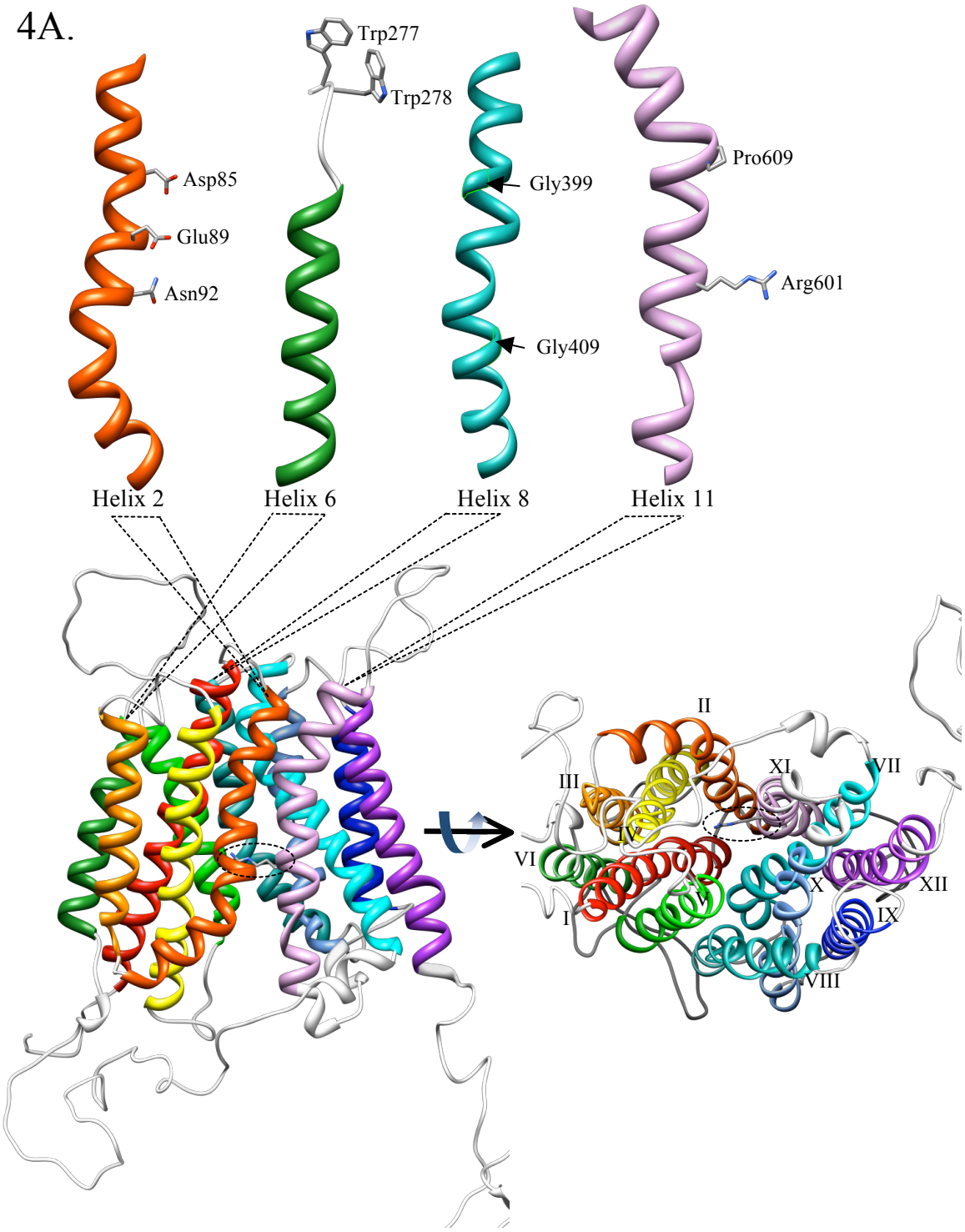
Trp277
Trp278
Asp85
Glu89
Asn92
Gly399
Gly409
Pro609
Arg601
Helix 2
Helix 6
Helix 8
Helix 11
II
III
XI
VII
IV
VI
X
XII
I
V
IX
VIII

4B.

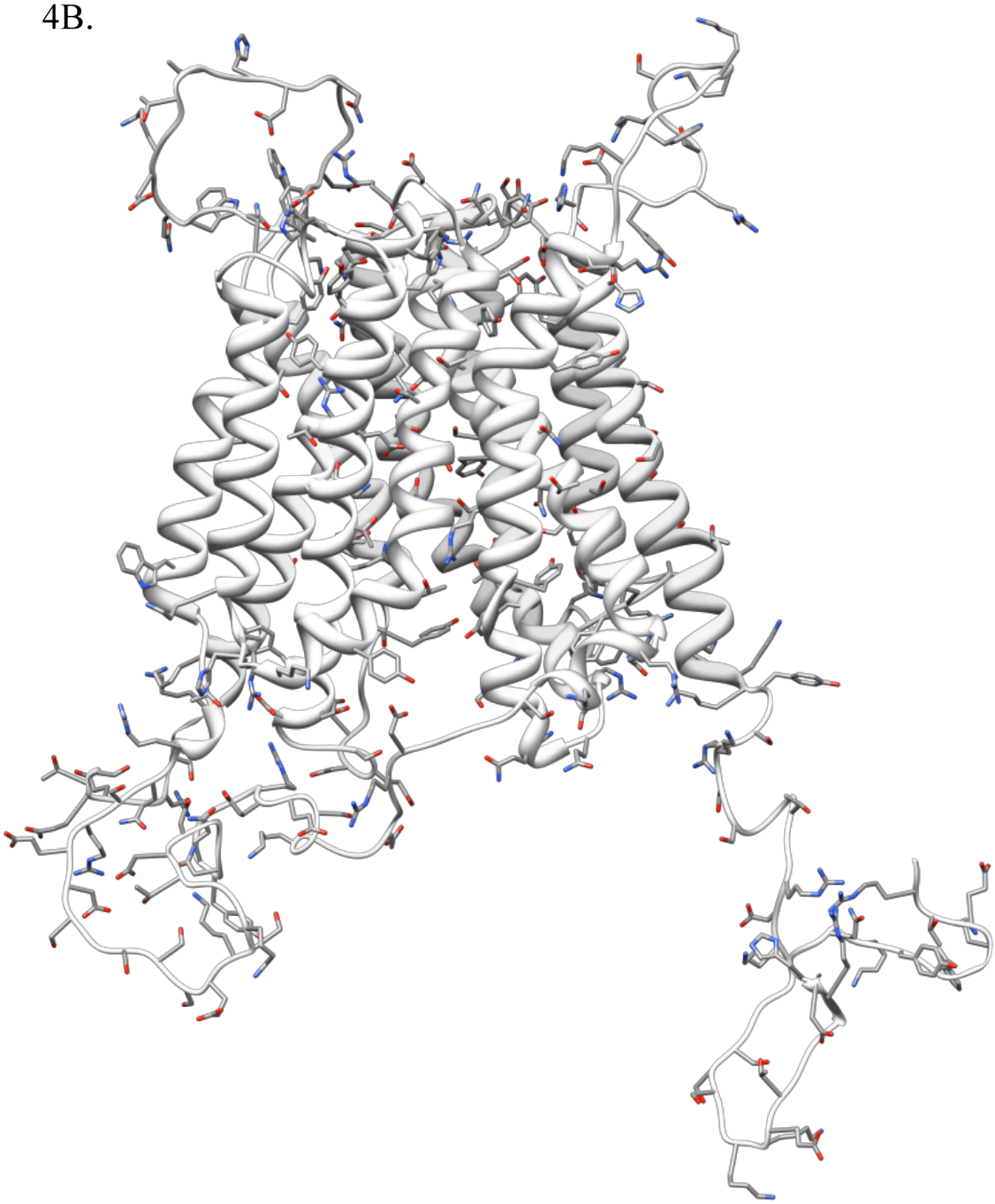

4C.

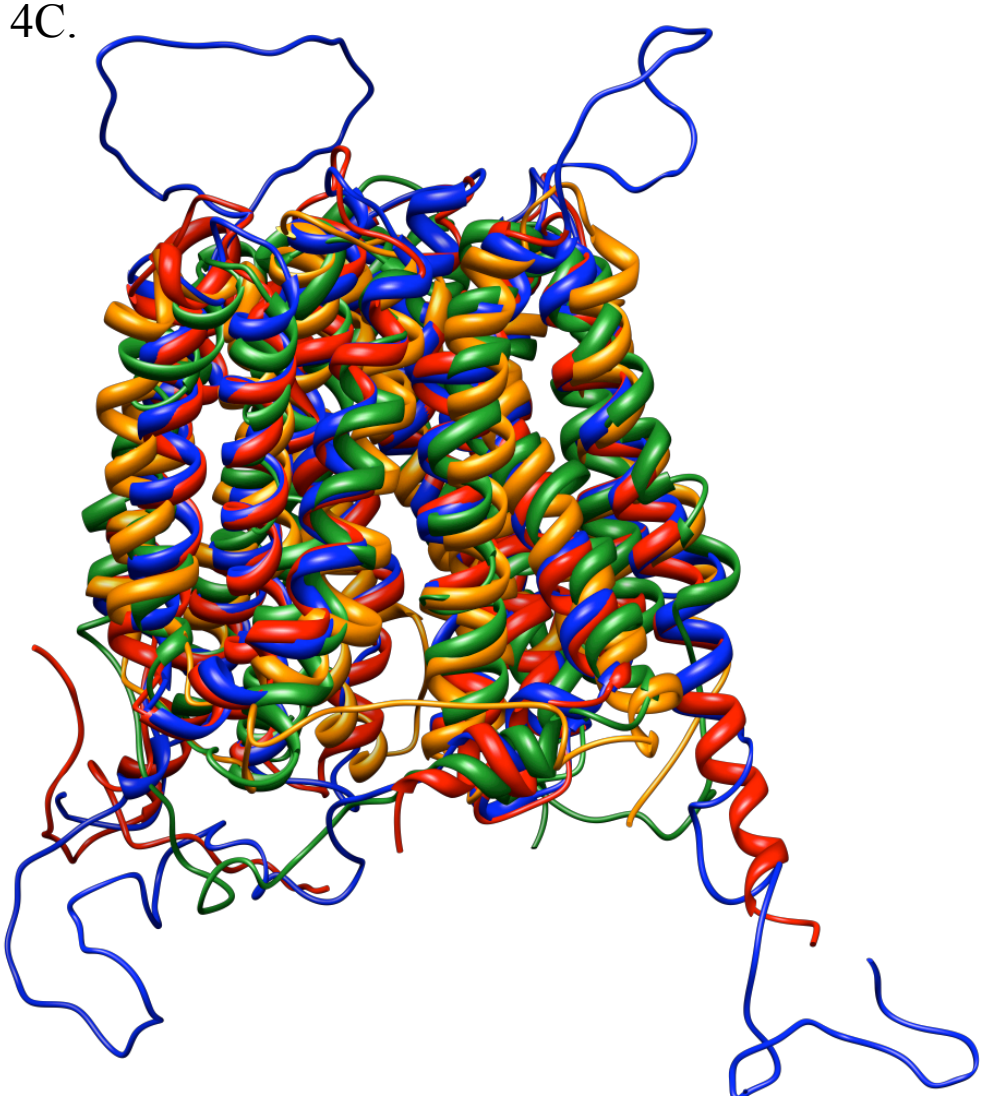

Figure 4. 3-dimensional homology model of Oatp1c1 structure. (A) Oatp1c1 side view with isolated helices with residues targeted for mutagenesis (left panel) and view looking down substrate channel from extracellular side of Oatp1c1 (right panel). The dashed oval in both left and right panels surrounds the exposed R601 residue. Colored coiled structures represent transmembrane alpha helices and gray lines represent extra- and intracellular portions of the Oatp1c1 protein. Transmembrane domains are numbered with Roman numerals (I-XII). (B) Side view with all polar amino acids exposed. Polar and charged amino acids are represented with gray stick figures. (C) Structural overlay of rat Oatp1c1 with 3 MFS proteins. GlpT is red, EmrD multidrug resistance transporter is orange, lactose permease is green, and rat Oatp1c1 is blue.

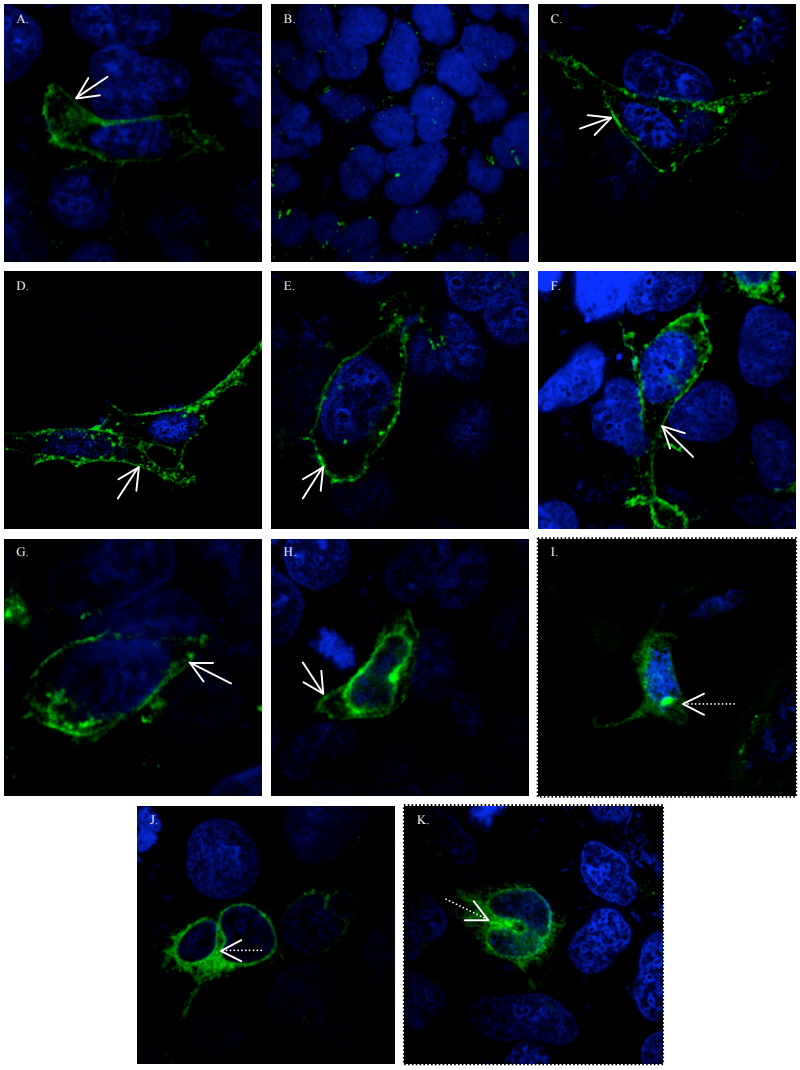

Figure 5. Subcellular localization of Oatp1c1 mutants using immunofluorescence. V5 primary and FITC-conjugated secondary antibodies were used to probe for expression of V5-tagged Oatp1c1 wild type and mutant constructs (A-K). WT Oatp1c1 (A) displayed plasma membrane staining (arrow), while empty pEF-DEST51 transfected cells showed only background staining (B). Oatp1c1 mutants W277A,W278A (C), W277F,W278F (D), G399A,G409A (E), G399V,G409V (F), R601S (G), displayed predominantly plasma membrane staining expression patterns as indicated by arrows. Oatp1c1 mutant P609A (H) displayed plasma membrane staining (arrows) with significant intracellular trapping (dashed arrows). Oatp1c1 mutants D85A (I), E89A (J), and N92A (K) displayed only intracellular staining (dashed arrows).

empty pEF-DEST51 vector transfected cells (Fig 5B). Oatp1c1 mutants including W277A,W278A, W277F,W278F, G399A,G409A, G399V,G409V and R601S also displayed the majority of staining at the plasma membrane (Figs 5C-G). P609A also displayed plasma membrane localization, however, a significant portion of the expressed protein was trapped within the cell in perinuclear regions (Fig 5H). Mutations of the polar conserved amino acids in transmembrane domain 2, including D85A, E89A and N92A showed no plasma membrane staining, with all observed expression occurring in peri-nuclear regions and punctate cytoplasmic deposits suggestive of Oatp1c1 trapping within the endoplasmic reticulum (ER) (Figs 5I-K).

Screen for mutant Oatp1c1 T4 transport activity

As a next step in the characterization of Oatp1c1 mutations, constructs were screened for T4 transport activity in an *in vitro* uptake assay. Cells were transiently transfected as in the immunofluorescence experiments, then assessed for uptake of 1nM ^{125}I-T4 at 10 min incubation periods at 37^{o}C (Fig 6). As expected, mutations in transmembrane domain 2 that resulted in intracellular trapping including D85A, E89A and N92A, showed no transport activity above empty vector transfected cells. The conservative W277F,W278F mutation in transmembrane 5 retained WT T4 transport activity, but the less conserved W277A,W278A mutation reduced T4 uptake to empty vector levels. In transmembrane domain 8, G399A,G409A and G399V,G409V mutants displayed near WT Oatp1c1 activity at 81% and 77% of control, respectively. Transmembrane domain 11 R601S and P609A resulted in attenuated T4 transport compared to WT Oatp1c1, however, transport was still significantly greater than empty

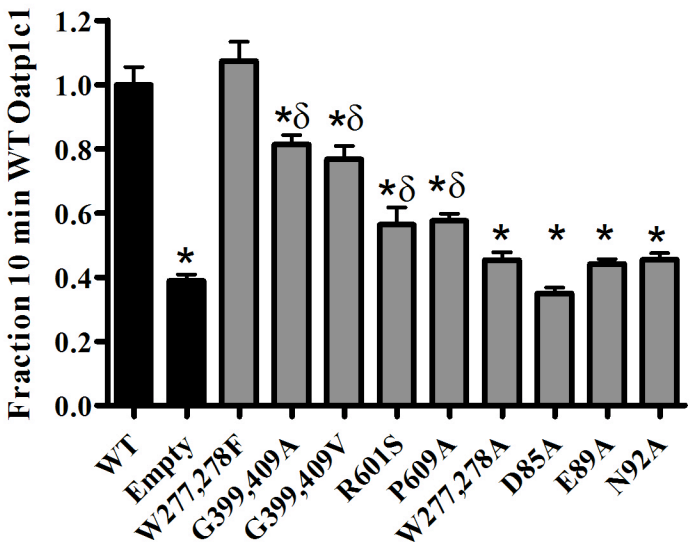

Figure 6. Screen for mutant Oatp1c1 T4 transport. Uptake of 1 nM ^{125}I-T4 was examined at 10 min timepoints in cells transiently transfected with WT Oatp1c1, empty vector pEF-DEST 51, and W277A,W278A, W277F,W278F, G399A,G409A, G399V,G409V, R601S, P609A, D85A, E89A, N92A Oatp1c1 mutants. Data is presented as fraction of WT Oatp1c1 ^{125}I-T4 uptake at 10 min at 37^{o}C. Asterisk (*) denotes statistical difference ($p<0.05$) compared to WT uptake as determined by ANOVA with a Bonferroni post hoc test (Graph Pad Prism). Delta (δ) denotes statistical difference ($p<0.05$) compared to empty vector uptake as determined by ANOVA with a Bonferroni post hoc test (Graph Pad Prism). Each point represents the mean uptake ± standard error (n=3).

vector uptake. At 10 min, R601S uptake was 56% of WT control, while P609A was 58% of WT control.

Kinetic Characterization of Oatp1c1 mutants

The four mutants that displayed no T4 transport activity above empty vector transfected cells, including D85A, E89A, N92A, and W277A,W278A were not further characterized. The kinetic characteristics of the remaining mutants were assessed with detailed T4 uptake time course and velocity vs. substrate concentration assays.

WT Oatp1c1 transiently transfected into HEK293 cells resulted in time dependent accumulation of ^{125}I-T4 at 37^{o}C. Uptake of 1nM ^{125}I-T4 increased linearly for the first 7.5 min, and remained at equilibrium thereafter (Fig 7A). Kinetic parameters were assessed at 4 min time points over a range of T4 concentrations (0.1-400nM). Total T4 concentrations were achieved using 1 nM ^{125}I-T4 either diluted or supplemented with increasing concentrations of cold T4. Similar to observations in Oatp1c1 stably transfected HEK293 cells (see Chapter 2), HEK293 cells transiently transfected with WT Oatp1c1 demonstrated multi-site, biphasic transport kinetics (Fig 7B). Such biphasic transport suggests the presence of high and low affinity binding sites. Uptake was best fit with a biphasic non-linear regression equation (R^2=0.98) resulting in a high affinity binding site K_{m1} of 2.0 nM. In support of biphasic Oatp1c1 T4 transport, when data from the WT velocity vs. substrate graph was replotted as an Eadie-Hofstee plot, a two phase profile resulted (Fig 7C).

W277F,W278F Oatp1c1 transported 1nM ^{125}I-T4 with a magnitude and time dependency similar to WT. Uptake was linear until approximately 7.5 min, then remained at equilibrium at subsequent time points (Fig 7D). The W277F,W278F amino

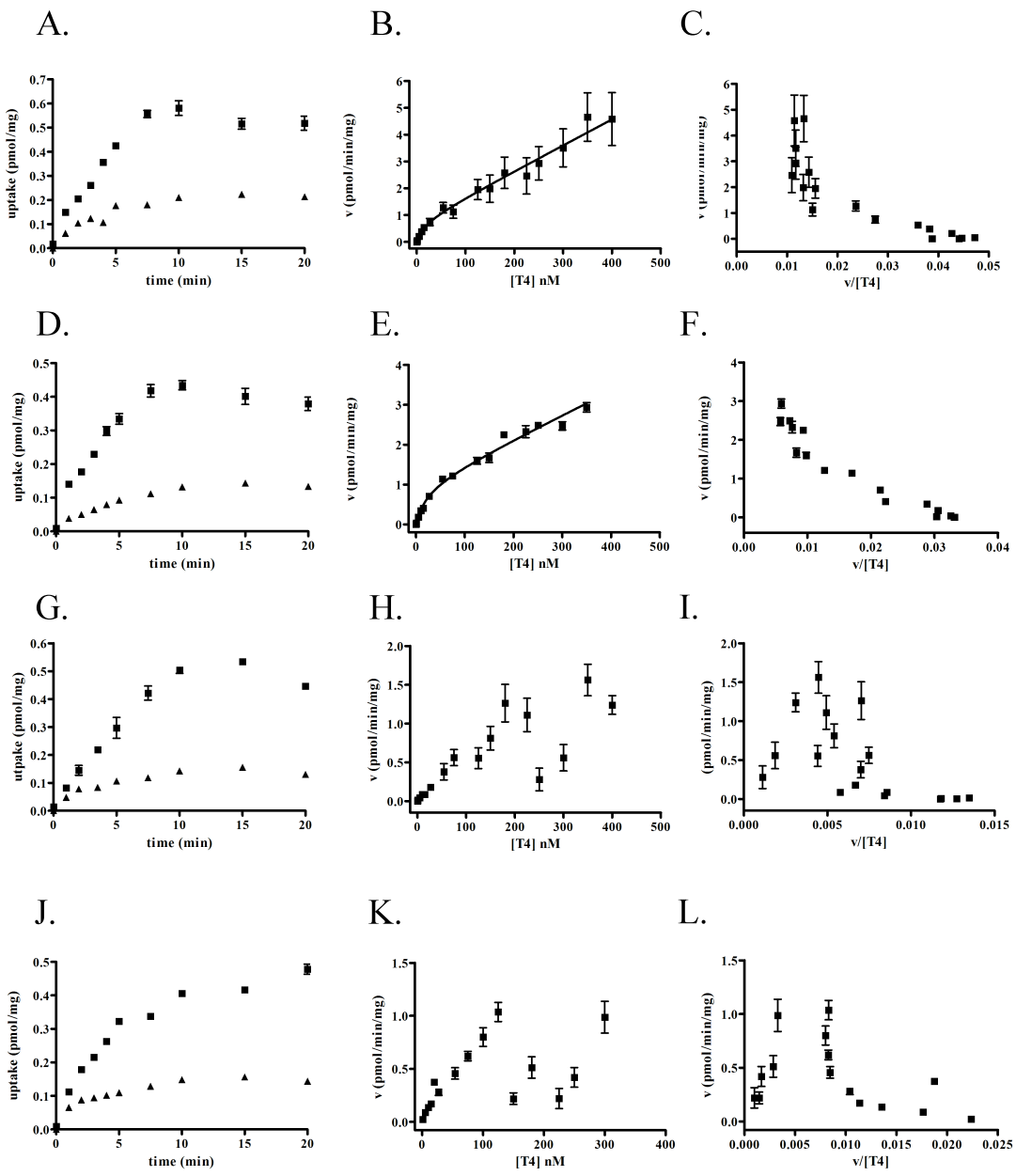
A.
B.
C.
D.
E.
F.
G.
H.
I.
J.
K.
L.
uptake (pmol/mg)
time (min)
v (pmol/min/mg)
[T4] nM
v/[T4]
utpake (pmol/mg)
(pmol/min/mg)

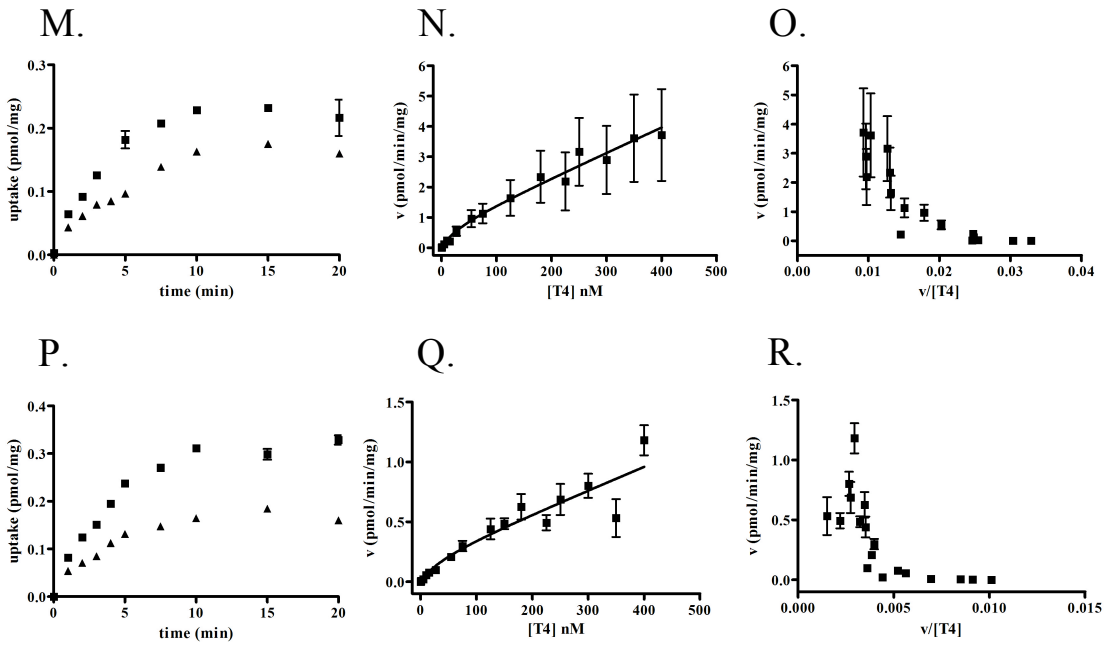

Figure 7. Characterization of mutant Oatp1c1 T4 transport kinetics (A-R). T4 transport kinetics in the form of time courses (left column), velocity vs. substrate concentration (middle column), and Eadie Hofstee plots (right column) were performed in transiently transfected HEK293 cells for WT Oatp1c1 (A-C), W277F,W278F (D-F), G399A,G409A (G-I), G399V,G409V (J-L), R601S (M-O), and P609A (P-R). For time courses (left column), uptake of ^{125}I-T4 was monitored at multiple timepoints in HEK293 cells transiently transfected with either Oatp1c1 construct (square) or empty pEF-DEST 51 (triangle). For velocity vs. substrate concentration experiments, uptake of varying concentrations of T4 was examined at 4 min at 37^{o}C, except for Oatp1c1 R601S and P609A, which were monitored at 4.5 min timepoints. For time courses, each point represents the mean uptake minus empty vector zero min uptake ± standard error (n=3). For velocity vs. substrate concentration experiments, each point represents the mean Oatp1c1 construct uptake minus empty vector contributions at equivalent time points and substrate concentrations ± standard error (n=3).

acid substitutions appeared to have a slight effect on the T4 concentration dependence of Oatp1c1 transport, slightly attenuating the discrete break point at approximately 50 nM between initial rapid increase in velocities and the slow rise at higher concentrations thereafter. Nonetheless, T4 uptake was best fit with biphasic equation (R^2=0.98), resulting in a high affinity K_{m1} of 22 nM (Fig 7E). The two phase profile of Eadie-Hofstee plot was also not as distinct as that observed with WT Oatp1c1, but a break from linearity occurred at higher velocities (Fig 7F).

In ^{125}I-T4 uptake time courses, the Oatp1c1 double glycine mutants G399A,G409A and G399V,G409V transported with similar characteristics to WT Oatp1c1. For G399A,G409A, T4 uptake was linear for the first 10 minutes, then reached equilibrium (Fig 7G). G399V,G409V exhibited linear ^{125}I-T4 uptake for at least the first 5 minutes and reached equilibrium at 10 min (Fig 7J). For both mutants the dynamic range of substrate uptake was similar to that of WT Oatp1c1. However, G399A,G409A and G399V,G409V transport kinetics varied from WT Oatp1c1 (Figs 7H and 7K, respectively). Initial velocities rapidly increased in a linear fashion at low T4 concentrations, but at T4 concentrations greater than 100 nM, velocities decreased. Because of the unique data patterns, velocity vs. substrate data were not fit and a K_m for T4 transport was not calculated. However, the decrease in velocities at high T4 concentrations suggests an apparent case of substrate inhibition, though data reorganization as Eadie-Hofstee plots for both G399A,G409A and G399V,G409V did not yield the arch profile characteristic of substrate inhibition (Figs 7I and 7L, respectively).

P601S mutants transported ^{125}I-T4 in a linear fashion for 5 min, then reached equilibrium at approximately 10 min (Fig 7M). However, the ^{125}I-T4 uptake dynamic

range between P601S and empty vector transfected cells was greatly reduced compared to WT Oatp1c1. Due to the small dynamic range, kinetic parameters were measured at 4.5 min to maximize the uptake difference between P601S and empty vector transfected cells, while still remaining in the linear range of uptake with respect to time. In velocity vs. substrate assays, the rate of initial velocity increases for R601S was 67% of WT Oatp1c1. This resulted in smaller initial velocity increases at low T4 concentrations (Fig 7N), producing more of a shallow hyperbolic uptake profile instead of the distinctive biphasic profile observed with WT Oatp1c1 (Fig 7B). However, in Eadie-Hofstee replots of kinetic data, R601S displayed a distinct biphasic profile with a sharp division between two transport phases, supportive of at least partial activity in multiple sites (Fig 7O). Informed by the biphasic Eadie-Hofstee plot, P601S transport data was fit with a biphasic equation resulting in a K_{m1} of 32 nM.

P609A-mediated uptake of 1nM ^{125}I-T4 increased linearly for the first 5 min, and reached at equilibrium at approximately 10 min (Fig 7P). Similar to R601S, the dynamic range between P609A and empty vector transfected cells was reduced. As a result, kinetic measurements were taken at 4.5 min to maximize the difference between P609A and empty vector transfected cells. The velocity vs. substrate concentration plots were suggestive of biphasic uptake, but velocities were reduced and high affinity K_{m1} was increased (42 nM) compared to WT (Fig 7Q). Eadie-Hofstee plots also displayed a biphasic profile (Fig 7R). Kinetic parameters for all Oatp1c1 constructs are summarized in Table 1.

Oatp1c1 Construct	High affinity K_{m1}
WT	2 nM
W277F,W278F	22 nM
R601S	32 nM
P609A	42 nM
G399A,G409A	n/a
G399V,G409V	n/a

Table 1. Summary of Oatp1c1 mutant K_{m1} values.

Discussion

In the present study we sought to identify and characterize Oatp1c1 amino acids responsible for the specificity filter employed in substrate recognition and discrimination. Through the use of eight predictive algorithms and a comparison of all rat Oatp amino acid sequences, an Oatp1c1 membrane consensus topology map was generated (Fig 2). Considerable evolutionary conservation was observed throughout the transmembrane domains (Fig 2), with 54% of the 13 similar amino acids, 49% of the 149 conserved amino acids, and 28% of the 25 invariable amino acids localized to the transmembrane domains. If the 9 invariable cysteines, previously shown to be required for Oatp function are ignored, 44% of the remaining 16 invariable amino acids are confined to the transmembrane domains. Overall, 87 out of the 256 amino acids (34%) comprising the Oatp1c1 transmembrane domains display either similar, conserved or invariable identity. This compares to 100 out of the 460 (22%) remaining amino acids in the extra- and intra-cellular Oatp1c1 domains displaying any degree of conservation. The level of conservation varied between the 12 predicted transmembrane domains. Transmembrane domain 2 displayed the highest level of conservation, with 79% amino acid conservation. Transmembrane domains 3, 6 and 11 also displayed a high degree of conservation, exhibiting 55%, 41%, and 43% conservation, respectively. Conserved and invariable amino acids within the transmembrane domains consisted of both structural amino acids such as glycines and prolines, as well as potentially functional amino acids including charged lysines, arginines, aspartates, and glutamates. Thus, the conserved amino acids within the Oatp1c1 transmembrane domains likely contribute to substrate translocation mechanisms or structural stabilization features common to all rat Oatps. Transmembrane

domains with higher degrees of conservation likely contribute more to these processes. Transmembrane domains 7 and 10 displayed very limited conservation (10% and 16%, respectively). Based on our assessments it is not possible to determine whether these transmembrane domains play an accessory role as helix stabilizers or contribute to Oatp1c1-specific functional properties. The lack of conservation in the N- and C-termini may be due to differences in polypeptide chain lengths between the different rat Oatp isoforms.

In addition, we created a 3-dimensional model of Oatp1c1 structure based on the known, high resolution crystal structures of the three MFS transporters containing 12 transmembrane domains: GlpT, lactose permease and EmrD (Figs 3 and 4A). The orientation and location of Oatp1c1 transmembrane domains was calculated using MODELLER. In order to augment homology to the 3 MFS transporters used as the template, the large hydrophilic domain between transmembrane domains 9 and 10 was removed during modeling. The majority of conserved and identical amino acids are facing the substrate pore. In addition, very few polar and no charged amino acids face the lipid bilayer (Fig 4B). The location of consensus transmembrane domains of rat Oatp1c1 as determined in the membrane topology was also used as an evaluation tool for the 3-dimensional Oatp1c1 model derived from sequence alignments with the three MFS transporters. The helices predicted with the eight algorithms coincided with those predicted in the alignment with GlpT, lactose permease and EmrD. Even though sequence homology between rat Oatp1c1 and the three MFS transporters is relatively low, there was high coincidence between the known transmembrane domains of the MFS transporters and rat Oatp1c1 homology model with the predicted rat Oatp1c1

transmembrane domains in the membrane topology. These features are consistent with the generation of a reliable 3-dimensional homology model.

Based on the resulting evolutionary conservation, localization to the transmembrane domains, and orientation within the pore in our 3-dimensional model, the contribution to Oatp1c1 structure function of residues D85, E89, N92, W277,W278, G399,G409, R601 and P609 were analyzed. In addition to the structural and evolutionary reasons for the examining the function of the conserved amino acids in this study, we hypothesized biochemical roles for the targeted amino acids in their native state based on the chemical character of the specific side chains.

As observed in Fig 5A and Fig 7A-C, WT Oatp1c1 was expressed at the plasma membrane and displayed biphasic uptake of T4 suggestive of multiple binding sites. However, all Oatp1c1 mutations appeared to have some degree of effect on either subcellular localization or T4 transport kinetics (Figs 5-7 and Table 1). Mutation of either D85 or E89, the only negatively charged amino acids in transmembrane domain 2, to alanine caused intracellular trapping of Oatp1c1 protein (Figs 5I and J). Both of these residues are at the N-terminal region of the transmembrane domain 2 alpha helix. In transmembrane proteins, alpha helices carry a dipole moment due to positive charge build-up at the N-terminal end and negative charge accumulation at the cytoplasmic C-terminal end (Agnati et al., 2005). It is possible that loss of the negative charge associated with the carboxyl group in both D85 and E89, destabilized the alpha helix dipole and/or protein wide macrodipole leading to misfolded Oatp1c1 protein. Mutated Oatp1c1 N92A also displayed intracellular expression patterns and no T4 transport activity (Figs 5K and Fig 6). It is most likely that the polar, but nonionizable N92 may be

involved in Oatp1c1 stabilizing interhelical contacts through hydrogen bonding with adjacent transmembrane alpha helices. However, Oatps are known to undergo N-glycosylation at asparagine residues within specific consensus sequences in putative extracellular Oatp domains (Bergwerk et al., 1996; Lee et al., 2003; Wang et al., 2008). Disruption of the glycosylation process leads to intracellular trapping of Oatp protein (Wang et al., 2008). However, N92 is within the putative transmembrane domain and thus likely unavailable for N-glycosylation. It is also possible the N92 residue is part of a consensus sequence within the Oatp/OATP polypeptide required to interact with binding partners involved with maintaining stable Oatp/OATP structure. One such Oatp/OATP binding partner required for function, PDZK1, has been identified (Wang et al., 2005). Analysis of C-terminal Oatp/OATP sequences has revealed, in some isoforms, PDZ consensus binding sites involved with interaction with PDZK1, an accessory protein of unknown function, but associated with a number of membrane proteins (Kocher et al., 1999). Evidence from PDZK1 knock-out mice, has shown this protein is required for plasma membrane expression of Oatp1a1 (Wang et al., 2005). In PDZK1 knock-out mice, Oatp1a1 liver expression was entirely sequestered intracellularly. It is unknown whether Oatp1c1 or other Oatps/OATPs contain protein binding consensus sequences elsewhere in the polypeptide sequence and/or additional binding/trafficking partners.

Oatp1c1 amino acids W277 and W278 are clearly important in T4 transport. When conservatively co-mutated to similar bulky aromatic phenylalanines, W277F,W278F displayed near WT transport activity in both time course and velocity vs. substrate concentration assays (Figs 7D-F). In addition, the biphasic uptake profile observed in WT Oatp1c1 velocity vs. substrate concentration and Eadie-Hofstee plots

was largely maintained, though the distinct velocity break point was slightly diminished. In contrast, when W277,W278 were replaced with alanines, Oatp1c1 transport activity was abolished (Fig 6). Based on these data, W277,W278 likely provide required steric constraints critical at the interface between the Oatp1c1 extracellular domain and substrate pore. These steric constraints were likely partially substituted by the bulk of the phenylalanines, but not by the much smaller alanines. In addition, the polarizable electron system may be important in developing electrostatic interactions with polar Oatp substrates.

Conserved glycines in transmembrane domain 8 are also important in Oatp1c1 transport kinetics (Fig 7G-I and J-L). T4 transport was relatively similar to WT Oatp1c1 in an initial uptake screen at 10 min (Fig 6). However, transport velocities were greatly reduced at high T4 concentrations with both G399A,G409A and G399V,G409V mutations (Figs 7H and K). The high entropic cost associated with the conformational flexibility of two glycines within the alpha-helix in transmembrane 8 in the face of high evolutionary conservation, suggest that these residues are critically important for proper Oatp1c1 function. The lack of a side chain on the glycines at 399 and 409 may produce a void volume within the pore critical for proper channel formation and/or binding. The lack of large effects on T4 transport at low T4 concentrations, suggest that the low affinity Oatp1c1 T4 binding site is affected to a greater degree than the high affinity binding site by these mutations. However, at T4 concentrations predicted to engage the low affinity site, binding at the high affinity site appears to be influenced as well (Figs 7H and K). This is supported by the observation that at high T4 concentrations, measured transport velocities fell below those previously achieved at lower T4 concentrations.

This is suggestive of substrate inhibition, perhaps as a result of non-productive binding of the low affinity binding site.

R601S displayed partial T4 transport activity compared to WT (Fig 6). Similar to WT Oatp1c1, R601S expression was predominantly at the plasma membrane (Fig 5G). As a result, reductions in transport could not be attributed to intracellular trapping. Velocity vs. substrate and particularly Eadie-Hofstee plots retained an overall biphasic profile (Fig 7 N,O). However, as seen in Table 1, the high affinity K_{m1} value (32 nM) was significantly increased compared to WT (2 nM). Canonical Oatp/OATP substrates contain a hydrophobic center, a hydrogen bond donor on one end, and negative charge on the opposite end (Yarim et al., 2005). The R601 residue may serve as a counter-charge for anionic binding to Oatp1c1 and may explain the reduced T4 transport capabilities in the R601S mutant compared to WT. However, mutation of R601 to alanine did not completely abolish Oatp1c1-mediated transport. It is possible that other charged residues within the transmembrane domains also assist in providing a counter charge. Additional arginines are located within or near Oatp1c1 transmembrane domains, including a non-conserved residue in transmembrane domain 4 and two conserved residues just outside transmembrane domains 10 and 12. However, R601 is the only conserved arginine within the middle of a transmembrane domain. In addition, multiple lysine residues are found within the transmembrane domains and may also provide a counter charge for anion binding. Four positively charged lysines are located in transmembrane domains 1, 5 and 9, with one conserved residue within transmembrane domain 1. Finally, Oatp/OATP transport may proceed without the presence of a positive counter charge as neutral and positively charged substrates have been identified for some Oatps/OATPs,

including Oatp1a1, OATP1A2 and Oatp1a4 (Hagenbuch and Meier, 2004). Thus, our data suggests that although a counter charge provided by a positively charged amino acid may increase binding affinity, it may not be required for Oatp/OATP substrate recognition and/or transport across the membrane.

Finally, P609A displayed partial T4 transport activity (Fig 6). However, when expression was monitored using immunofluorescence, along with plasma membrane staining, significant intracellular trapping of P609A was observed compared to WT Oatp1c1 (Fig 5H). Thus, it was undetermined whether the partial activity of the P609A mutant could be attributed to reduced appearance of Oatp1c1 at the plasma membrane or changes in T4 binding capabilities. P609 may introduce helical constraints by generating a kink in the alpha helix, perhaps allowing the different surfaces of the helix to face the pore. The significant intracellular trapping suggests that P609 may be playing a role in trafficking Oatp1c1 to the plasma membrane. However, the increase in the K_m value suggests the P609 residue may also play a role in T4 binding.

As mentioned in the introduction, several lines of evidence exist suggesting the presence of multiple binding sites within Oatps. This property is not unique to Oatp/OATP transporters. Additional multispecific transporters have are known to possess multiple substrate binding sites including P-gp and MRP1 (Aller et al., 2009; Karwatsky and Georges, 2004). Interestingly, these transporters also accept many of the same substrates as Oatps/OATPs, including T4 and $E_2$17βG, suggesting there may be common mechanisms and/or structural motifs involved in generating atypical transport kinetics between the various superfamilies of transporters. Our previous work has demonstrated the presence of high and low affinity binding sites in Oatp1c1 involved in

the transport of two substrates, T4 and $E_2$17βG. In the current study, in addition to gaining basic information about which amino acids are involved in creating the general specificity filter for Oatp1c1 substrate recognition, we sought to identify specific amino acids that define the discrete binding sites. Based on our expression and initial screen for transport activity, the only amino acids in our group of mutations available for testing for preferential effects on one binding site or the other were those mutants that retained partial or full activity. Oatp1c1 mutations that resulted in intracellular trapping, such as D85A, E89A and N92A may be involved with protein-substrate interactions, but their role in this process cannot be determined due to the lack of functional Oatp1c1 protein at the plasma membrane. Thus, only Oatp1c1 mutants W277F,W278F, G399A,G409A, G399V,G409V, R601S, and P609A allow evaluation of functional effects on Oatp1c1 binding sites. Concentration dependent T4 uptake displayed as both velocity vs. substrate concentration or Eadie-Hofstee plots suggested both binding sites remained at least partially functional in W277F,W278F, R601S, and P609A mutants. In these cases, a biphasic equation was used to fit the data, although as previously described, K_{m1} values were higher than those observed with WT (Fig 7, Table 1). This suggests that these residues are likely involved in a substrate recognition mechanism common to both high and low affinity sites. Concentration dependent T4 uptake by Oatp1c1 mutants G399A,G409A, G399V,G409V, however, suggests these mutations may have preferential effects on the low affinity binding site, while leaving the high affinity T4 binding site intact. The drastic lowering of T4 transport velocities at T4 concentrations predicted to engage the low affinity site, suggests the G399A,G409A and G399V,G409V mutations produce non-productive binding at the low affinity site.

Evaluating the transport capabilities of the functional Oatp1c1 mutants using substrates other than T4 may also reveal more about the substrate binding site organization. The characteristics and specificity of substrate interaction with the multiple binding sites within an individual Oatp/OATP cannot be applied to all substrates of that transporter. For example, numerous Oatps/OATPs, including Oatp1a4 and Oatp1c1, have revealed substrate-dependent inhibition, where a single inhibitor affects transport of two substrates of the same transporter differently (Sugiyama et al., 2002; Tohyama et al., 2004). Characterizing the transport capabilities of the Oatp1c1 mutants discussed here with other substrates may provide an additional platform to assess complementary Oatp1c1-substrate surfaces.

Most of the current data on the mutational effects of amino acids in Oatps/OATPs comes from pharmacogenetic studies on naturally occurring polymorphic OATPs (Konig et al., 2006; Marzolini et al., 2004). Use of a targeted mutagenesis approach provides another means to understand Oatp/OATP structure and function. Nonetheless, data on polymorphic OATPs can be useful in modeling Oatp/OATP structure and function. Although polymorphic data is based on human OATP sequences, much sequence and functional conservation exists between rodent and human Oatps/OATPs and thus meaningful comparisons can be made. Most pharmacogenetic studies have been performed in members of the OATP1 family, including members OATP1A2, OATP1B1, and OATP1B3 (Badagnani et al., 2006; Kameyama et al., 2005; Lee et al., 2005; Nozawa et al., 2002). Of the numerous nonsynonomous polymorphisms identified, most are in putative extracellular domains, suggesting there is selective pressure to maintain sequence integrity in OATP transmembrane domains, where direct substrate contact

occurs (Konig et al., 2006; Marzolini et al., 2004; Tirona et al., 2001). Despite the relative paucity of polymorphisms within the transmembrane domains, some polymorphisms resulting in amino acid substitutions within putative transmembrane domains have been identified and functionally characterized. Some of the biochemical consequences of these polymorphisms are in agreement with our results, allowing us to apply our results to Oatps/OATPs in general. For example, a polymorphism in OATP1A2 resulting in an R168C substitution in transmembrane 4, results in reduced uptake of estrone-3-sulfate and methotrexate (Badagnani et al., 2006). This supports our finding that the loss of a positively charged transmembrane residue, possibly serving as a counter charge for anion transport, reduces but does not abolish Oatp/OATP transport activity. In another study, an OATP1B1 polymorphism resulting in a P336R substitution in transmembrane domain 7, was associated with decreased total and nonrenal pravastatin clearance in a healthy Japanese subject with this polymorphism (Nishizato et al., 2003). This polymorphic protein, when examined within an OATP1B1*15 +1007C<G haplotype in transiently transfected HEK293 cells, resulted in reduced transport capacity and partial intracellular trapping (Kameyama et al., 2005). These combined data are supportive of a role for transmembrane prolines in generating stable and functional Oatp/OATP structures. Additional biochemical characterization of other polymorphic OATPs, along with more extensive site-directed mutagenesis, will assist in creating Oatp/OATP binding pocket and structural models, as well as delineating the rules for Oatp/OATP substrate recognition.

In conclusion we have predicted and characterized amino acids involved with maintenance of Oatp1c1 structural integrity and T4 transport function. Future structure-

function studies along with CoMFA analysis will allow mapping of complementary Oatp1c1 and substrate surfaces, with the ultimate goal of identifying novel Oatp1c1 substrates as well as targeting this family of transporters for drug delivery.

Chapter 4

Competitive inhibition of Oatp1c1-mediated thyroxine transport by the fenamate class of nonsteroidal anti-inflammatory drugs

Daniel E. Westholm, David D. Stenehjem, Jon N. Rumbley, Lester R. Drewes, Grant W. Anderson

The entire contents of this chapter were published in:

Endocrinology 2009 Feb;150(2):1025-32.

Abstract

The organic anion transporter Oatp1c1 is a high affinity thyroxine (T4) transporter with narrow substrate specificity expressed at the blood-brain barrier. A transport model using cells over-expressing Oatp1c1 was created to identify novel Oatp1c1 substrates and inhibitors. Rat Oatp1c1 was cloned and stably expressed in HEK293 cells. Oatp1c1-transfected HEK293 cells transported ^{125}I-labeled T4 in a time dependent manner which was completely abolished in the presence of excess unlabeled T4. Next, various compounds including inhibitors of thyroid hormone uptake were screened for inhibitory effects on Oatp1c1-mediated T4 uptake. Phenytoin (64%), indocyanine green (17%) and fenamic acid (68%) diclofenac (51%) and meclofenamic acid (33%) all reduced T4 uptake by Oatp1c1 when assayed at concentrations of 10μM. Dose response assays for the fenamic acids, iopanoic acid, indocyanine green and phenytoin revealed IC_{50}s for Oatp1c1 T4 uptake below or near the blood plasma levels after therapeutic doses. Further kinetic assays and reciprocal plot analyses demonstrated that the fenamic acid diclofenac inhibited in a competitive manner. Finally, microvessels were isolated from adult rat brain and assessed for T4 uptake. 10μM fenamate concentrations inhibited T4 microvessel uptake with a similar hierarchical inhibition profile (fenamic acid (43%), diclofenac (78%) and meclofenamic acid (85%) as observed for Oatp1c1 transfected cells. Oatp1c1 is expressed luminally and abluminally in the BBB endothelial cell and exhibits bidirectional transport capabilities. Together, these data suggest that Oatp1c1 transports fenamates into, and perhaps across, brain barrier cells.

Introduction

Organic anion transporting polypeptides (rodents and other animals, Oatps; human, OATPs) are a large and multi-faceted group of membrane-bound solute carriers mediating the transport of amphipathic organic substrates across cellular plasma membranes (Hagenbuch and Meier, 2003). Structurally, all Oatps/OATPs contain 12 transmembrane spanning domains, a superfamily signature of 13 amino acids and 11 extra-cellular cysteine residues (Meier-Abt et al., 2005). Substrates of these transporters include; steroid conjugates, bile salts, organic dyes, thyroid hormones and various drugs (Hagenbuch and Meier, 2004). Oatp/OATP transport mechanism is sodium-independent and likely accomplished through anion exchange (Hagenbuch and Meier, 2003). Currently, the driving force is unclear, but intracellular glutathione is a potential candidate (Li et al., 1998). Many Oatps/OATPs are expressed ubiquitously, but more specialized members are expressed exclusively in a limited number of tissues (Hagenbuch and Meier, 2004). Oatp1c1/OATP1C1 is an Oatp/OATP superfamily member that follows the latter expression and functional pattern. Oatp1c1/OATP1C1 is a high affinity T4 transporter (reported K_m=180-720nM) expressed in the blood-brain barrier (BBB), choroid plexus, human ciliary body epithelium and Leydig cells of the testis (Chu et al., 2008; Gao et al., 2005; Pizzagalli et al., 2002). Other known substrates include 3,3',5' triiodothyronine (reverse T3), cerivastatin and estradiol-D-17 β-glucuronide ($E_2$17βG) (Sugiyama et al., 2003). Of the Oatps expressed at the BBB, Oatp1c1 has the lowest identified K_m for T4, a prohormone which plays a crucial role in the timing of multiple neurological development processes (Sidney Jones, 2005).

An extensive network of microvessels infiltrates the brain and is comprised of brain capillary endothelial cells that together form the BBB. Unlike other tissues in which solutes in the blood enter the parenchyma through diffusion between endothelial cells, brain capillary endothelial cells possess tight junctions that prevent paracellular diffusion. As a result, solutes must cross the luminal and abluminal membranes of the brain capillary endothelial cell to enter the brain parenchyma. Such transport is accomplished by a number of solute carriers including the Oatps (Kusuhara and Sugiyama, 2005; Westholm et al., 2008).

Oatp1c1 is the fourth most abundant transporter expressed in rat brain endothelial cells (Enerson and Drewes, 2006; Tohyama et al., 2004). Oatp1c1 protein has been localized to both the luminal and abluminal side of brain endothelial cells and implicated in the transport of T4 across the BBB. T4 is an important regulator of brain development (Anderson, 2001; Sugiyama et al., 2003; Tohyama et al., 2004). In addition, Oatp1c1 is also localized to cells comprising the blood-cerebrospinal fluid barrier. Unlike other regions of the brain, choroid plexus vasculature is fenestrated and the barrier is formed through tight junctions between epithelial cells (Segal, 2000). Currently, Oatp1c1 is thought to be localized to the basolateral membrane of choroid plexus epithelial cells (Hagenbuch and Meier, 2003). Identifying Oatp1c1 and other brain transporter substrates is important in understanding drug-drug interactions or drug-hormone interactions and for the rational design of new drugs. A comprehensive knowledge of substrate specificity will assist in the design of drugs to facilitate or inhibit uptake via brain transporters.

Compared to other Oatps, Oatp1c1 has relatively narrow substrate specificity. Our current study sought to identify novel Oatp1c1 substrates. In addition, we sought to

elucidate possible functional consequences of Oatp1c1-mediated transport of these substances.

Candidates were identified from known competitive inhibitors of thyroid hormone transport (Hennemann et al., 2001). As T4 is transported by Oatp1c1, we hypothesized some of these known thyroid hormone transport inhibitors may be specific Oatp1c1 inhibitors and/or substrates. Amiodarone, bilirubin, phenytoin, iopanoic acid, indocyanine green and members of the fenamic acid family of non-steroidal anti-inflammatory drugs (NSAIDs) were among the compounds tested for Oatp1c1-specific T4 transport inhibition using a model cell line overexpressing Oatp1c1. We found that the fenamic acid diclofenac competitively inhibited T4 uptake by Oatp1c1. In addition, the fenamates inhibited T4 uptake in isolated rat brain microvessels using an *ex vivo* transport assay. Molecular modeling of T4 and fenamates revealed striking structural commonalities in electrostatic surface potential and steric bulk. Together, these data suggest Oatp1c1 may contribute to fenamate influx into, and perhaps across, brain endothelial cells.

Materials and Methods

Cloning of Oatp1c1 and plasmid construction

To clone rat Oatp1c1, cDNA was reverse transcribed from post-natal day 15 (PN15) total rat brain RNA using Superscript III Reverse Transcriptase (Invitrogen Corp.; Carlsbad, CA). PCR was then performed against Oatp1c1 using forward and reverse primers designed against Oatp1c1 sequences obtained in the National Center for Biotechnology Information database (Accession ID NM_053441). Forward primers (5'-GGGGACAAGTTTGTACAAAAAAGCAGGCTTCGAAGGAGATAGAACCATGGC CGACACTTCATCCAAAGAAAATGCCC-3') and reverse primers (5'-GGGGACCACTTTGTACAAGAAAGCTGGGTCAAGTCGGGTCTCTTGCCTG-3') were flanked on their 5' end by *att* B sites for use in Gateway cloning (Invitrogen Corp.; Carlsbad, CA). The stop codon was removed in the reverse primer for fusion with a C-terminal tag in the expression vector pEF-DEST 51 (Invitrogen). Oatp1c1 PCR products were gel-purified using a GeneClean kit (Qbiogene; Irvine, CA) to remove *att* B primers and primer dimers and then further purified using a QIAquick PCR purification kit (QIAGEN, Inc; Valencia, CA). *Att* B flanked PCR products were directionally cloned into *att* P containing Gateway pDONR 221 entry vectors (Invitrogen) in a 4 h BP recombination reaction catalyzed by BP clonase according to the manufacturers instructions resulting in *att* L containing Oatp1c1-pDONR 221 entry clones. Oatp1c1 was subcloned from pDONR 221 to the *att* R containing expression vector pEF-DEST 51 in a 5 h LR recombination reaction. pEF-DEST 51 contains a C-terminal fusion V5 epitope tag for antibody detection. The Oatp1c1 insert along with upstream elements and the V5 tag were sequence verified.

Stable transfection of Oatp1c1-pEF-DEST51 in HEK293

HEK293 cells were grown to 50% confluence in minimal essential medium (MEM) with 10% fetal bovine serum, sodium pyruvate (1mM) and non-essential amino acids (1X) without antibiotics. Linearized Oatp1c1-pEF-DEST 51 was introduced into the cells through lipofection using the reagent lipofectin (Invitrogen). Transfected cells were split 1:5 and cultured in the presence of blasticidin (10μg/ml) for 2 weeks. Surviving cells were pooled and cultured in MEM with 10% fetal bovine serum, sodium pyruvate (1mM), non-essential amino acids (1X) and a maintenance concentration of blasticidin (2 μg/ml).

Western Blot

One confluent well of a 6-well plate of Oatp1c1-pEF-DEST 51 transfected HEK293 cells was washed once with ice-cold PBS and then lysed with 150 μl RIPA buffer ((50 mM Tris-HCl pH 8, 150 mM NaCl, 1.0% NP-40, 0.1% SDS, 0.5% sodium deoxycholate, 50 mM NaF, 50 mM EDTA) containing Complete Mini Protease Inhibitor (Roche Diagnostics; Penzberg, Germany). Cell lysate was boiled for 5 min and 15 μl was run on a 10% SDS-polyacrylamide gel containing 0.36 g/ml urea. Protein was transferred to a nitrocellulose membrane at 100 volts for 1 h and blocked in blotto (50 mM Tris pH 8, 2 mM CaCl, 80 mM NaCl, 0.2% Tween 20, 5% non-fat dry milk) for 1 h at room temperature. The membrane was then incubated with anti-V5 antibodies (Invitrogen)(1:4,000 in blotto) for 1 h at room temperature. After 4 ten min washes with TBST (Tris-buffered saline pH 8, 0.1% Tween 20) at room temperature, the membrane was incubated with the secondary horseradish-peroxidase conjugated secondary antibody (1:20,000) for 1 h at room temperature. The membrane was then washed 3 times for ten

min in TBST and developed in West Pico Chemiluminescent substrate (Pierce; Rockford, IL) for 5 min. Finally, the membrane was imaged using a Fluorochem 8000 (San Leandro, CA).

Immunocytochemistry

Transfected cells were plated in a 12-well plate containing #1 round glass coverslips (Dynalab Corp.; Rochester, NY). Cells were then washed in PBS, pH 7.4, followed by a rinse in room temperature methanol, and fixed in -20^{o}C methanol for 12 h. Next cells were washed, permeabilized and blocked during three 5 min washes in PBSA/TX100 (PBS, 1% bovine serum albumin, 0.1% Triton X100). Primary anti-V5 mouse IgG antibodies (Invitrogen) were diluted 1:100 in PBSA/TX100 and applied to the coverslips for 1 h in a humidity chamber placed in a 37^{o}C incubator. Following primary antibody incubation, cells received three 5 min washes in PBS. Next, goat anti-mouse fluorescein isothiocyanate (FITC) conjugated secondary antibodies (Jackson ImmunoResearch Laboratories, Inc.; West Grove, PA) were applied (1:75) and incubated and washed using the identical procedure as with the primary antibody. Cells were then mounted on slides with Prolong anti-fade Reagent (Molecular Probes, Inc.; Eugene, OR). Slides were examined using a Nikon TE300 inverted fluorescent microscope (Nikon; Melville, NY).

Transport Assay

Cell-culture transport assays were carried out using a method based on a procedure published by Sugiyama et al (Sugiyama et al., 2003). 1x10^{5} cells/well were plated in four-well plates (Nunc; Rochester, NY) in standard culture medium (see stable transfection). Twenty-four h before the assay, media was changed and supplemented

with 10mM sodium butyrate, and 10% stripped serum. Stripped serum was prepared by incubating 50 ml of FBS and 0.3 μCi of ^{125}I-T4 with 2.5 g of Dowex 1x8, 50-100 mesh, ion exchange resin (Acros Organics; Geel, Germany) 3 times for 2 h at room temperature. After the final incubation, the beads were pelleted with centrifugation and the serum was filter sterilized. Thyroid hormone removal was assessed by monitoring ^{125}I-T4 tracer elimination. To perform the assay, cells were washed and incubated with Krebs-Henseleit buffer (142 mM NaCl, 23.8 mM $NaHCO_3$, 12.5 mM HEPES, 5 mM glucose, 4.83 mM KCl, 1.53 mM $CaCl_2$, 1.2 mM $MgSO_4$, and 0.96 mM KH_2PO_4, pH 7.4). Uptake was commenced with the addition of Krebs-Henseleit containing 1nM ^{125}I-T4 (307 μCi/ml, Perkin Elmer; Wellesley, MA) and ended at specific timepoints with two washes of Krebs-Henseleit without radio-labeled ligand. Cells were then lysed with TritonX100 (Sigma; St. Louis, MO) and the associated radioactivity measured with a Beckman gamma counter (Beckman Coulter, Inc.; Fullerton, CA). Protein concentrations were determined with a BCA Protein Assay kit (Pierce). Background radioactivity associated with the empty vector zero time point was subtracted from all samples. Zero time points were performed as follows. Following equilibration in Krebs-Henseleit buffer, the buffer was aspirated from cells and 200 μl of isotopic media was overlaid on confluent HEK293 cells and immediately removed. Cells were then rapidly washed 2 times with fresh Krebs-Henseleit buffer. The ^{125}I-T4 associated counts at zero min account for approximately 10% of uptake at 2 min for Oatp1c1-transfected cells. Uptake was calculated from the proportion of radioactivity associated with the cell lysate as compared to total radioactivity associated with the isotopic Krebs-Henseleit buffer and expressed in units of pmol/min/mg protein. The uptake units were expressed as a cell-to-

medium ratio of associated radioactivity derived from the following equality: counts in isotopic standard/volume of standard = counts in lysate sample/"volume" taken up by cells in lysate sample. The volume units were then converted to picomolar units by equating sample uptake volume to the standard volume which had a known T4 concentration. In all experiments, 125I-T4 concentrations were 1 nM and supplemented with unlabeled T4 to achieve higher total T4 concentrations when needed. All unlabeled compounds used in inhibition assays were purchased from Sigma.

Rat Cerebral Microvessel Isolation

Cerebral microvessels were isolated from adult Sprague–Dawley rats. Adult rats weighed approximately 250 g. Rats were anesthetized with Nembutal 50mg/kg i.p., exsanginated and decapitated. The brains were immediately removed and pooled. The brain matter was minced in 10 ml of ice cold Buffer A (MEM supplemented with 25mM HEPES and 1% Dextran) into approximately 5mm cubes. The minced brain matter was homogenized via 10 strokes in a glass-Teflon homogenizer with a clearance of 0.25 mm using a motor driven drill press. The homogenate was passed over a 350 μm nylon mesh, followed by 3 washes with 5ml of ice cold Buffer A. The flow thru was passed over a 110 μm nylon mesh and washed 3 times, with 5 ml of ice cold Buffer A. The resulting flow thru was thoroughly mixed with an equal part of ice cold Buffer A + 40% Dextran. The mixture was centrifuged in a swinging bucket rotor at 5000 X g for 15 min at 4°C. The supernatant was aspirated and the pellet was resuspended in 5 ml of ice cold Buffer A. The microvessels were collected by passing the resuspended pellet over a 25 μm nylon mesh and the trapped microvessels were washed 3 times with 5 ml of ice cold buffer A. The nylon mesh containing the trapped microvessels was placed in a 12 ml

centrifuge tube and washed with 5 ml of ice cold buffer A to remove the adherent microvessels. The microvessel collection procedure on the 25μm nylon mesh was repeated for a total of 6 times with the resulting flow through. The microvessel preparation was assessed microscopically for purity. All animal use and protocols were approved by the University of Minnesota Institutional Animal Care and Use Committee. Animals were maintained in accordance with the NIH Guide for the Care and Use of Laboratory Animals.

Rat Cerebral Microvessel Uptake Assay

The determination of T4 uptake in rat cerebral microvessels is based on the filter binding methodology of Inoue et al (Inoue et al., 1984). In brief, purified microvessels were washed with Krebs-Henseleit buffer at 37°C and resuspended to 1μg/μl in Krebs-Henseleit buffer and incubated at 37°C for 15 min. Protein concentration was determined using a BCA Protein Assay kit (Pierce). The uptake assay was begun by the addition of 0.344 μCi ^{125}I-T4 in 100 μl of Krebs-Henseleit to 100 μg of purified microvessels for a total volume of 200 μl. The reaction was incubated at 37°C for the indicated time (0, 30, 60, 120 sec). To terminate the reaction 800 μl of ice-cold Krebs-Henseleit buffer was added to the reaction followed by immediate filtration on nitrocellulose filter disks (Millipore HAWP-02500) with suction. The filter disk was rapidly washed three times with approximately 10ml of PBS. The filters were placed in vials and 10 min gamma counts were performed. Controls were included for non-specific binding of ^{125}I-T4 to the filter, which was typically 1.2% of total activity.

Determination of kinetic parameters

Dose response and uptake curves were fitted using non-linear regression with Graph Pad Prism Version 4 (San Diego, CA). Dose-response curves followed the "four-parametric logistic equation" of the form: $Response=Bottom+(Top-Bottom)/[1+10^{(LogIC50-[Drug])}]$. Uptake curves followed the Michaelis-Menten equation: $v=Vmax*[S]/[S]+K_m$.

Substrate-Inhibitor Comparison

Structures of the T4 and Oatp1c1 inhibitors were retrieved from PubChem in SMILES notation and converted into their three dimensional structures using Sybyl 7.2 (Tripos, Inc.). The structures were minimized by the Powell method in Sybyl 7.2 using the Tripos force field, atomic charges assigned by the Gasteiger-Marsili method. To optimize the structural alignment simulated annealing was used to sample conformational space. Ten cycles of heating to 700K for 1000fs and cooling to 200K for 1000fs using an exponential temperature versus time decay were used. The energetics were calculated as above. The simulation was followed by another minimization and the process repeated until structural minima were obtained having a high degree of structural overlap. The structural alignments were done using the Multifit algorithm in Sybyl 7.2. MOLCAD was used to compare the electrostatic potential surface of T4 and meclofenamic acid.

Results

Oatp1c1 Cloning and expression in HEK293 cells

The coding sequence of Oatp1c1 was PCR amplified from PN15 rat brain total RNA, inserted into the Gateway expression vector pEF-DEST 51 and sequence verified. Western blot and immunocytochemistry was performed to verify full-length expression and proper sub-cellular localization of Oatp1c1-pEF-DEST51 transfected HEK293 cells. Oatp1c1 was expressed with an apparent molecular mass of ~75 kDa, consistent with predicted size, along with a lower weight band likely resulting from a degradation product or incomplete denaturing of the protein (Fig 1a). Immunocytochemical analysis revealed expected Oatp1c1 plasma membrane localization along with deposition in the endoplasmic reticulum and/or Golgi apparatus in transfected HEK293 cells (Fig. 1b, 1c).

Establishing a cell based model for assessing Oatp1c1-mediated transport

^{125}I-T4 was used as a model high affinity Oatp1c1 substrate for all assays. Oatp1c1 transported ^{125}I-T4 in a time-dependent manner into transfected HEK293 cells (Fig. 2). ^{125}I-T4 uptake was higher in Oatp1c1 transfected cells compared to empty-vector transfected cells at all time points assessed. The addition of excess unlabeled T4 quenched labeled T4 transport.

Inhibition of Oatp1c1-mediated T4 transport

Next, putative inhibitors of Oatp1c1-mediated T4 uptake were screened at 10 μM concentrations. We first tested the known thyroid hormone transport inhibitors (amiodarone, bilirubin, indocyanine green, iopanoic acid, phenytoin and fenamic acid) to assess Oatp1c1-specific transport inhibition. Additional NSAIDS were tested including

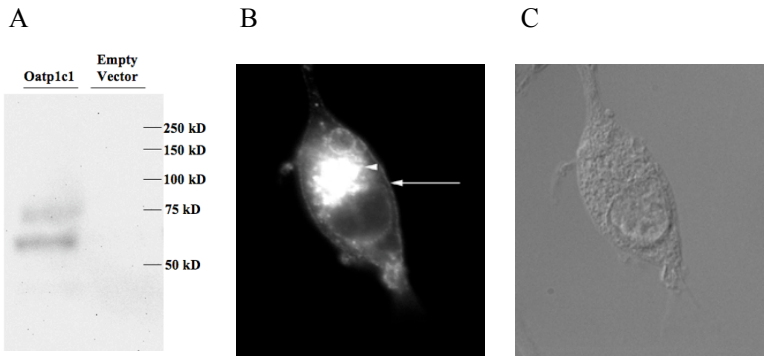

Figure 1. Oatp1c1 expression in transfected HEK293 cells. (A) Full Length Oatp1c1 is expressed in transfected Hek293 cells. Lysate from HEK293 cells transfected with Oatp1c1-pEF-DEST 51 (Lane 1) and empty vector (Lane 2) was transferred to a nitrocellulose membrane and probed with anti-V5 antibodies. (B and C) Oatp1c1 is expressed at the plasma membrane (arrow) and perinuclear regions (arrowhead) in transfected HEK293 cells. Methanol fixed HEK293 cells expressing Oatp1c1 were probed with anti-V5 antibodies to reveal V5 tagged Oatp1c1 localization. Green stain corresponds to Oatp1c1 localization.

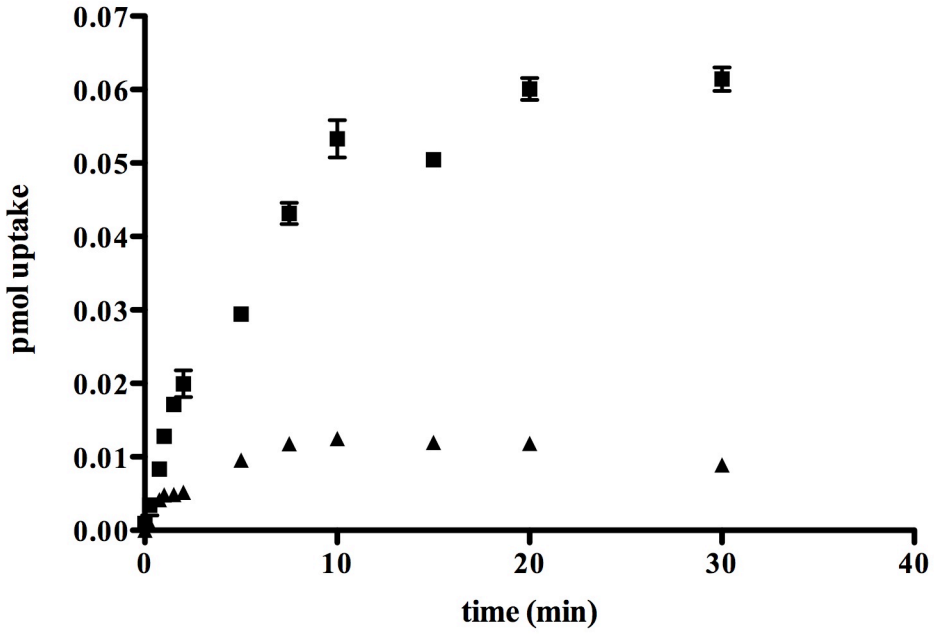

Figure 2. T4 is transported in a time dependent manner by Oatp1c1-pEF-DEST 51 transfected HEK293 cells. Uptake of ^{125}I-T4 was examined at different timepoints in cells transfected with Oatp1c1-pEF-DEST 51 (square) or empty vector (triangle) at 37^{o} C. The zero time point was subtracted from each time point to account for background. Each point represents the mean uptake ± standard error (n=3).

the fenamates diclofenac and meclofenamic acid. Aspirin, flurbiprofen, ibuprofen, and indomethacin had no effect on T4 uptake (Fig. 3). Amiodarone, bilirubin, phenytoin, fenamic acid, diclofenac, meclofenamic acid and indocyanine green all reduced T4 uptake significantly (Fig. 3). Indocyanine green was the most potent inhibitor (82.5 ± 1.5%), followed by members of the fenamic acid family (diclofenac 48.5 ± 4.6%; meclofenamic acid 66.8 ± 2.9%) and iopanoic acid (58.8 ± 1.0%).

Dose response analyses were carried out for the fenamates, phenytoin, ICG and iopanoic acids (Table 1). IC_{50}s followed the same pattern as the initial inhibition screen, with ICG displaying the lowest value, followed by meclofenamic acid, iopanoic acid, diclofenac, phenytoin and fenamic acid (Fig. 4). T4 is light sensitive and known to undergo photodegradation in the presence of colored compounds. Therefore, we examined whether the measured inhibition by the fenamates, ICG, phenytoin and iopanoic acid was due to interactions with Oatp1c1 or photodegradation of the ^{125}I-T4. To test this, we assessed ability of these six compounds to inhibit Oatp1c1-mediated transport when co-incubated under ambient light with ^{125}I-T4 immediately and 1 h before uptake was measured. We found that the time of light exposure had no effect on the degree of inhibition, suggesting photodegradation did not occur in our assays (data not shown).

Identification of competitive inhibitors of Oatp1c1-mediated T4 transport

We determined initial velocities at 2 min time points of Oatp1c1 T4 uptake at varying concentrations in the presence of diclofenac. As seen in Figure 5, increasing concentrations of T4 attenuated, then abolished diclofenac inhibition, suggesting competitive inhibition by this fenamic acid.

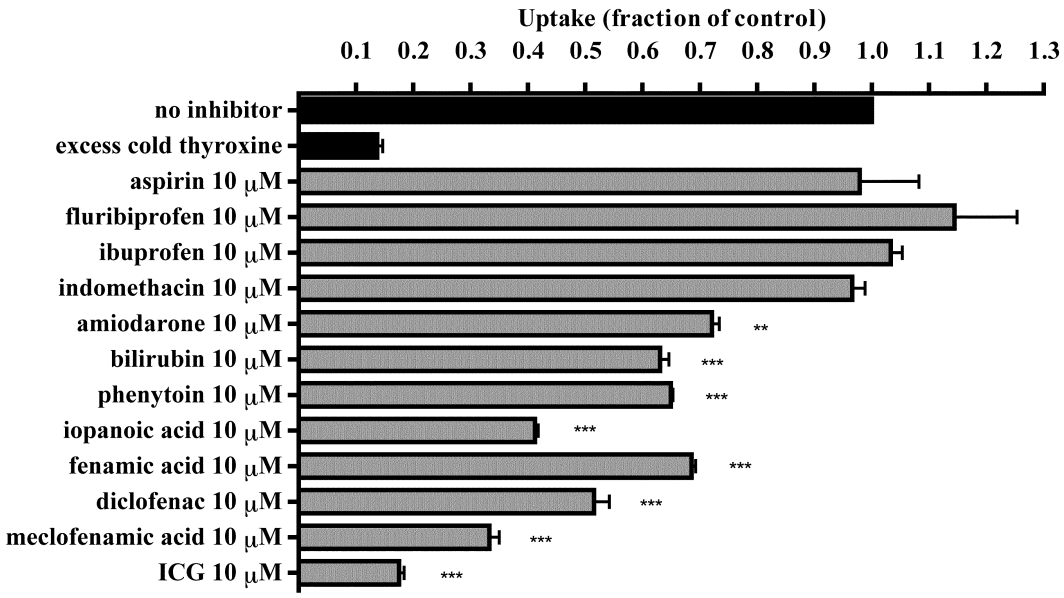

Figure 3. Fenamic acids, ICG, iopanoic acid and phenytoin inhibit Oatp1c1-mediated T4 transport. The effect of various unlabeled compounds (10 μM) on Oatp1c1-mediated ^{125}I-T4 (1 nM) transport was examined at 2 min time points at 37^{o}C. Each graph represents the mean uptake ± standard error (n=3). ** denotes $p \leq 0.01$ and *** denotes $p \leq 0.001$

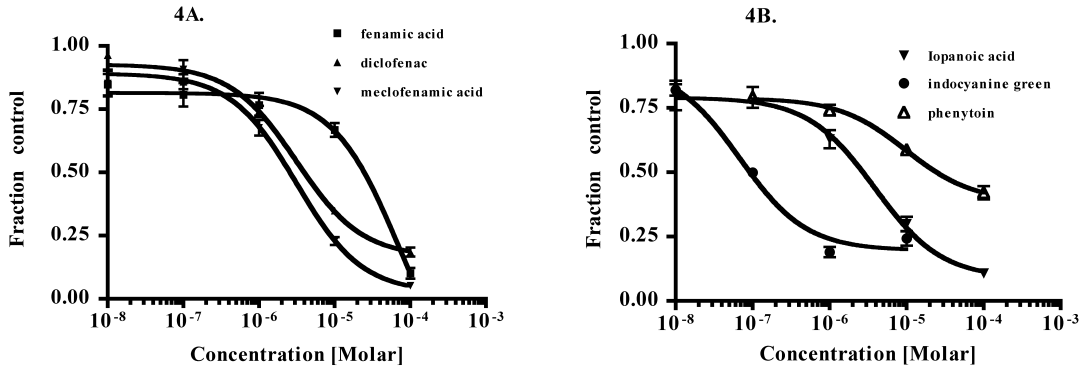

Figure 4. Fenamate, iopanoic acid, ICG and phenytoin dose responses for Oatp1c1-mediated T4 transport. Uptake of ^{125}I-T4 was examined in the presence of different concentrations of (A) fenamic acid, diclofenac, meclofenamic acid, (B) iopanoic acid, ICG and phenytoin. Dose response curves were fitted and IC_{50}s were calculated using non-linear regression analysis (Graph Pad Prism). Each point represents the mean uptake ± standard error (n=3).

Compound	IC_{50}
Fenamic acid	25 μM
Diclofenac	4 μM
Meclofenamic acid	3 μM
Iopanoic acid	3 μM
ICG	0.1 μM
Phenytoin	26 μM

Table 1. IC_{50} values for inhibitors of Oatp1c1-mediated transport

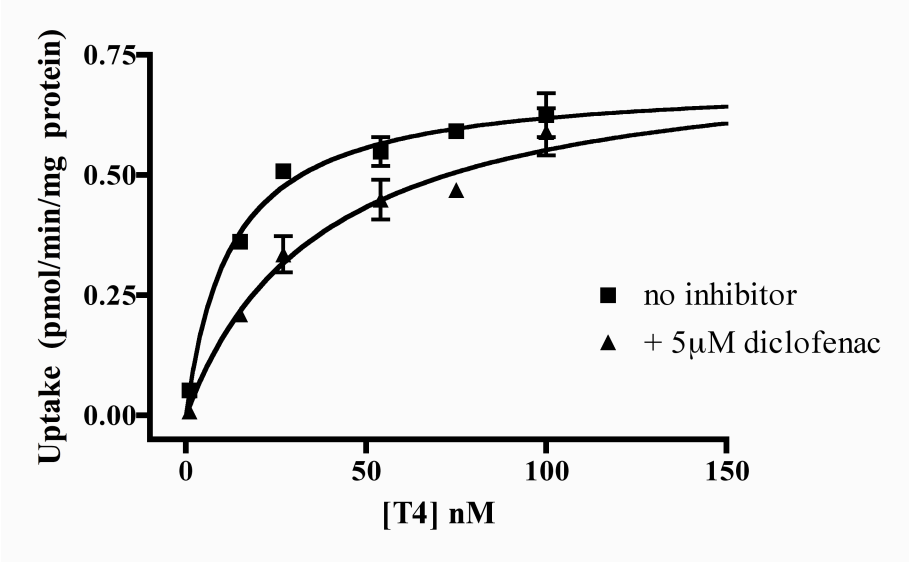

Figure 5. Characterization of Oatp1c1-mediated T4 uptake inhibition. Uptake of increasing concentrations of ^{125}I-T4 supplemented with cold T4 (total concentration 1-100 nM) was monitored at 2 min at 37^{o}C with and without the inhibitor diclofenac. Each point represents the mean velocity ± standard error (n=3).

Inhibition of T4 uptake into microvessels

Since Oatp1c1 is expressed nearly exclusively at the BBB, the physiological relevance of NSAID inhibition of T4 uptake was examined utilizing an *ex vivo* transport system isolated brain microvessels. T4 uptake inhibition into microvessels was most strongly inhibited by meclofenamic acid (14.82 ± 3.11%), followed by diclofenac (19.87 ± 6.56%) and fenamic acid (28.54 ± 4.73%), duplicating the hierarchy of inhibition assumed in the *in vitro* cell culture model (Fig. 6).

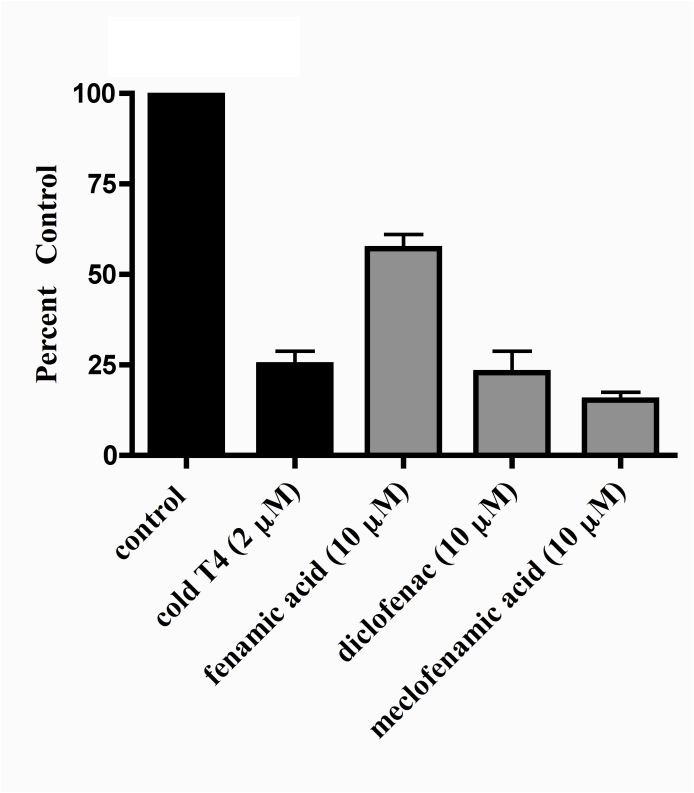

Figure 6. Fenamic acids inhibit ^{125}I-T4 uptake in rat microvessels. Effect of fenamic acid, diclofenac and meclofenamic acid (10 μM and 100 μM) on the uptake of ^{125}I-T4 in adult rat cerebral microvessels over 5 min at 37^{o}C. Values represent mean uptake ± standard error (n=3-5).

Discussion

Chalmers and colleagues previously observed inhibition of 3,3',5 triiodothyronine (T3) uptake in cultured hepatocytes in the presence of mono and disubstituted fenamic acids (Chalmers et al., 1993). We now report that members of the fenamic acid family of NSAIDs inhibit Oatp1c1-mediated T4 transport in a competitive manner suggesting that Oatp1c1 transports this family of drugs across the plasma membrane. Interestingly, meclofenamic acid is the strongest T4 transport competitor, followed by diclofenac and fenamic acid. Similar to our data (Fig. 3), when a library of 26 fenamic acid derivatives was screened for L-T3 uptake inhibition in H4 rat hepatoma cells, meclofenamic acid was the most potent inhibitor (Chalmers et al., 1993). This hierarchical pattern of Oatp1c1-mediated T4 transport inhibition mirrors the degree of cyclooxygenase 1 (COX-1) inhibition in a whole blood assays by these NSAIDs (Vane, 2000). Thus, the relatively stronger COX inhibitory effect of meclofenamic acid may reflect enhanced intracellular delivery.

COX-1 and COX-2 are endoplasmic reticulum (ER) localized enzymes responsible for prostaglandin synthesis. NSAIDs inhibit COX activity through binding to the active site in the ER lumen. Interestingly, our immunocytochemistry data suggests that Oatp1c1 protein is localized both to plasma and perinuclear membranes (Fig. 1B). Oatp expression in perinuclear membranes such as the ER may have functional significance. For example, ER localized Oatps may facilitate NSAID delivery into the ER lumen where the drug is now free to bind to the COX active site. In support of a role for Oatps in ER transport, Gollan et al. have demonstrated saturable transport of the Oatp substrate $E_2$17βG across ER derived microsomal membranes (Battaglia and Gollan,

2001). Interestingly, this transport process was inhibited by model organic anions including bromosulfophthalein (Battaglia and Gollan, 2001).

A structural comparison suggests why the fenamates are able to inhibit T4 transport and presumably can themselves be transported by Oatp1c1 (Fig. 7). A structural overlay (Fig. 7 Upper panel) was optimized by searching conformational space using simulated annealing for alternative low energy conformations until the resulting structures could be superimposed. The superposition shows alignment of the carboxylate (upper left) and one benzylic ring as well as a number of atoms between them. The electrostatic surface potential in Fig. 7 (Lower panel) further highlights these commonalities. The volume occupied by meclofenamic acid also correlates very highly with T4 (Fig. 7 Lower panel). These features compare well to the determinants of binding affinity identified in a recent Oatp1a5 QSAR paper (Yarim et al., 2005). Also in that paper, it was shown that additional steric bulk near the negative charge can have a positive effect on binding. Though Oatp1c1 substrates may differ in detail, this may play a role in the fenamates binding affinity, having the steric bulk of a 6-membered ring near the carboxylate. In addition, the higher affinity of meclofenamic acid for Oatp1c1 could be due to the added steric bulk of the methyl group on its benzylic ring, also shown to be important in the previous study (Yarim et al., 2005). Not obvious from that work is the importance of the iodine or chlorine substituents on the benzene ring. The increase in affinity of diclofenac with respect to fenamic acid to Oatp1c1 suggests this substitution is important. Further, it improves the volume overlap with the very high affinity T4.

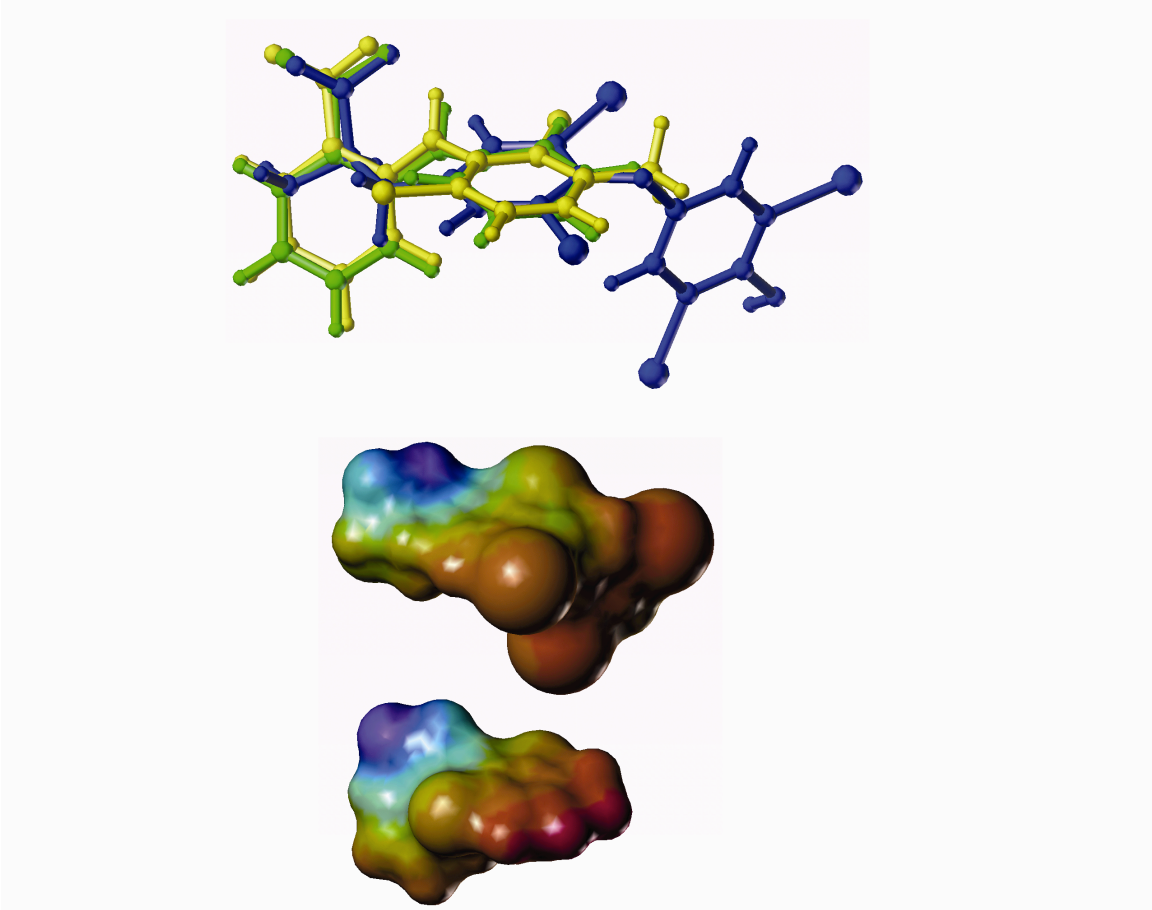

Figure 7. Structural and electrostatic comparison of T4 and fenamate inhibitors of Oatp1c1. (Upper panel) Overlay of T4 (blue), fenamic acid (green), and meclofenamic acid (yellow) using Multifit in Sybyl 7.2. Twelve atoms in each molecule were used in the alignment. Simulated annealing was used to sample viable structural conformations. (Lower panel) Electrostatic surface potential of T4 (top) and meclofenamic acid (bottom). The electrostatic potential was mapped onto the Connolly surface using MOLCAD.

Tight junctions prevent paracellular diffusion of molecules into brain interstitial spaces. Compounds of smaller molecular weights with high lipophilicity and low polarizability and hydrogen bonding potential are more likely to passively diffuse across the BBB (Habgood et al., 2000). Most NSAIDs are lipophilic with ClogP values (logP octanol/water) approximately in the 4-6 range for fenamic acid analogs (Chalmers et al., 1993). Despite the inherent lipophilic nature of these compounds, over 99% of NSAIDs circulate as organic anions due to their acidic character (pKa<6) (Parepally et al., 2006). This severely limits availability of the diffusible non-ionized fraction. As a result, NSAIDs must cross the BBB through carrier-mediated transport at the plasma membrane (Chen et al., 2004). In our study, all fenamates tested significantly inhibited T4 uptake in isolated rat brain microvessels, likely due in part through inhibition of Oatp1c1 (Fig. 6). In addition to our present studies, other work implicates Oatps in NSAID transport at the BBB. For example, Oatp1a4 transport, another Oatp expressed at the BBB, is inhibited by ketoprofen and indomethacin at high concentrations, and in addition to the fenamates, Oatp1c1 transports ketoprofen with low affinity (Shitara et al., 2002; Sugiyama et al., 2003).

In addition to transporting NSAIDs across the BBB, Oatp-mediated NSAID uptake into the endothelial cell may have direct functional consequence as these cells express both COX-1 and COX-2 isoforms (Glasgow and Middleton, 2001; Parfenova et al., 1997; Parfenova et al., 2002; Parfenova et al., 2001). Endothelium-derived vasodilatory prostanoids are critical mediators of cerebral blood flow under both basal and stimulated conditions. Oatp1c1 transported fenamic acids, active on both COX-1 and COX-2, could potentially inhibit endothelial prostanoid synthesis. Under certain

conditions, this event could have potentially severe consequences in the regulation of cerebral circulation and result in serious neurological complications including hypoxic injuries, especially in the developing neonate (Parfenova et al., 2002).

In addition to the fenamates, iopanoic acid, phenytoin and ICG also inhibited Oatp1c1-mediated T4 uptake. Iopanoic acid inhibits T4 uptake in cultured hepatocytes (Topliss et al., 1989). This radioopaque, cholecystographic agent is a known inhibitor of type II deiodinase (D2), the enzyme that catalyzes the outer ring deiodination of T4 to produce the active thyroid hormone T3 (Coppola et al., 2005). This drug is used to treat T4 overdoses and hyperthyroidism (Bal et al., 2005). The reasons behind the efficacious nature of iopanoic acid treatment are likely two-fold. In addition to D2 activity, iopanoic acid may also reduce T4 transport (via Oatp1c1 in some tissues), leading to decreased intracellular T4 availability for T3 conversion. The anticonvulsant phenytoin has multiple effects on the thyroid hormone system, including inhibiting anterior pituitary cell T3 uptake (Lim et al., 1996; Smith and Surks, 1984). This drug acted as a partial antagonist of Oatp1c1 T4 uptake as complete inhibition was not achieved. Indeed, T4 uptake was quenched nearly maximally at phenytoin concentrations near the IC_{50}. ICG, a dye used in measuring cardiac output, was the most potent inhibitor of Oatp1c1-mediated T4 uptake. This model organic anion also inhibits transport by other Oatps, but the inhibitory effect is not global among family members. For example, $E_2$17βG uptake is inhibited by ICG in Oatp1a4, but not Oatp1b3 transfected HEK293 cells (Cui et al., 2001). It is conceivable that T4 binding site similarities in Oatp1c1 and Oatp1a4 account for the ICG inhibition observed in cells transfected with these two transporters.

The fenamic acids, phenytoin, ICG and iopanoic acids are all clinically used. Our T4 dose response assays indicated that ICG, phenytoin, iopanoic acid, and all fenamic acid analogs have IC_{50}s below or near the blood plasma levels after therapeutic dose administration. Thus, antagonistic drug-hormone interactions may influence the uptake of Oatp1c1 substrates into the brain. In our *in vitro* transport system, inhibition assays were performed with Krebs-Henseleit buffer in the absence of serum. Therefore, our reported IC_{50} measurements (Table 1) correspond to the capacity of free drug concentrations to inhibit uptake of 1 nM ^{125}I-T4 uptake. Reported blood plasma levels after therapeutic dosing refer to total drug concentrations, of which, a significant portion is protein bound. For example, 99% of diclofenac circulates bound to plasma albumin (Davies and Skjodt, 2000). The blood plasma concentration of diclofenac after standard dosage is 7.1 μM (Voltaren, 2003). Therefore, the pharmacologically active free concentration is 71 nM. In contrast, free T4 concentrations in adult humans are approximately 12 pM. Thus, diclofenac blood plasma levels achieved after standard dosing maintain the potential to influence T4 uptake via Oatp1c1. However, full inhibition of T4 transport will not likely occur as free drug levels are well below the measured Oatp1c1 IC_{50}. This pattern repeats for the other inhibitors tested. Meclofenamic acid, ICG, iopanoic acid and phenytoin all have IC_{50}s (Table 1) near the blood plasma levels after standard dosing (16.2 μM, 3.6 μM, 8 μM, 6.7 μM, respectively), but are highly bound in plasma (Kennedy and van Rij, 2006; Meyer et al., 2001; Moss et al., 1979). Thus, the unbound fraction of these drugs is well below the IC_{50} for Oatp1c1 T4 transport. Nonetheless, the rate of T4 transport will likely be reduced. Given the time dependent developmental regulation of many thyroid hormone

responsive brain genes, this delay may exert a deleterious biological effect (Anderson et al., 2003). In addition, drug-drug interactions between these tested compounds are possible, if administered simultaneously.

In conclusion, we have identified multiple inhibitors of Oatp1c1 T4 transport. These compounds, including the fenamic acids, iopanoic acid, ICG and phenytoin demonstrated IC_{50}s in the low micromolar to high nanomolar range. The competitive nature of fenamate inhibition of T4 transport along with structural alignments suggests Oatp1c1 transports this family of NSAIDs. Oatp1c1 expression in brain endothelial cells suggests an important role for Oatps in brain NSAID transport. Future animal experiments will further elucidate the *in vivo* scope and relevance of Oatp1c1-T4-fenamate interactions.

Chapter 5

Molecular determinants required for Oatp1c1 substrate specificity

Daniel E. Westholm, Joseph A. Schneider, Grant W. Anderson, Jon N. Rumbley

Abstract

Organic anion transporting polypeptides (Oatps/OATPs) are a superfamily of bidirectional solute carriers selectively expressed in tissues including the blood-brain barrier (BBB) endothelial and blood-cerebrospinal fluid barrier epithelial cells. Multispecific Oatps/OATPs transport substrates as structurally divergent as iodinated thyronines, glucuronidated sterols, and prostanoids. Our limited understanding of substrate-transporter recognition represents an important problem because rational design of new drugs able to effectively penetrate the brain barriers requires incorporating chemical structures recognized by bidirectional and influx transporters expressed in brain barrier cells into drug design. Therefore, in the present study we performed an analysis of substrates and inhibitors of the BBB high affinity thyroxine (T4) transporter Oatp1c1 to determine common structural characteristics required for activity at the Oatp1c1 active site. Oatp1c1 is an ideal candidate for rationally designing drugs for central nervous system (CNS) penetrance as this transporter is expressed in the BBB endothelial cell and mediates transport of neuroactive hormones (e.g. T4) and drugs (e.g. fenamates). K_i values for Oatp1c1-mediated ^{125}I-T4 transport inhibition were obtained for a panel of Oatp1c1 substrates and competitive inhibitors including 4-methylumbelliferone sulfate (4-MUS), AZT, bromosulfophthalein, diclofenac, $E_2$17βG, $E_3$17βG, estrone-3-sulfate, fenamic acid, ketoprofen, iopanoic acid, meclofenamic acid, pravastatin, PFOS, PFOA, prednisilone-21G, taurocholate and T3. Competitive inhibition of Oatp1c1-mediated T4 transport was determined using Lineweaver-Burk plots. In addition, K_i values for Oatp1c1-mediated ^{125}I-T4 transport inhibition were determined for five thyroid hormone derivatives: T4, T3, T4-amine, T1-amine, and T4-acetic acid. Partial atomic point

charges and electrostatic surface potential maps were determined for all compounds tested. This information, combined with the measured K_i values were used to create an Oatp1c1 pharmacophore model. It was found that two distinct hydrophobic centers and a negative charge were characteristic for high affinity Oatp1c1 binding.

Introduction

Organic anion transporting polypeptides (Oatps, rodents; OATPs, humans) are membrane transporters of structurally diverse organic solutes, ranging from conjugated sterols, bile salts, hormones drugs and toxins (Hagenbuch and Meier, 2003). Most members are widely expressed throughout the body in organs such the brain, liver, kidney, and intestine (Hagenbuch and Meier, 2003). Within these organs, Oatps/OATPs are expressed in a variety of polarized barrier cells important in the deposition and elimination of multiple endogenous compounds, drugs and their metabolites (Ito et al., 2005). In addition, Oatps/OATPs have been implicated in a variety of drug-drug interactions at these sites (Kim, 2003; Shitara et al., 2004). Thus, the identification of complementary features between Oatp/OATP protein and substrates will aid in both the design of drugs to preferentially target Oatps/OATPs and the avoidance of potentially harmful drug-drug interactions involving Oatps/OATPs. For a complete picture of Oatp-substrate binding site interactions, investigations should be approached from both the perspective of the substrate and the transporter (Chang and Swaan, 2006). When approaching transporter-substrate interactions from the protein point of view, high resolution 3-dimensional structures are the gold standard for substrate binding site(s) and docking analyses. However, membrane proteins, such as Oatps/OATPs, have proven difficult to isolate and crystalize (Winiwarter and Hilgendorf, 2008). Therefore, studies examining Oatp protein structure are reliant on targeted mutagenesis of the protein, homology modeling to the few 12 transmembrane transporters with solved 3-dimensional structures, or ab initio modeling whereby 3-dimensional structure is inferred based on primary polypeptide sequence (Chang and Swaan, 2006). Such studies, such as those

performed in Chapter 3, are useful in assessing structure-function relationships, but are relatively time consuming and often assess the interactions between the protein and a single substrate. To augment these studies, substrate based structural studies in the form of CoMFA, QSAR and pharmacophore analyses are used as a complimentary and rapid assessment of transporter substrate relationships using substrates of varied affinities and structures.

A limited number of substrate structure-based studies have been performed in Oatps/OATPs. Yarim et al. performed a 3D-QSAR analysis on a heterogenous training set of 18 substrates of Oatp1a5 (Yarim et al., 2005). The authors developed a hypothetical pharmacophore model containing a negatively charged group on one end, an extended hydrophobic domain in the central part of the structure, and a hydrogen bond donor at the opposite end. Chang et al. performed a meta-pharmacophore analysis of Oatp1a1 and OATP1B1 substrates using combined data set from the literature (Chang et al., 2005). The authors created a training set for rat Oatp1a1 that contained 26 molecules with a range of K_m values from 0.015 to 3300 μM. In general, the results reported by Chang et al. were in agreement with those published by Yarim et al. The pharmacophore generated in this case contained two hydrogen bond acceptors and three hydrophobes. Again, the polar groups (hydrogen bond acceptors) were located on the opposite ends of the molecules. Finally Gui et al. performed a CoMFA analysis of OATP1B1 inhibitors (Gui et al., 2009). The authors screened 39 known nuclear receptor ligands for inhibition activity of OATP1B1-mediated $E_2$17βG transport. A CoMFA model based on a training set of 18 of the newly identified inhibitors was then developed, using molecular structures and experimentally determined K_is. They concluded that an ideal OATP1B1

substrate contains a central hydrophobic region, a flanking negatively charged region, as well as another negatively charged or polar region critical for interacting with OATP1B1 channel surfaces.

The polyspecific nature of Oatp/OATP transport results in partially overlapping substrate specificities of individual Oatp/OATP members (Hagenbuch and Meier, 2004). Thus, it is not surprising that the results from the Yarim, Chang and Gui studies are in general agreement. Moreover, the same transporter, OATP1B1, was used in two of the studies, and the other two transporters, Oatp1a1 and Oatp1a5, are in the same Oatp subfamily, share significant sequence homology and predominantly transport the same catalog of substrates. Still, significant differences in substrate specificity and affinity exist between the various Oatp/OATP isoforms. For example, the cardiac glycoside digoxin is a high affinity substrate of Oatp1a4 (K_m=0.24μM), whereas this molecule is not a substrate of some members of the same Oatp1 family, including Oatp1c1 (Noe et al., 1997; Sugiyama et al., 2003). In addition, multiple Oatps transport thyroxine (T4), including 3 isoforms in rat brain: Oatp1a4, Oatp1a5 and Oatp1c1. However, Oatp1c1 transports T4 with significantly greater affinity compared to Oatp1a4 and Oatp1a5, suggesting the Oatp1c1 binding site is selectively tuned to accept T4 (Suzuki and Abe, 2008). Finally, other Oatps/OATPs transport a very limited panel of substrates, such as Oatp2a1 which functions primarily as a prostaglandin transporter (Kanai et al., 1996; Schuster, 1998). Thus, pharmacophore data derived from one Oatp/OATP isoform cannot necessarily be applied to all Oatps/OATPs.

In the present study we performed an analysis of the substrate structural determinants for Oatp1c1 binding. Compared to other Oatps/OATPs, Oatp1c1 has a

relatively narrow substrate specificity and K_m values are determined for only a few substrates (Sugiyama et al., 2003). In addition, as described in Chapter 2, one of the Oatp1c1 binding sites appears selectively adjusted for T4 binding. These features suggest that the Oatp1c1 pharmacophore may be unique compared to that of other Oatps/OATPs. To begin, K_i values of known Oatp1c1 substrates were experimentally determined for inhibition of Oatp1c1-mediated T4 transport in Oatp1c1 stably transfected HEK293 cells. Next, energy minimized structures, partial atomic point charges and electrostatic surface potential maps were created for all compounds tested, along with competitive inhibitors previously identified in Chapters 2 and 4. These data, combined with the corresponding K_i values were then used to identify structural motifs that support interaction with the Oatp1c1 binding site.

Materials and Methods

Chemicals and Reagents

Radiolabeled ^{125}I-T4 was purchased from Perkin Elmer Life Sciences (specific activity 1080-1320uCi μCi/μg; Wellesley, MA). Unlabeled Oatp1c1 substrates and inhibitors 4-methylumbelliferone sulfate (MUS), 3′-Azido-3′-deoxythymidine (AZT), bromosulfophthalein (BSP), diclofenac, estradiol 17-β-D-glucuronide ($E_2$17βG), estriol 17-β-D-glucuronide ($E_3$17βG), estrone-3-sulfate, fenamic acid, ketoprofen, meclofenamic acid, pravastatin, prednisolone 21-β-D-glucuronide (P-21G), taurocholate, T3, T4, and T4-acetic acid) were purchased from Sigma (St. Louis, MO). Iodothyronamines (T4-amine and T1-amine) were a generous gift from Dr. Thomas Scanlon (Oregon Health and Science University). Perfluorooctylsulfonic acid (PFOS) and perfluorooctanoic acid (PFOA) were generous gifts from 3M Corporation (St. Paul, MN). Cell culture reagents, including blasticidin were obtained from Gibco/Invitrogen (Carlsbad, CA), except for fetal bovine serum from Atlanta Biologicals (Lawrenceville, GA). Except for ketoprofen, chemical mixtures were stereochemically pure.

Cell Culture

HEK293 cells were maintained in 10 cm culture dishes (Sarstedt, Nümbrecht Germany) using Minimum Essential Media containing 10% fetal bovine serum, 10 mM sodium pyruvate, and non-essential amino acids. Cells were incubated at 37^{o}C in a CO_2 incubator.

Generation of stable cell line expressing Oatp1c1

Rat Oatp1c1 was cloned as described in Chapter 4 (Westholm et al., 2009). Briefly, total RNA was isolated and then cDNA reverse transcribed from PN15 rat brain.

PCR was performed on cDNA using *attB*-flanked primers specific for Oatp1c1, resulting in full-length rat Oatp1c1 PCR products flanked with *attB* recombination sequences. *attB*-flanked Oatp1c1 PCR products were then cloned into pDONR221 vector and then subcloned into a pEF-DEST51 expression vector, containing a blasticidin resistance gene (Invitrogen). Next, Oatp1c1-pEF-DEST51 constructs were linearized and transfected into HEK293 cells with lipofectin (Invitrogen). 72 hours after transfection cells were split at low dilution and Oatp1c1 transfected cells were selected using 10 μg/ml blasticidin supplemented in the culture medium. Surviving positive cells were pooled and maintained with standard culture media as described above, supplemented with 2 μg/ml blasticidin.

Transport assays

Transport assays were performed as described in Chapter 2. To begin, cells were plated on 24 well plates coated with rat-tail collagen (Gibco; Carlsbad, CA) at a density of $2x10^5$ cells/well. The next day, 24 hours before the assay, media was changed to MEM supplemented with 10% stripped fetal bovine serum (to remove endogenous bovine T4), 10 mM sodium pyruvate, non-essential amino acids, and 10 mM sodium butyrate (a histone deacetylase inhibitor). Stripped serum was prepared as described in Chapter 2. To begin the assays, media was aspirated and cells were washed twice and then preincubated with fresh Krebs-Henseleit assay buffer (142 mM NaCl, 23.8 mM $NaHCO_3$, 12.5 mM HEPES, 5 mM glucose, 4.83 mM KCl, 1.53 mM $CaCl_2$, 1.2 mM $MgSO_4$, and 0.96 mM KH_2PO_4, pH 7.4) for 10 minutes in a CO_2 incubator. Plates were allowed to cool to room temperature and transport was commenced with the addition of 1 nM ^{125}I-T4 (1080-1320μCi μCi/μg) suspended in Krebs-Henseleit buffer to the cells. Cells were

incubated at room temperature for designated time periods, then isotopic media was removed and cells were washed twice with fresh Krebs-Henseleit buffer. Cells were then lysed with 0.5% TritonX100 and radioactivity of lysate was measured with a WIZARD^2 Automatic Gamma Counter (Perkin Elmer). Uptake was corrected for protein content which was assessed with a BCA assay (Pierce; Rockford IL). Specific assays in the form of dose responses and Lineweaver-Burks were performed as described in Chapter 2. Non-linear regression was performed using Graph Pad Prism version 4.0 (Graph Pad Software; San Diego, CA) as described in Chapter 2.

Structural computations

Structural computations in the form of energy minimization, partial atomic point charges calculations, and electrostatic surface potential maps were performed similarly for all compounds discussed in this chapter. Chemical structures were initially mined using PubChem (http://pubchem.ncbi.nlm.nih.gov). Stereocenters were verified by examining the same structures listed at ChemSpider (http://www.chemspider.com) and previously published studies using them. Chemical structures in isomeric SMILES format were imported into ChemDraw Ultra 11.0 (Cambridgesoft; Cambridge, MA) to generate 2-D structures. 2-D structures were then transferred to ChemDraw 3D Ultra (Cambridgesoft) to produce energy minimized structures with the built-in MOPAC 6.0 program with PM3 function. With these programs, the energy minimized conformation is achieved when consecutive perturbations result in no changes in the minimum potential energy surface of the structure.

Once optimized structures were achieved, partial atomic point charges were calculated with a Mulliken population analysis in MOPAC. With this program, electron

populations and densities across the entire molecule were determined to calculate partial point charges. The structures with calculated partial atomic point charges were saved in SYBL Mol2 format. This information was then used to calculate electrostatic surface potential for each structure using the SYBL 8.0 modeling package MOLCAD (Tripos, Inc.; St. Louis, MO).

To generate an Oatp1c1 pharmacophore, a molecular database was assembled containing 17 structures with associated partial atomic point charges and K_i values (see results section). With this information, an alignment between all 17 structures was performed using GALAHAD (Tripos, Inc.). The GALAHAD alignment was produced using molecular features alignment as opposed to an individual atom alignment. With the GALAHAD alignment, characteristic charges, sterics, and hydrophobic regions were determined for each molecule. During this process, molecular flexibility was allowed, giving the program a large amount of conformational space to sample. Based on these features, the structures were aligned to generate an Oatp1c1 pharmacophore. Overall, 20 pharmacophore models were generated, of which, 4 contained reasonable conformers of T4, the highest affinity substrate. The model represented here accommodated the largest number of measured inhibitors and is predicted to have the highest discriminatory ability against a random database search for novel compounds.

Results

A list of known and potential Oatp1c1 substrates was compiled to determine K_i values for inhibition of Oatp1c1-mediated ^{125}I-T4 transport and develop an overall Oatp1c1 pharmacophore model. Based on a literature search and our own data, BSP, AZT, taurocholate, pravastatin, ketoprofen, estrone-3-sulfate, $E_2$17βG, $E_3$17βG, P-21G, fenamic acid, diclofenac, meclofenamic acid, iopanoic acid, PFOS, PFOA, 4-MUS, T4, T3, T4-acetic acid, T4AM, T1AM, were identified as known or potential Oatp1c1 substrates. K_i values for all of these compounds along with associated energy minimized structures and partial atomic point charges were used to inform the Oatp1c1 pharmacophore model. The structures of all compounds used in the dose responses and pharmacophore model are shown in Figure 1.

Oatp1c1 time course for ^{125}I-T4 transport

To establish a more high throughput assay system we converted our transport assay conditions from 37^{o}C to room temperature. Therefore, a new Oatp1c1 T4 transport time course was required to establish linear conditions for room temperature Oatp1c1-dependent T4 transport. As observed at 37^{o}C, Oatp1c1 transfected cells transported ^{125}-T4 in a time dependent manner at room temperature. Uptake was linear for the first 7.5 min, then slowly transitioned from the initial linear phase until equilibrium was reached at approximately 45 min (Fig 2).

Oatp1c1 dose response for ^{125}I-T4 transport inhibition

K_i values for known and putative Oatp1c1 substrates were calculated using dose responses for inhibition of Oatp1c1-mediated T4 transport. Oatp1c1-mediated uptake of 1nM ^{125}I-T4 was monitored at 5 min room temperature incubations in the presence of

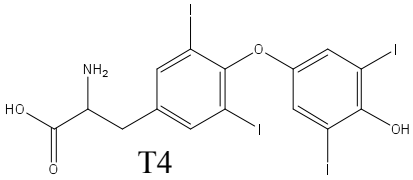

T4

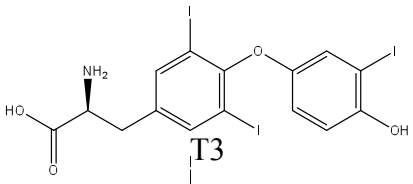

T3

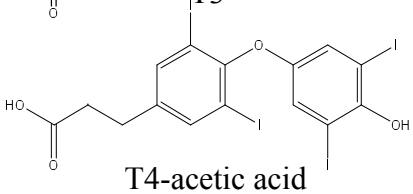

T4-acetic acid

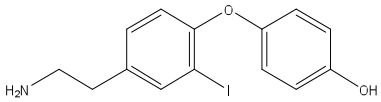

T1 amine

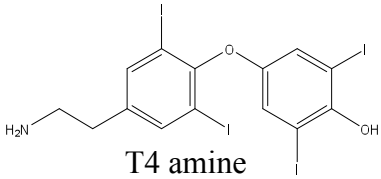

T4 amine

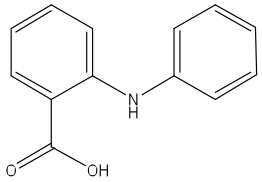

Fenamic Acid

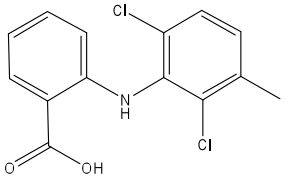

Meclofenamic Acid

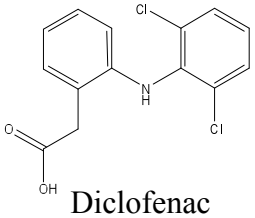

Diclofenac

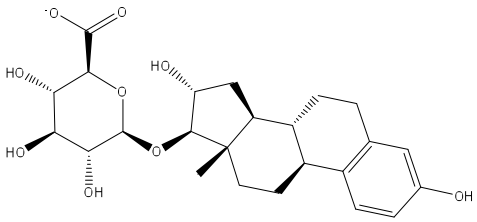

$E_3$17βG

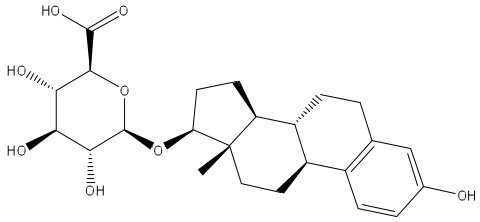

$E_2$17βG

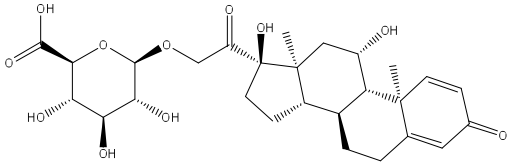

P-21G

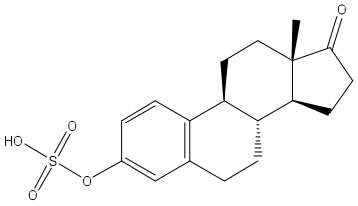

Estrone 3-sulfate

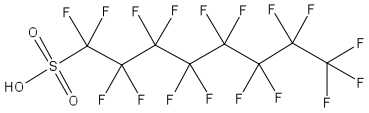

Perfluorooctylsulfonic acid

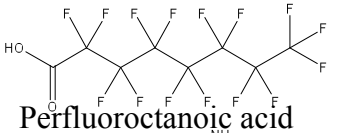

Perfluoroctanoic acid

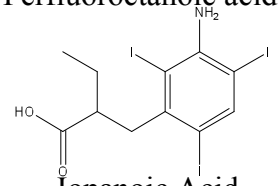

Iopanoic Acid

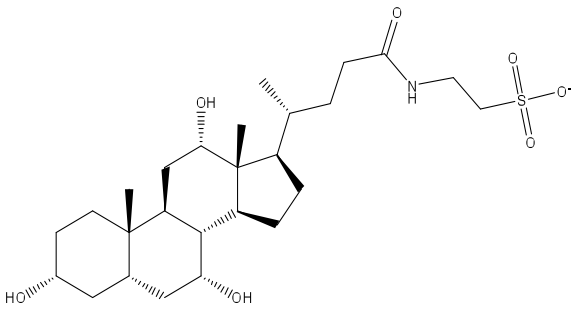

Taurocholate

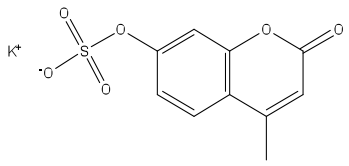

4-methylumbelliferyl sulfate

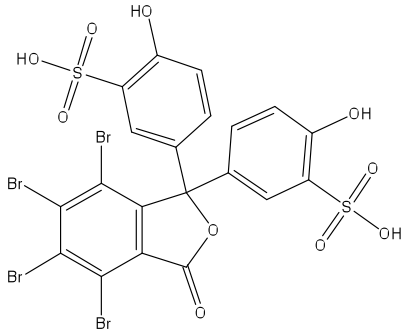

Bromosulfophthalein (BSP)

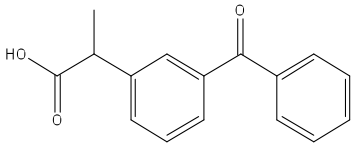

Ketoprofen

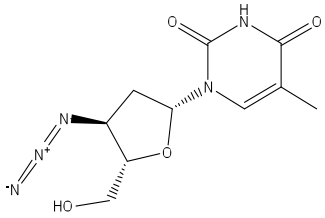

3’-Azido-3’-deoxythymidine (AZT)

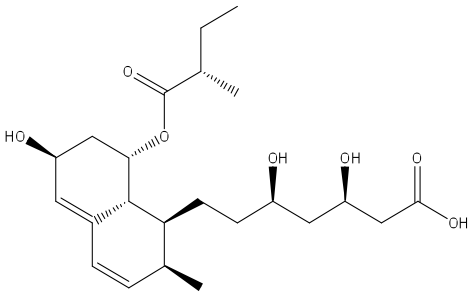

Pravastatin

Figure 1. Chemical structures of the model substrate T4, and 17 additional Oatp1c1 substrates and competitive inhibitors. These structures were selected based on their known activity within the Oatp1c1 active site and/or structural similarity to T4.

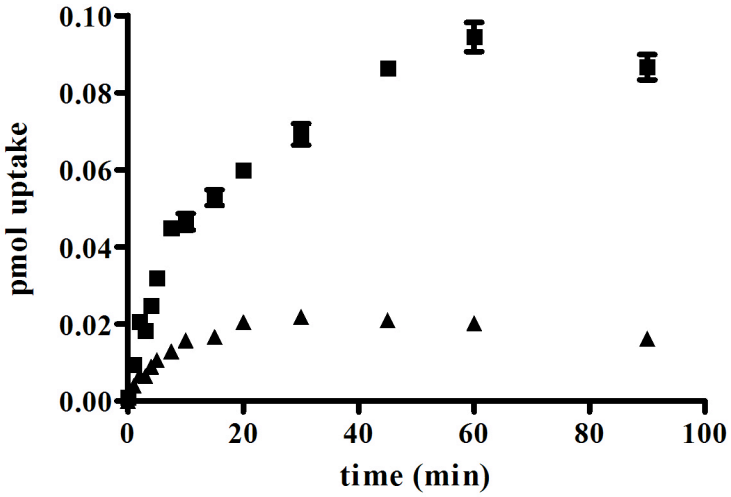

Figure 2. ^{125}I-T4 is transported at room temperature in a time dependent manner by Oatp1c1 stably transfected HEK293 cells. Oatp1c1 transfected cells (squares) and empty vector transfected cells (triangles) were incubated in the presence of 1 nM ^{125}I-T4 for increasing amounts of time. Each point represents the mean uptake ± standard error (n=3) at different periods of time.

increasing concentrations of each compound (Fig 3). T4 and T4-acetic acid were the strongest inhibitors, followed by BSP, T4AM, T3, estrone-3-sulfate, iopanoic acid, meclofenamic acid, diclofenac, PFOS, TIAM, PFOA, fenamic acid, P-21G, taurocholate, $E_2$17βG, $E_3$17βG, pravastatin, and ketoprofen. Table 1 displays the K_i values calculated from the dose responses, along with those previously determined in Chapter 2 and 4. AZT did not inhibit, while a dose response could not be fit for 4-MUS.

For inhibitors without proven substrate specificity, Lineweaver-Burk plots were performed to diagnose the type of Oatp1c1 inhibition. Fenamic acid, meclofenamic acid, iopanoic acid, and PFOS and PFOA displayed competitive inhibition, as revealed by y-axis intersections of linear regression lines in both the presence (dashed lines) and absence (solid line) of inhibitor (Figure 4 A-E). Competitive inhibition by $E_2$17βG, $E_3$17βG, P-21G was demonstrated in Chapter 2 (see Chapter 2, Fig 5) and competitive inhibition by diclofenac was demonstrated in Chapter 4 (see Chapter 4, Fig 5). Lineweaver-Burk plots for T4AM and T1AM were not generated due to insufficient provided quantities of these two compounds.

Calculation of partial atomic point charges and electrostatic surface potential maps

Partial atomic point charges were calculated for all structures used in the Oatp1c1 pharmacophore analysis using a Mulliken population analysis in MOPAC. In all cases, correct charge distribution was observed across different molecular regions, for example in conjugated ring systems and oxygen atoms of carboxyl groups. The verified partial atomic point charges were then used for calculating electrostatic surface potential maps.

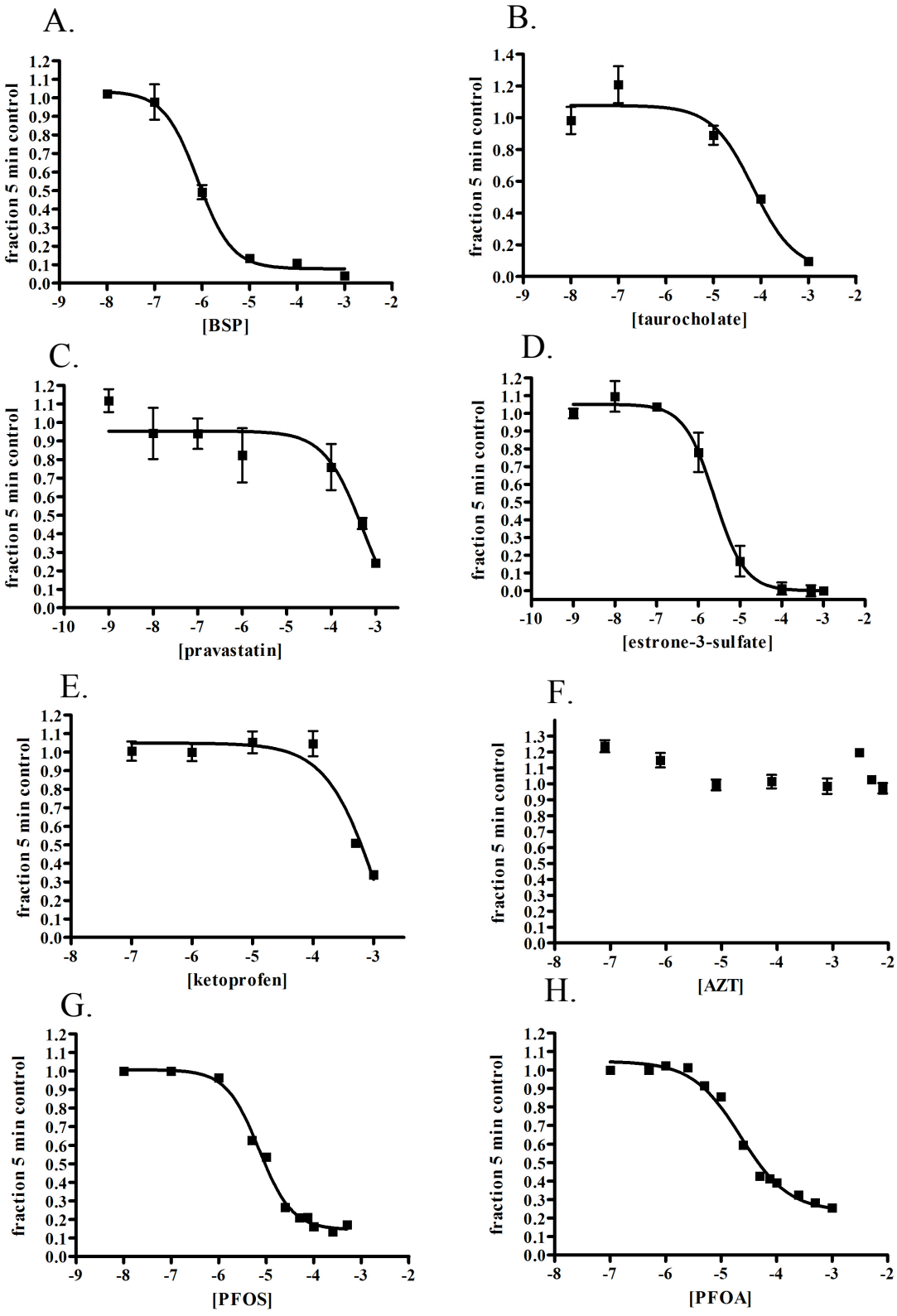
A.
fraction 5 min control
[BSP]
B.
fraction 5 min control
[taurocholate]
C.
fraction 5 min control
[pravastatin]
D.
fraction 5 min control
[estrone-3-sulfate]
E.
fraction 5 min control
[ketoprofen]
F.
fraction 5 min control
[AZT]
G.
fraction 5 min control
[PFOS]
H.
fraction 5 min control
[PFOA]

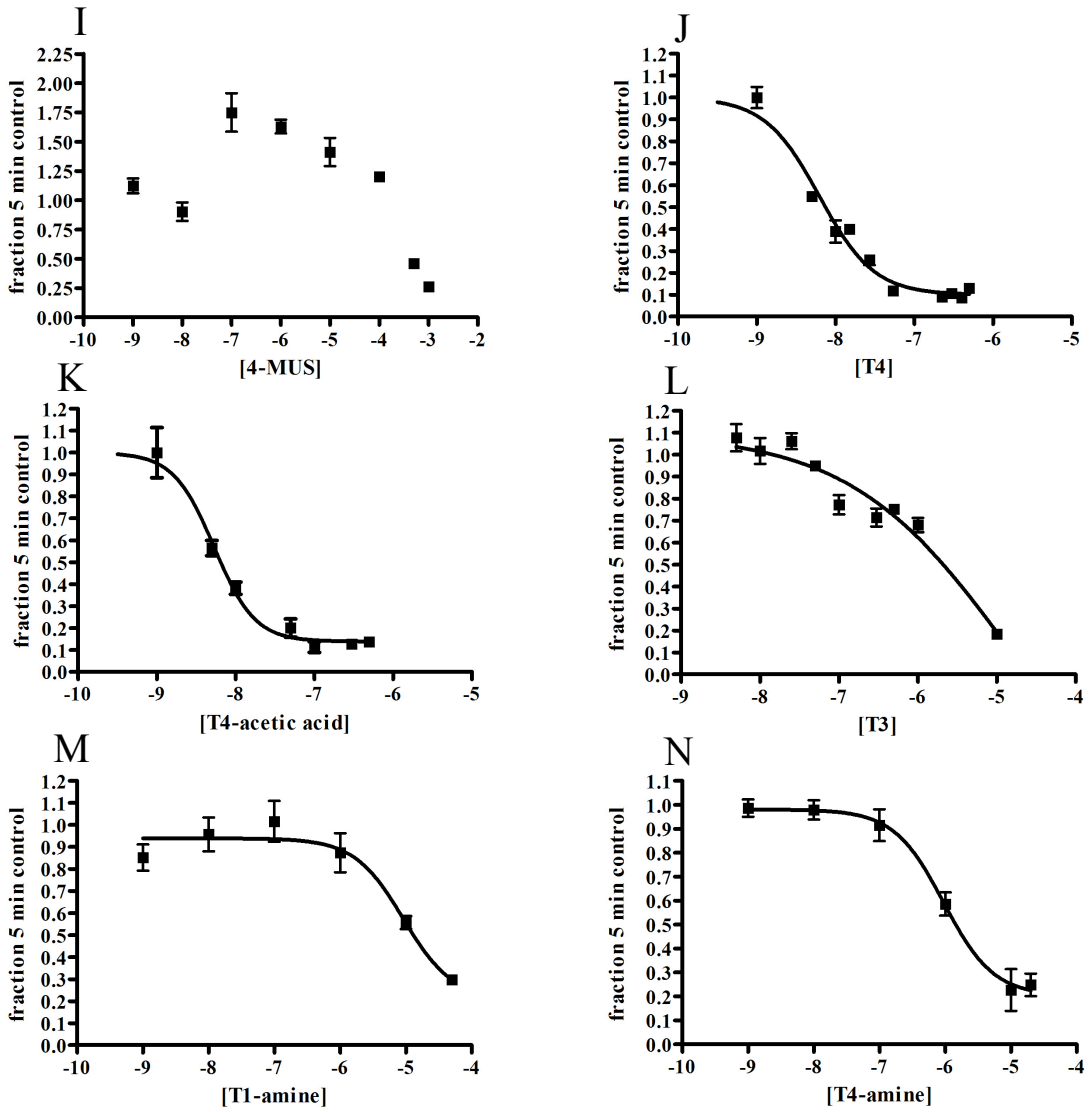

Figure 3. Inhibition of Oatp1c1-mediated T4 transport by various known Oatp1c1 substrates and thyroid hormone derivatives (A-N). Uptake of 1 nM ^{125}I-T4 in the presence of increasing concentrations of inhibitors was examined with 5 min incubations at room temperature. Dose response curves were fitted using non-linear regression (Graph Pad Prism). Each point represents the mean uptake ± standard error (n=3).

Inhibitor	**K_i (μM)**
BSP	0.81
Taurocholate	68.6
Pravastatin	518
Ketoprofen	1300
Estrone-3-sulfate	2.5
T4	0.0062
T3	2.1
T4AM	0.95
T1AM	9.1
T4-acetic acid	0.0053
AZT	did not inhibit (tested to 8 mM)
4-MUS	undetermined
Fenamic acid	25
Diclofenac	4
Meclofenamic acid	3
Iopanoic acid	3
PFOS	7.1
PFOA	20
$E_2$17bG	81
$E_3$17bG	98
P-21G	61

Table 1. Summary of K_i values for Oatp1c1-mediated T4 transport inhibition.

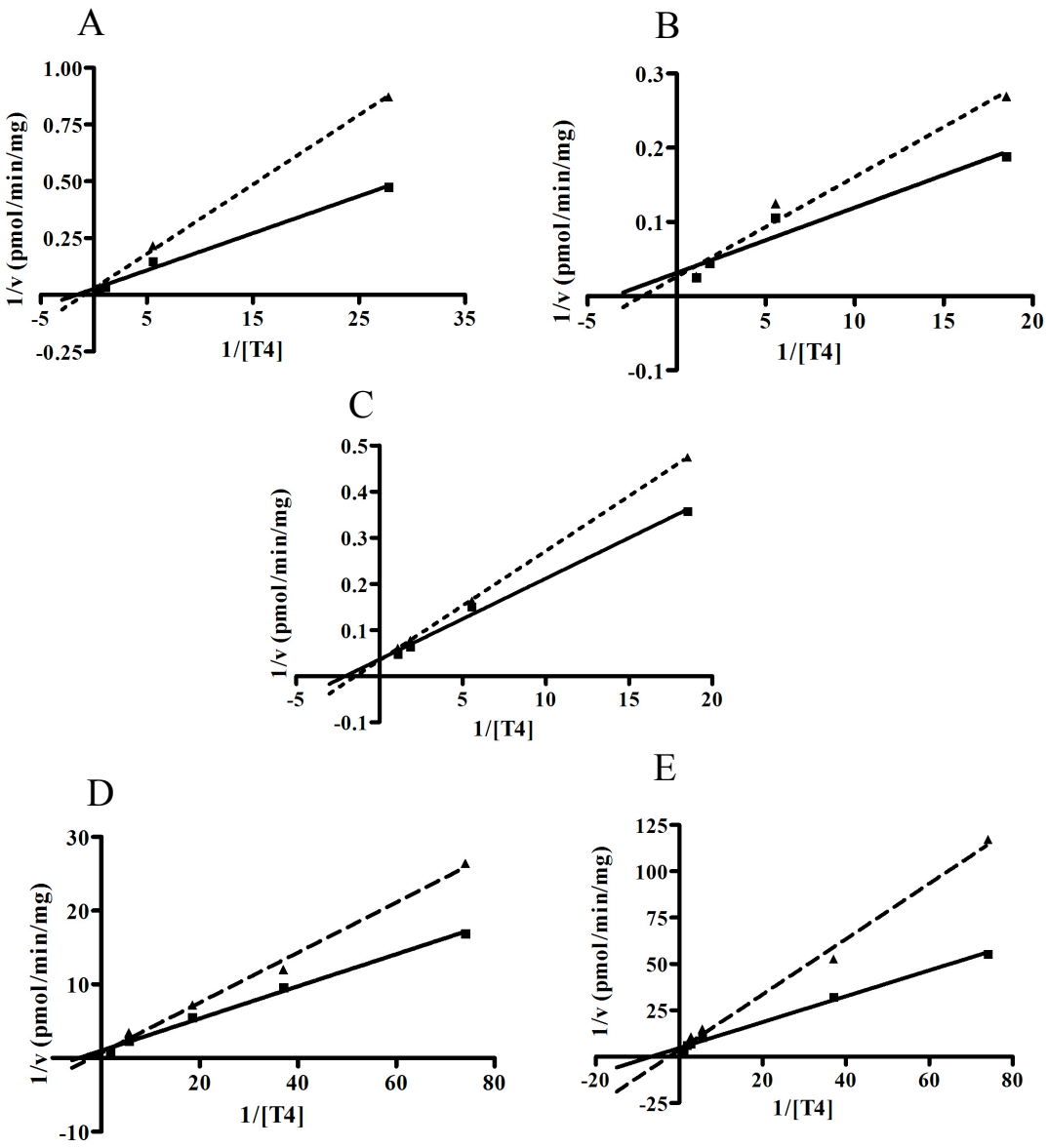

Figure 4. Fenamic acids, iopanoic acid and perflourinated compounds competitively inhibit Oatp1c1-mediated T4 transport. Uptake of varying concentrations of T4 was examined in the presence of fenamic acid (A), meclofenamic acid (B), iopanoic acid (C), PFOS (D), and PFOA (E). Lineweaver-Burk plots were graphed as the reciprocal of velocity versus the reciprocal of T4 concentration. Each point represents the mean velocity (n=3).

To identify the molecular characteristics that lead to divergent affinities for Oatp1c1, a comparison of partial point charges and electrostatic surface potentials was performed for a high affinity and low affinity Oatp1c1 substrate. For this analysis, T4 was chosen as the canonical high affinity Oatp1c1 substrate and pravastatin the low affinity Oatp1c1 substrate (Table 1). Partial point charges and electrostatic surface potentials for T4 and pravastatin are displayed in Figure 5. Overall, pravastatin had much greater positive potential distributed across its molecular surface (Fig 5D). In contrast, T4 trended more toward neutral and negative electrostatic potential across its surface (Fig 5B). In addition, the volumetric distribution of pravastatin is distinct from that of T4 leading to unique steric surfaces presented to the Oatp1c1 binding site.

Generation of Oatp1c1 pharmacophore

To more thoroughly map the molecular features associated with Oatp1c1 substrates, we next extended our substrate structural studies to computing an Oatp1c1 pharmacophore. K_i data calculated from the dose responses displayed in Fig 3, along with K_i data generated in Chapters 2 and 4 for $E_2$17βG, $E_3$17βG, P-21G, fenamic acid, diclofenac, meclofenamic acid, and iopanoic acid were used to create an Oatp1c1 pharmacophore. The modeling program GALAHAD generated an Oatp1c1 pharmacophore based on structural alignments using the energy minimized structures, partial atomic point charges, and K_i values of 17 different Oatp1c1 substrates and competitive inhibitors (BSP, diclofenac, $E_2$17βG, $E_3$17βG, estrone-3-sulfate, fenamic acid, iopanoic acid, meclofenamic acid, pravastatin, PFOS, PFOA, P-21G, taurocholate, T4, T3, T4AM, and T1AM). Ketoprofen was not included in the analysis because a

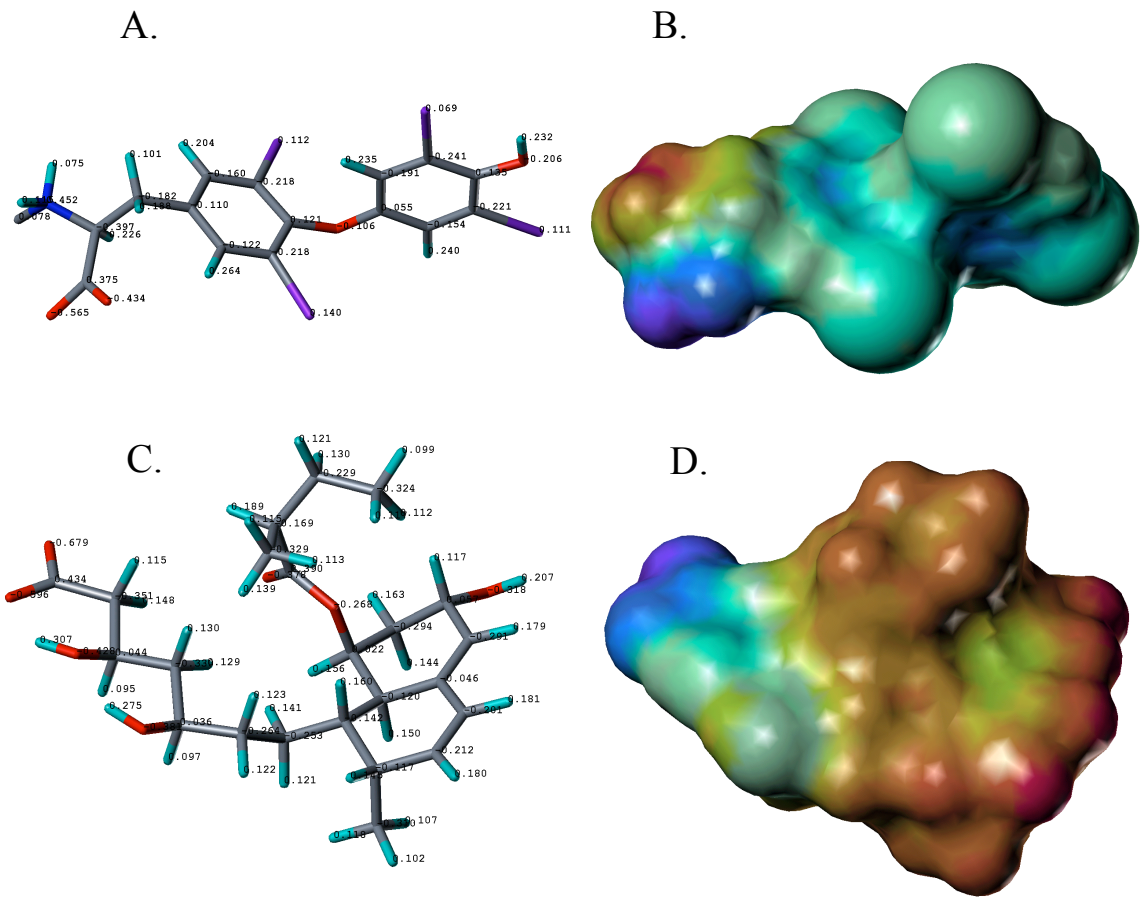

Figure 5. Comparison of partial atomic point charges and electrostatic surface potentials of T4 and pravastatin. Partial atomic point charges were determined on energy minimized structures using a Mulliken population analysis in MOPAC for T4 (A) and pravastatin (C). Partial point charges were then used to calculate electrostatic surface potentials for T4 (B) and pravastatin (D) using the SYBL 8.0 modeling package MOLCAD.

racemic ketoprofen solution was used during the dose response. GALAHAD computations produced a total of 20 different Oatp1c1 pharmacophore models. The pharmacophore model represented in this chapter had the highest spatial score (how well molecules are ordered with respect to one another in space) and hydrogen-bond score (how well all potential hydrogen bond donors and acceptors align with the pharmacophore), and also fit T4 structure the best with respect to the other models (Fig 6). Associated with each pharmacophore model is a score representing the number of the original structures used in the overlay that fit the resulting pharmacophore. Of the 20 models produced by GALAHAD, this model had the most structures (14 of the original 17) that reasonably fit the pharmacophore model.

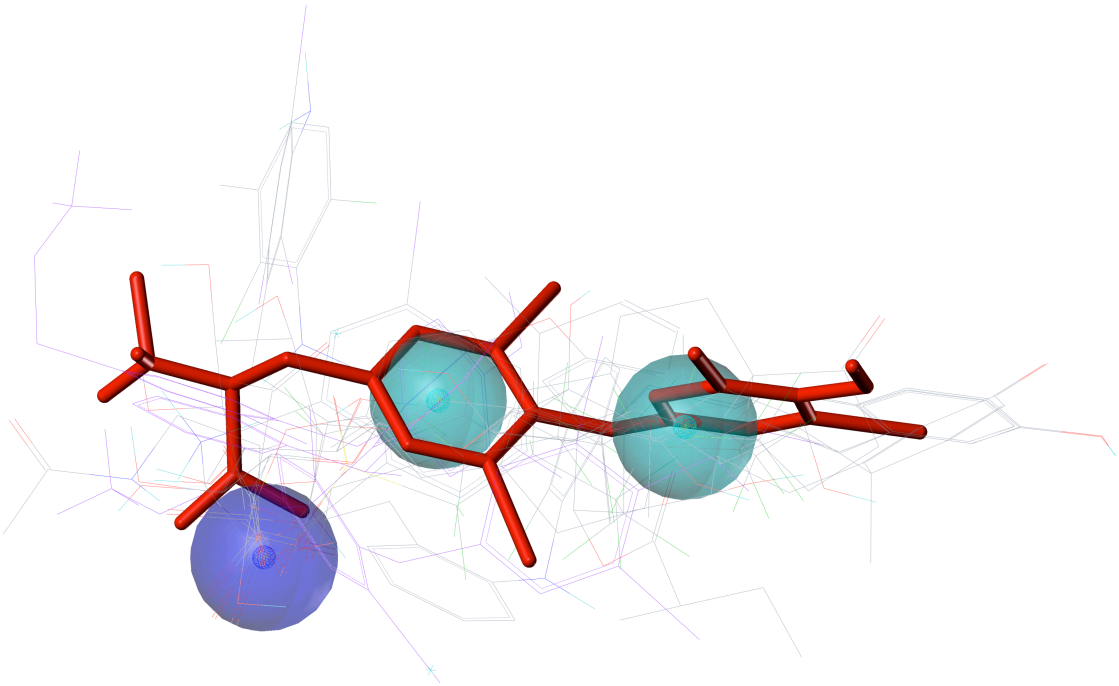

Figure 6. Structural alignment of 17 compounds (stick figures) used in training set for Oatp1c1 pharmacophore generation. Pharmacophore features are represented by blue sphere (negative center) and cyan sphere (hydrophobic centers).

Discussion

In the present study, we determined K_i values and performed structural alignments of multiple substrates and competitive inhibitors of Oatp1c1. The K_i data was combined with electrostatic surface potential maps to generate an Oatp1c1 pharmacophore predictive of the molecular determinants required for Oatp1c1 substrate specificity.

Dose responses for Oatp1c1-mediated transport inhibition using Oatp1c1 substrates identified in a literature search (BSP, estrone-3-sulfate, ketoprofen, pravastatin, taurocholate, 4-MUS, and AZT) yielded K_i values ranging from 0.81 μM to 1.3 mM (Fig 3, Table 1) (Chu et al., 2008; Sugiyama et al., 2003). In dose response assays measuring inhibition of Oatp1c1-mediated T4 transport, the overall carbon structure of the inhibitor did not appear to influence the degree of inhibition as strongly as other characteristics, such as electronegativity and charge of the molecule. For example, the strongest inhibitor of this group, BSP, had a carbon backbone structure quite different than of T4, consisting of four heterogeneous carbon ring structures (Fig 1). One of the weakest inhibitors of the group, pravastatin, has a basic carbon structure more similar to that of T4, with two aromatic 6-member carbon rings connected to an aliphatic carbon chain with a carboxyl group bonded at one end. However, unlike the heavily iodinated T4, pravastatin has no halogenic substitutions, whereas BSP structure contains 4 bromines. This suggests the increase in electronegativity and volume associated with halogen substitutions is important for Oatp1c1 substrate recognition. The pattern of halogenic substitutions leading to increases in Oatp1c1 T4 transport inhibition was also observed with the fenamic acids as discussed in Chapter 4. Fenamic acid, containing no halogenic

substitutions, was a weaker inhibitor than other fenamic acids, including diclofenac and meclofenamic acid, which possessed two chlorine substitutions. For sterol-based structures, the presence of a sulfate significantly increased the affinity for Oatp1c1 inhibition/binding. Estone-3-sulfate yielded a K_i of 2.5 μM, significantly lower than those of the 17 and 21 position glucuronidated sterols, which displayed K_i values of approximately 100 μM. The difference is particularly striking when estrone-3-sulfate inhibition is compared to that of sterols glucuronidated in the 3 postion, including $E_1$3βG (see Chapter 2). The addition of a sulfate, instead of a glucuronide in the 3 position, lowered the K_i of the estrone conjugate by nearly 500-fold. Interestingly, AZT did not inhibit Oatp1c1-mediated T4 transport. A recent report by Chu et al. identified AZT as an inhibitor of Oatp1c1-mediated $E_2$17βG transport, with a K_i of 4.2 mM (Chu et al., 2008). It is possible that AZT binds to regions of the Oatp1c1 binding site occupied by $E_2$17βG, but not T4. These data provide additional support for the two site binding hypothesis for Oatp1c1 transport kinetics.

Dose responses with multiple thyroid hormone derivatives yielded information regarding the moieties of T4 structure important for Oatp1c1-mediated transport. Inhibition of Oatp1c1-mediated T4 transport was assessed with five different thyroid hormone based structures: T4, T3, T4AM, T1AM, and T4-acetic acid. These compounds possess highly similar chemical structures, and thus provided a powerful opportunity to elucidate the regions of T4 structure that are most important in interactions with Oatp1c1. Compared to T4 structure, T3 lacks an outer ring 5' iodine, T4-acetic acid lacks an amine group, T4AM lacks the terminal carboxyl group, and T1AM lacks the terminal carboxyl group, as well as both outer ring and one inner ring iodine (see Fig 1).

The K_i for T4-acetic acid inhibition was nearly identical to that of T4, suggesting that amine group is not important for Oatp1c1 T4 binding. Interestingly, in the case of T3, losing a single outer ring iodine, results in a dramatic decrease in the affinity for the Oatp1c1 binding site. These results repeat the Chu et al. report that T3 is a weak inhibitor of Oatp1c1-mediated T4 influx (Chu et al., 2008). The reasons for the large loss in affinity are likely three fold. First, the sterics of T3 are changed with respect to T4. Iodine is a large atom, thus the replacement of iodine with a hydrogen atom results in a changed steric surface and volume of thyroid hormone. Second, the electrostatics between T4 and T3 are changed. Each iodine contributes a significant amount of electronegativity to the overall thyroid hormone structure due to the high effective nuclear charge associated with this atom. Finally, the removal of an iodine, in the case of T3, may result in freer rotation about the two ring structures, as a result of decreased steric hindrance. A theoretical increase in bond rotation of T3 would lead to an increase in entropy associated with the T3 structure compared to T4. Thus the increase in entropy associated with T3 would make binding more difficult, In order for binding to occur, the atoms must become restrained, drastically reducing the structure's degree of freedom, contributing to a significant entropic penalty for binding. Compared to T4 binding, this would lead to a thermodynamic penalty for T3 binding. However, an initial molecular dynamics simulation of T3 and T4 did not show significant differences in bond rotation (data not shown). Thus, changes in structure volume and electrostatic surface, likely account for the differences between T3 and T4 affinity for Oatp1c1.

The two thyronamines tested, T4AM and T1AM, also displayed reduced affinity to the Oatp1c1 binding site compared to T4, suggesting the T4 carboxyl group is a strong

determinant in Oatp1c1 binding. T4AM displayed a K_i an order of magnitude lower than T1AM, likely due to retention of the 4 iodines on its ring structures. Together, these data suggest that the 5' iodine and carboxyl group are extremely important in T4-Oatp1c1 interactions, while the amine group is less critical. Although substrate specificity was not proven, the ability of both thyronamines to inhibit Oatp1c1-mediated T4 transport suggests these compounds may themselves be transported by Oatp1c1. This is significant, because T1AM is an endogenous form of thyroid hormone and has demonstrated biological activity (Scanlan et al., 2004). T1AM is a ligand of the G protein-coupled receptor, trace amine-associated receptor (TAAR1) and may play a neuromodulary role through interactions with the dopamine and norepinephrine reuptake transporters (Hart et al., 2006; Snead et al., 2007). To date, thyronamine transporters have not been conclusively identified, although Oatp/OATP thyronamine transport has not been exhaustively tested (Ianculescu et al., 2009). Oatp1c1, or other thyroid hormone transporting Oatps/OATPs may be responsible for thyronamine movement across the plasma membrane.

An Oatp1c1 pharmacophore was generated with GALAHAD using alignments based on comparisons of energy minimized structures, electrostatic surface potentials, and K_i values for inhibition of Oatp1c1-mediated T4 transport for 17 different Oatp1c1 substrates and competitive inhibitors. The resulting Oatp1c1 pharmacophore model contains two hydrophobic centers (cyan spheres) and a negative charge area (blue sphere) (Fig 6). The pharmacophore in Figure 6 was chosen to be the best representative amongst 20 other Oatp1c1 pharmacophores predicted by GALAHAD (see results). Of all the pharmacophores predicted, the one represented in Fig 6 had the best fit scores (as

described in results) and best fit the features of T4, the presumed highest affinity substrate. In all dose response experiments, ^{125}I-T4 concentrations were kept at 1 nM. At these concentrations, we predict T4 will only occupy the high affinity binding site. Pharmacophore information derived from the K_i values determined in these experiments, models the key features for binding at the putative Oatp1c1 high affinity T4 binding site. Thus, a pharmacophore model that fits T4 structural features is likely the most accurate. Significant differences exist between our predicted Oatp1c1 pharmacophore model and those predicted using other Oatp/OATP isoforms. First, both the Yarim et al. study and the Gui et al. study predicted a pharmacophore with a single central hydrophobic region (Gui et al., 2009; Yarim et al., 2005). In addition, both of these studies predicted negative charges and/or polar groups at both ends of the substrate. In our Oatp1c1 pharmacophore, only a single negative charge is indicated. These differences likely arise from the bias towards T4-like structures in our alignment and the apparent higher specificity of Oatp1c1 for T4.

The position of T4 within the overlays and accompanying pharmacophore is displayed in bold in Fig 6. The conjugated ring systems of T4 orient well with the hydrophobic centers of the pharmacophore and the carboxylic acid aligns with the negative charge region of the pharmacophore. Confirmatory of the dose response data with T4-acetic acid, a positively charged region (i.e. amino group of T4) is not identified in the Oatp1c1 pharmacophore as important for binding. In addition, the distance between the negative charge and the hydrophobic centers appears to be significant in the Oatp1c1 pharmacophore. This distance constraint may account for some of the dramatic differences in Oatp1c1 affinity between substrates that contain the pharmacophore

requirements of a negative charge and hydrophobic regions. For example, both T4 and pravastatin have negatively charged carboxyl groups, but in pravastatin, the carboxyl group is separated from the hydrophobic plane of its ring system by 7 carbon-carbon bonds. In contrast, the carboxyl group in T4 is separated from the first hydrophobic center by 3 carbon-carbon bonds. The difference in distance between the negative charge and hydrophobic center may have energetic implications for binding surface presentations as well as entropic repercussions with respect to mobility of carboxyl group.

The current Oatp1c1 pharmacophore is an early model. However, most of the molecules used in the pharmacophore calculation fit at least part of the model. GALAHAD has no *a priori* knowledge of structures. Thus, it is has no knowledge that structures like fenamic acid, diclofenac and meclofenamic acid are related. As a result, some molecules with highly similar structures did not overlay in the alignment exactly the same way. This is an important source of error in this initial Oatp1c1 pharmacophore model. The model will be refined through optimized manual alignments where needed and allowing all molecules to explore conformer space.

After optimization, we will use the Oatp1c1 pharmacophore in a number of ways. By searching for the features of the Oatp1c1 pharmacophore amongst structures in a chemical database, potential Oatp substrates may be found and tested for substrate specificity. Oatp1c1 binding activity of candidate substrate will demonstrate the predictive validity of the pharmacophore. In addition, the features of the pharmacophore could be used to rationally design drugs to target Oatp1c1. This is an appealing possibility, as expression at the BBB places Oatp1c1 in a position to facilitate brain

penetration of CNS active drugs. Finally, the refined Oatp1c1 pharmacophore will yield structural information about the Oatp1c1 binding pocket, facilitating the mapping of specific contacts between Oatp1c1 and its substrates.

Chapter 6

Comprehensive discussion, conclusions and future directions

Oatp1c1 transport kinetics

The studies presented in this dissertation were designed to characterize the biochemical properties of the BBB high affinity thyroxine transporter Oatp1c1. To achieve this goal, I assessed Oatp1c1 transport kinetics and structure/function properties, and identified molecular determinants required for recognition of substrates by the transporter.

Oatps/OATPs are multispecific transporters of a large range of amphipathic organic anions (Hagenbuch and Meier, 2003). The promiscuous nature of Oatp/OATP transport dictates that the substrate binding site(s) accept a range of structurally diverse compounds. Examples of identified Oatp substrates range from iodinated thyronines to glucuronidated sterols. This apparent flexibility of Oatp/OATP transport suggests the presence of an extremely plastic binding pocket, capable of handling divergent steric surfaces during substrate recognition and transport. One way Oatps/OATPs may accomplish this multispecific substrate transport is through the use of multiple substrate binding sites, instead of a single, rigid binding pocket. Indeed, several Oatps/OATPs, including Oatp1a4, Oatp1c1, OATP1B1, OATP1B3, OATP2B1, and Oatp4C1, display properties suggestive of multiple binding sites in the form of substrate-dependent inhibition, transport stimulation and atypical kinetics (Grube et al., 2006; Gui et al., 2008; Hagenbuch and Gui, 2008; Mikkaichi et al., 2004; Noe et al., 2007; Sugiyama et al., 2002). Understanding the nature of Oatp/OATP mediated transport will allow more accurate prediction of drug-hormone and drug-drug interactions, as well as facilitate the rational targeting of these transporters for therapeutic drug delivery to the brain.

Based on previously published data demonstrating weaker than predicted transport inhibition between Oatp1c1 substrates T4 and $E_2$17βG, we performed detailed kinetic assessments of Oatp1c1-mediated transport of these two substrates (Chu et al., 2008; Tohyama et al., 2004). Oatp1c1-mediated transport of both T4 and $E_2$17βG was best fit with a biphasic uptake equation, suggesting high and low affinity binding sites for these two substrates exist within Oatp1c1. In addition, it appeared that these substrates interacted with both Oatp1c1 binding sites, but had reciprocal affinities for them. This conclusion is supported by results demonstrating higher cis-inhibition K_i values than transport K_m values for both T4 and $E_2$17βG. In addition, Oatp1c1-mediated T4 transport was competitively inhibited by $E_2$17βG. Thus, I conclude that although T4 and $E_2$17βG interact with Oatp1c1 binding sites with different preference, they interact with the same binding sites.

The teleologic reason for the evolution of multiple substrate binding sites in Oatps/OATPs and other transporters is unknown. Multiple substrate binding sites and/or atypical kinetics have been identified in large number of transporters (Oatps/OATPs, P-gp, MRP1, Na^+ nucleoside transporter type 2) and enzymes (multiple CYP450s, UDP-glucuronosyl transferases (UGTs)) (Gaganis et al., 2007; Karwatsky and Georges, 2004; Li et al., 2001; Shapiro et al., 1999; Tracy, 2006). All of these transporters and enzymes possess the common characteristic of recognizing a broad range of substrates. The presence of multiple binding sites within an Oatp/OATP or other transporter is likely the result of evolutionary selection to allow broader substrate coverage without requiring the generation of a novel gene through gene duplication. In addition, the broad and overlapping substrate specificity of Oatps/OATPs, presumably facilitated through engagement of multiple binding

sites, may play a role in a remote signaling network between various tissues and fluid compartments throughout the body (Ahn and Nigam, 2009).

Oatp1c1 Structure and Function

In Chapter 3, Oatp1c1 structural characteristics and the functional contributions of conserved amino acids within Oatp1c1 were examined. Based on polypeptide sequence conservation between all rat Oatps and the use of eight predictive algorithms, conserved amino acids and putative transmembrane domains of Oatp1c1 were identified. Consensus Oatp1c1 membrane topology yielded 12 transmembrane domains, with the transmembrane domains displaying a higher level of conservation compared to extra- and intracellular domains. A 3-dimensional crystal structure does not yet exist for Oatps/OATPs. However, high resolution crystal structures for three members of the Major Facilitator Superfamily (MFS) of transporters with 12 transmembrane domains have been solved (GlpT, lactose permease, and EmrD) (Abramson et al., 2003; Huang et al., 2003; Yin et al., 2006). Using MODELLER, Oatp1c1 3-dimensional structure was then modeled using the MFS transporters as templates. Polar amino acids in the Oatp1c1 3-dimensional structure were largely oriented towards the substrate pore or intra- and extracellular domains, suggestive of a valid model. I next examined the contributions of conserved amino acids to Oatp1c1 T4 transport and structure. Based on overall conservation, localization within the transmembrane domains, and orientation within the putative substrate pore, D85, E89, N92, W277,W278, G399,G409, R601 and P609 residues were targeted for mutagenesis. D85, E89 and N92 in transmembrane domain 2 all were critical in generating a stable structure for insertion into the plasma membrane. Oatp1c1 amino acids W277,W278, R601 and P609 all play roles in T4 transport, but appear to leave both Oatp1c1 T4 binding sites at least partially functional.

However, conserved glycines within putative transmembrane domain 8 may be involved in defining one of the Oatp1c1 binding sites. When glycines at position 399 and 409 were mutated to alanines in Oatp1c1, concentration dependent T4 transport was near normal until high concentrations of T4 were achieved. At that point, transport velocities were significantly reduced, suggesting the low affinity Oatp1c1 T4 binding site requires glycines at positions 399 and 409 for full functionality.

These initial mutagenesis studies will be used to inform the next set of mutations. For example, R601S and P609 both disrupted T4 transport. These mutations are localized in regions predicted to comprise transmembrane domain 11. Additional mutations targeting amino acids flanking these residues will be generated in order to define the breadth and contributions this region has on Oatp1c1 transport. As a whole, this work will guide the identification of Oatp1c1 binding pockets and the specific amino acids defining the pockets, thus delineating the molecular characteristics required for Oatp1c1 binding and transport. A comprehensive understanding of the molecular determinants of Oatp1c1 required for substrate transport may facilitate the future design of CNS penetrant drugs.

Molecular determinants for Oatp1c1 substrate recognition

Data from Chapters 2, 4, and 5 provided insight into structural moieties required for small molecules to interact with Oatp1c1. In Chapter 2, multiple sterol glucuronides were found to inhibit Oatp1c1-mediated T4 and $E_2$17βG transport. The inhibition by sterol glucuronides had a strong positional effect. Sterols glucuronidated in the 17 or 21 position were more potent inhibitors than those glucuronidated in the 3 position by an order of magnitude. Although fenamates were not directly shown to be Oatp1c1 substrates, in Chapter 4, I established this class of NSAIDs as competive inhibitors of Oatp1c1-mediated T4

transport. Based on structural overlays with T4, the presence of a carboxyl group bonded to a six-membered carbon ring structure appeared to be important in Oatp1c1 recognition. T4 has 4 large, electro-dense iodines on the two tyrosine derived rings. The increase in electronegativity associated with the chlorine substitutions in both diclofenac and meclofenamic acid, may have been responsible for the increase in affinity to Oatp1c1 compared to fenamic acid. In addition, fenamates inhibited T4 uptake into isolated rat brain microvessels.

The potential Oatp1c1-mediated transport of fenamates may prove important clinically. NSAIDS function to inactivate both COX-1 and COX-2. This class of drugs is transported into the target cell, passes through the cytoplasm, is transported into the ER, and binds to the COX active site thereby inhibiting the synthesis of prostaglandins (PG). In adults, epidemiologic evidence indicates that NSAID use is associated with a lower incidence risk of Alzheimer Disease (AD) (Hendrie, 1997; McGeer, 2000; McGeer et al., 1996; O'Banion, 1999; Pasinetti, 2001). AD exhibits a strong inflammatory component initiated and/or exacerbated by fibrillar -beta-sheet beta-amyloid deposits. Prostaglandins, proinflammatory cytokines, and other mediators of inflammation are elevated in and around the senile plaques present in AD brains. Thus, potentiating NSAID uptake, such as Oatp1c1-mediated fenamate transport, to inhibit PG synthesis represents a therapeutic opportunity to combat alzheimers.

In chapter 5, an Oatp1c1 pharmacophore was presented. K_i values for Oatp1c1 inhibition, energy minimized structures, and partial atomic point charges were calculated for known and putative Oatp1c1 substrates. This information was used to inform the generation of an Oatp1c1 pharmacophore. The resulting pharmacophore contained two distinct

hydrophobic centers and a negative charge on one end. As the pharmacophore model is refined in subsequent iterations, novel Oatp1c1 substrates may be predicted, drugs may be rationally designed to target Oatp1c1 for transport, and specifics of substrate interactions with Oatp1c1 may be elucidated.

Oatp transport roles

Data presented in this thesis and elsewhere suggest that Oatps/OATPs, including Oatp1c1 are involved in the membrane transport of various conjugated molecules, including those conjugated with glucuronic acid, sulfate and glutathione (Hagenbuch and Meier, 2004). Metabolic conjugation reactions are accomplished by syntheses such as UDP-glucuronosyl transferases (UGTs), glutathione-S-tranferases (GSTs), and sulfotransferases (SULTs) whereby a functional group (e.g. alcohol, phenol, amine) is masked by the addition of a new group (e.g. acetyl, sulfate, glucuronic acid moieties) which further increase the polarity of the endo- or xenobiotic substrate. Polar compounds produced by conjugation are more soluble in the aqueous portion of the blood, which facilitates trafficking of the conjugated compound to the bile duct, kidney, or other compartment for excretion out of the body. However, the polarity also limits substrate diffusion across lipid bilayers. Thus, these substrates require membrane spanning transporters, such as Oatps/OATPs, to move the conjugates between the blood and target tissues (Strazielle et al., 2004). Transporters such as the Oatps/OATPs are integral partners for the production and elimination of metabolized substrates. Previously, Oatp1c1 was known to transport five conjugated substrates, E3S, $E_2$17βG, troglitazone-sulfate, 4MU-sulfate and 4MU-glucuronide. Data presented in Chapter 2 expanded the list of known conjugated compounds that interact with Oatp1c1. $E_3$17βG and P-21G, previously untested as Oatp1c1 substrates or inhibitors, were shown to competitively

inhibit Oatp1c1-mediated T4 transport, suggesting these two glucuronidated molecules may also be transported by Oatp1c1. These data will assist in predicting excretion pathways for these two compounds. This may be particularly important for prednisolone, a widely used immunosuppressant and chemotherapeutic drug. In all assays, transport was measured from the extracellular side. Glucuronides and sulfonated compounds are generated within the ER and cytoplasm, respectively. Thus, these compounds will initially interact with Oatps/OATPs from the intracellular side of the protein when first generated within the cell. However, Oatps have been shown to operate bidirectionally. Thus, transport/inhibition data generated from uptake assays can likely be accurately applied to the role of Oatps/OATPs as an efflux transporter. The multifaceted roles of Oatps/OATPs as a bidirectional transporter of hormones, drugs, conjugated metabolites is summarized in Figure 1.

Future Directions

Although significant progress was made in this thesis in the understanding of the structure and function of Oatp1c1, much remains to be elucidated about the diverse roles and function of Oatps/OATPs. First, Oatp1c1 binding sites need to be physically mapped to fully comprehend Oatp/OATP transport mechanism and substrate-protein interactions. This could be accomplished through more extensive mutagenesis, or photoaffinity labeling as has been done for the active efflux transporter MRP1 (Karwatsky and Georges, 2004). Kast et al. showed there are three distinct binding regions within the transmembrane domains MRP1 for the substrate Iodo-aryl azido-rhodamine 123 (Kast and Gros, 1997).

In addition, novel functions of Oatps/OATPs need to be assessed, such as potential transport roles in intracellular compartments such as the ER. For many Oatp substrates,

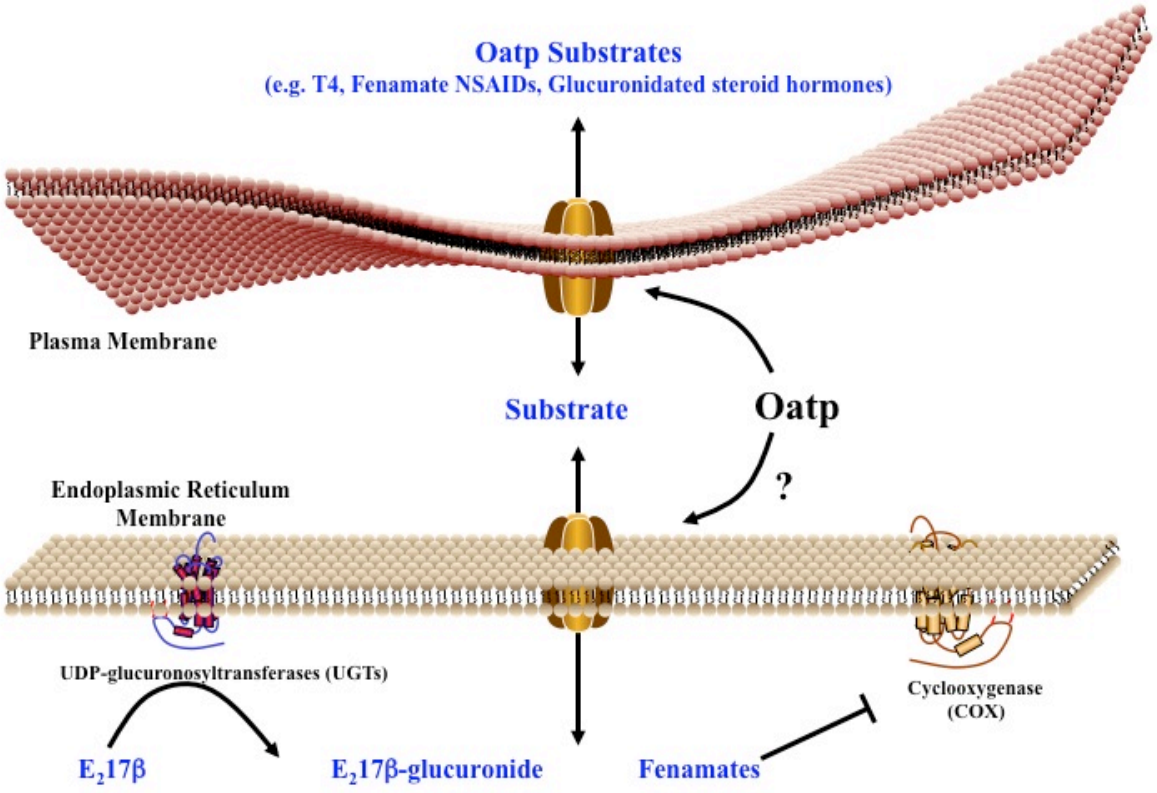

Figure 1. Summary of known and potential Oatp/OATP cellular transport roles. At the plasma membrane Oatps/OATPs mediate the bidirectional transport of numerous organic anions, including T4, glucuronidated sterols and fenamates. A potential intracellular Oatp/OATP role exists at the endoplasmic reticulum membrane, where Oatps/OATPs may deliver drugs, like fenamates to their site of action, or eliminate glucuronidated metabolites.

carrier-mediated transport is required at more than the plasma membrane for effective movement throughout the body/cell. For example, glurcuonides are generated within the lumen of the ER and require transport processes to traverse the ER membrane back into the cytoplasm for subsequent efflux from the cell. Conversely, polar NSAIDs must pass from the cytoplasm through the ER membrane to gain access to the active site of the COX enzyme in the ER lumen. In support of such a role, pharmacologic inhibition data from Battaglia et al. examining $E_2$17βG transport across isolated liver endoplasmic reticulum microsomes, suggested Oatps may be functionally operational at the ER membrane. Solid supportive evidence in the form of subcellular localization of Oatp/OATP protein in the ER and transport assays in highly purified ER microsomes is needed to rigorously test this hypothesis. Additional experiments are needed to assess questions such as how Oatp/OATP protein is differentially trafficked between ER and plasma membranes (e.g. through post-translational modifications, alternative splicing, etc.).

Finally, in-depth CoMFA and QSAR analyses are needed for Oatp/OATP substrates. Such studies will more fully classify the range of Oatp/OATP substrates, leading to a better understanding of Oatp/OATP physiological roles and accessory functions as a xenobiotic drug transporter. One exciting possibility stemming from CoMFA/QSAR studies is targeting Oatps/OATPs for therapeutic delivery of drugs to the brain. Oatp/OATP expression at various barriers throughout the body, including the BBB, leaves this group of transporters as an attractive vehicle for targeted drug delivery. A thorough understanding of the molecular characteristics of Oatp/OATP substrates may allow the rational design of drugs to specifically target Oatps/OATPs for transport across the barrier cells, while bypassing efflux transporters expressed in the same barrier cells. There are several examples targeting carrier

mediated transporters expressed at the BBB for precision delivery of drugs to the CNS (del Amo et al., 2008; Gynther et al., 2009). For example, LAT-1 has been targeted to deliver the amino derivative L-DOPA (3,4-dihydroxy-L-phenylalanine, Levodopa®) across the BBB for the treatment of Parkinson's Disease. Parkinson's disease is characterized by the degeneration of dopaminergic neurons in the substantia nigra region of the midbrain. Dopamine does not cross the BBB, and thus simple administration of dopamine is not an effective approach to treat Parkinson's disease. However, LAT-1 mediates the transport of L-DOPA across the BBB into the brain parenchyma, where L-DOPA is then decarboxylated by the actions of L-aromatic amino acid decarboxylase resulting in DOPA replacement. LAT-1 has also been used to facilitate the brain delivery of other drugs, such as ketoprofen. Gynther et al. joined ketoprofen to the phenolic hydroxyl group of L-tyrosine, resulting in LAT-1 mediated transport of the conjugated ketoprofen molecule and subsequent delivery into the brain (Gynther et al., 2008; Uchino et al., 2002). A similar targeted delivery of ketoprofen and indomethacin was performed Gynther et al. using GLUT-1 as transporter. In these studies, a glucose promoiety was attached to both ketoprofen and indomethacin allowing GLUT-1 specific transport of both conjugates (Gynther et al., 2009). The success of these so-called "Trojan Horse" delivery methods serve as a powerful impetus to examine the feasibility of using Oatps/OATPs in a similar role.

The OATP/Oatp superfamily of solute carriers plays a pivotal role in the disposition and flux of multiple endo- and xenobiotics in the CNS. The studies contained in this dissertation demonstrated Oatp1c1 possesses multiple binding sites for T4 and $E_2$17βG, as evidenced by atypical transport kinetics for both substrates. In addition, significant progress was made in elucidating Oatp1c1 structure/function through computational modeling and

mutagenesis of conserved transmembrane residues. Finally, basic common structural characteristics of Oatp1c1 substrates were determined using inhibition assays and mapping of electrostatic surface potentials of Oatp1c1 substrates. These data serve as a first step in charting complementary Oatp1c1-substrate surfaces and the prediction of novel Oatp1c1 substrates. The potential for strong physiologic and pharmacologic impacts in the CNS and elsewhere mediated by OATPs/Oatps is clear. Further study, including the generation of Oatp1c1 knockout mice, will continue to build on the current knowledge of the role of OATPs/Oatps at the BBB and BCSFB while possibly revealing novel functions of this versatile superfamily of transporters.

Bibliography

Abramson J, Smirnova I, Kasho V, Verner G, Kaback HR and Iwata S (2003) Structure and mechanism of the lactose permease of Escherichia coli. *Science (New York, NY* **301**(5633):610-615.

Adachi H, Suzuki T, Abe M, Asano N, Mizutamari H, Tanemoto M, Nishio T, Onogawa T, Toyohara T, Kasai S, Satoh F, Suzuki M, Tokui T, Unno M, Shimosegawa T, Matsuno S, Ito S and Abe T (2003) Molecular characterization of human and rat organic anion transporter OATP-D. *Am J Physiol Renal Physiol* 285(6):F1188-1197.

Agnati LF, Guidolin D, Genedani S, Ferre S, Bigiani A, Woods AS and Fuxe K (2005) How proteins come together in the plasma membrane and function in macromolecular assemblies: focus on receptor mosaics. *J Mol Neurosci* **26**(2-3):133-154.

Ahn SY and Nigam SK (2009) Toward a Systems Level Understanding of Organic Anion and Other Multispecific Drug Transporters: A Remote Sensing and Signaling Hypothesis. *Molecular pharmacology*.

Aller SG, Yu J, Ward A, Weng Y, Chittaboina S, Zhuo R, Harrell PM, Trinh YT, Zhang Q, Urbatsch IL and Chang G (2009) Structure of P-glycoprotein reveals a molecular basis for poly-specific drug binding. *Science (New York, NY* **323**(5922):1718-1722.

Aller SG, Yu J, Ward A, Weng Y, Chittaboina S, Zhuo R, Harrell PM, Trinh YT, Zhang Q, Urbatsch IL and Chang G (2009) Structure of P-glycoprotein reveals a molecular basis for poly-specific drug binding. *Science (New York, NY* **323**(5922):1718-1722.

Anderson GW (2001) Thyroid hormones and the brain. *Front Neuroendocrinol* 22(1):1-17.

Anderson GW, Schoonover CM and Jones SA (2003) Control of thyroid hormone action in the developing rat brain. *Thyroid* 13(11):1039-1056.

Atkins WM (2005) Non-Michaelis-Menten kinetics in cytochrome P450-catalyzed reactions. *Annual review of pharmacology and toxicology* **45**:291-310.

Badagnani I, Castro RA, Taylor TR, Brett CM, Huang CC, Stryke D, Kawamoto M, Johns SJ, Ferrin TE, Carlson EJ, Burchard EG and Giacomini KM (2006) Interaction of methotrexate with organic-anion transporting polypeptide 1A2 and its genetic variants. *The Journal of pharmacology and experimental therapeutics* 318(2):521-529.

Bal CS, Kumar A and Chandra P (2005) Effect of iopanoic acid on radioiodine therapy of hyperthyroidism: long-term outcome of a randomized controlled trial. *J Clin Endocrinol Metab* **90**(12):6536-6540.

Battaglia E and Gollan J (2001) A unique multifunctional transporter translocates estradiol-17beta -glucuronide in rat liver microsomal vesicles. *J Biol Chem* **276**(26):23492-23498.

Beitz E (2000) T(E)Xtopo: shaded membrane protein topology plots in LAT(E)X2epsilon. *Bioinformatics (Oxford, England)* **16**(11):1050-1051.

Bergwerk AJ, Shi X, Ford AC, Kanai N, Jacquemin E, Burk RD, Bai S, Novikoff PM, Stieger B, Meier PJ, Schuster VL and Wolkoff AW (1996) Immunologic distribution of an organic anion transport protein in rat liver and kidney. *The American journal of physiology* **271**(2 Pt 1):G231-238.

Borst P, Zelcer N and van de Wetering K (2006) MRP2 and 3 in health and disease. *Cancer Lett* 234(1):51-61.

Briz O, Romero MR, Martinez-Becerra P, Macias RI, Perez MJ, Jimenez F, San Martin FG and Marin JJ (2006) OATP8/1B3-mediated cotransport of bile acids and glutathione: an export pathway for organic anions from hepatocytes? *The Journal of biological chemistry* 281(41):30326-30335.

Cavallaro T, Martone RL, Stylianopoulou F and Herbert J (1993) Differential expression of the insulin-like growth factor II and transthyretin genes in the developing rat choroid plexus. *J Neuropathol Exp Neurol* 52(2):153-162.

Ceballos A, Belinchon MM, Sanchez-Mendoza E, Grijota-Martinez C, Dumitrescu AM, Refetoff S, Morte B and Bernal J (2009) Importance of monocarboxylate transporter 8 for the blood-brain barrier-dependent availability of 3,5,3'-triiodo-L-thyronine. *Endocrinology* **150**(5):2491-2496.

Chalmers DK, Scholz GH, Topliss DJ, Kolliniatis E, Munro SL, Craik DJ, Iskander MN and Stockigt JR (1993) Thyroid hormone uptake by hepatocytes: structure-activity relationships of phenylanthranilic acids with inhibitory activity. *J Med Chem* **36**(9):1272-1277.

Chang C and Swaan PW (2006) Computational approaches to modeling drug transporters. *Eur J Pharm Sci* **27**(5):411-424.

Chang C, Pang KS, Swaan PW and Ekins S (2005) Comparative Pharmacophore Modeling of Organic Anion Transporting Polypeptides: A Meta-analysis of Rat Oatp1a1 and Human OATP1B1. *J Pharmacol Exp Ther* 314(2):533-541.

Chen RL, Kassem NA and Preston JE (2006) Dose-dependent transthyretin inhibition of T4 uptake from cerebrospinal fluid in sheep. *Neurosci Lett* 396(1):7-11.

Chen Y, Dalwadi G and Benson HA (2004) Drug delivery across the blood-brain barrier. *Curr Drug Deliv* **1**(4):361-376.

Chen ZS, Guo Y, Belinsky MG, Kotova E and Kruh GD (2005) Transport of bile acids, sulfated steroids, estradiol 17-beta-D-glucuronide, and leukotriene C4 by human multidrug resistance protein 8 (ABCC11). *Mol Pharmacol* 67(2):545-557.

Cheng X, Maher J, Chen C and Klaassen CD (2005) Tissue distribution and ontogeny of mouse organic anion transporting polypeptides (Oatps). *Drug Metab Dispos* 33(7):1062-1073.

Chu C, Li JY, Boado RJ and Pardridge WM (2008) Blood-brain barrier genomics and cloning of a novel organic anion transporter. *J Cereb Blood Flow Metab* **28**(2):291-301.

Clark R, Kerr ID and Callaghan R (2006) Multiple drugbinding sites on the R482G isoform of the ABCG2 transporter. *British journal of pharmacology* **149**(5):506-515.

Coppola A, Hughes J, Esposito E, Schiavo L, Meli R and Diano S (2005) Suppression of hypothalamic deiodinase type II activity blunts TRH mRNA decline during fasting. *FEBS Lett* **579**(21):4654-4658.

Cui Y, Konig J, Leier I, Buchholz U and Keppler D (2001) Hepatic uptake of bilirubin and its conjugates by the human organic anion transporter SLC21A6. *J Biol Chem* **276**(13):9626-9630.

Davies NM and Skjodt NM (2000) Choosing the right nonsteroidal anti-inflammatory drug for the right patient: a pharmacokinetic approach. *Clin Pharmacokinet* **38**(5):377-392.

del Amo EM, Urtti A and Yliperttula M (2008) Pharmacokinetic role of L-type amino acid transporters LAT1 and LAT2. *Eur J Pharm Sci* **35**(3):161-174.

Drewes LR (2001) Molecular architecture of the brain microvasculature: perspective on blood-brain transport. *J Mol Neurosci* 16(2-3):93-98; discussion 151-157.

Dumitrescu AM, Liao XH, Weiss RE, Millen K and Refetoff S (2006) Tissue-specific thyroid hormone deprivation and excess in monocarboxylate transporter (mct) 8-deficient mice. *Endocrinology* **147**(9):4036-4043.

Enerson BE and Drewes LR (2006) The rat blood-brain barrier transcriptome. *J Cereb Blood Flow Metab* **26**(7):959-973.

Fenstermacher J, Gross P, Sposito N, Acuff V, Pettersen S and Gruber K (1988) Structural and functional variations in capillary systems within the brain. *Ann N Y Acad Sci* 529:21-30.

Friesema EC, Jansen J, Milici C and Visser TJ (2005) Thyroid hormone transporters. *Vitamins and hormones* 70:137-167.

Gaganis P, Miners JO and Knights KM (2007) Glucuronidation of fenamates: kinetic studies using human kidney cortical microsomes and recombinant UDP-glucuronosyltransferase (UGT) 1A9 and 2B7. *Biochemical pharmacology* **73**(10):1683-1691.

Gao B, Huber RD, Wenzel A, Vavricka SR, Ismair MG, Reme C and Meier PJ (2005) Localization of organic anion transporting polypeptides in the rat and human ciliary body epithelium. *Exp Eye Res* 80(1):61-72.

Gao B, Stieger B, Noe B, Fritschy JM and Meier PJ (1999) Localization of the organic anion transporting polypeptide 2 (Oatp2) in capillary endothelium and choroid plexus epithelium of rat brain. *J Histochem Cytochem* 47(10):1255-1264.

Girardin F (2006) Membrane transporter proteins: a challenge for CNS drug development. *Dialogues Clin Neurosci* 8(3):311-321.

Glasgow JF and Middleton B (2001) Reye syndrome--insights on causation and prognosis. *Arch Dis Child* **85**(5):351-353.

Grube M, Kock K, Karner S, Reuther S, Ritter CA, Jedlitschky G and Kroemer HK (2006) Modification of OATP2B1-mediated transport by steroid hormones. *Molecular pharmacology* **70**(5):1735-1741.

Gui C and Hagenbuch B (2008) Amino acid residues in transmembrane domain 10 of organic anion transporting polypeptide 1B3 are critical for cholecystokinin octapeptide transport. *Biochemistry* **47**(35):9090-9097.

Gui C, Miao Y, Thompson L, Wahlgren B, Mock M, Stieger B and Hagenbuch B (2008) Effect of pregnane X receptor ligands on transport mediated by human OATP1B1 and OATP1B3. *European journal of pharmacology* **584**(1):57-65.

Gui C, Wahlgren B, Lushington GH and Hagenbuch B (2009) Identification, K i determination and CoMFA analysis of nuclear receptor ligands as competitive

inhibitors of OATP1B1-mediated estradiol-17beta-glucuronide transport. *Pharmacol Res* 60(1):50-56.

Gynther M, Laine K, Ropponen J, Leppanen J, Mannila A, Nevalainen T, Savolainen J, Jarvinen T and Rautio J (2008) Large neutral amino acid transporter enables brain drug delivery via prodrugs. *Journal of medicinal chemistry* **51**(4):932-936.

Gynther M, Ropponen J, Laine K, Leppanen J, Haapakoski P, Peura L, Jarvinen T and Rautio J (2009) Glucose promoiety enables glucose transporter mediated brain uptake of ketoprofen and indomethacin prodrugs in rats. *Journal of medicinal chemistry* **52**(10):3348-3353.

Habgood MD, Begley DJ and Abbott NJ (2000) Determinants of passive drug entry into the central nervous system. *Cell Mol Neurobiol* 20(2):231-253.

Hagenbuch B (2007) Cellular entry of thyroid hormones by organic anion transporting polypeptides. *Best practice & research* **21**(2):209-221.

Hagenbuch B and Gui C (2008) Xenobiotic transporters of the human organic anion transporting polypeptides (OATP) family. *Xenobiotica; the fate of foreign compounds in biological systems* **38**(7-8):778-801.

Hagenbuch B and Meier PJ (2003) The superfamily of organic anion transporting polypeptides. *Biochimica et biophysica acta* **1609**(1):1-18.

Hagenbuch B and Meier PJ (2004) Organic anion transporting polypeptides of the OATP/ SLC21 family: phylogenetic classification as OATP/ SLCO superfamily, new nomenclature and molecular/functional properties. *Pflugers Arch* **447**(5):653-665.

Hanggi E, Grundschober AF, Leuthold S, Meier PJ and St-Pierre MV (2006) Functional analysis of the extracellular cysteine residues in the human organic anion transporting polypeptide, OATP2B1. *Mol Pharmacol* 70(3):806-817.

Hart ME, Suchland KL, Miyakawa M, Bunzow JR, Grandy DK and Scanlan TS (2006) Trace amine-associated receptor agonists: synthesis and evaluation of thyronamines and related analogues. *Journal of medicinal chemistry* **49**(3):1101-1112.

Hendrie HC (1997) Epidemiology of Alzheimer's disease. *Geriatrics* **52 Suppl 2**:S4-8.

Hennemann G, Docter R, Friesema EC, de Jong M, Krenning EP and Visser TJ (2001) Plasma membrane transport of thyroid hormones and its role in thyroid hormone metabolism and bioavailability. *Endocr Rev* **22**(4):451-476.

Hillier AP (1970) The binding of thyroid hormones to phospholipid membranes. *The Journal of physiology* 211(3):585-597.

Houston JB and Kenworthy KE (2000) In vitro-in vivo scaling of CYP kinetic data not consistent with the classical Michaelis-Menten model. *Drug metabolism and disposition: the biological fate of chemicals* **28**(3):246-254.

Hsiang B, Zhu Y, Wang Z, Wu Y, Sasseville V, Yang WP and Kirchgessner TG (1999) A novel human hepatic organic anion transporting polypeptide (OATP2). Identification of a liver-specific human organic anion transporting polypeptide and identification of rat and human hydroxymethylglutaryl-CoA reductase inhibitor transporters. *The Journal of biological chemistry* 274(52):37161-37168.

Huang Y, Lemieux MJ, Song J, Auer M and Wang DN (2003) Structure and mechanism of the glycerol-3-phosphate transporter from Escherichia coli. *Science (New York, NY* **301**(5633):616-620.

Hutzler JM and Tracy TS (2002) Atypical kinetic profiles in drug metabolism reactions. *Drug metabolism and disposition: the biological fate of chemicals* 30(4):355-362.
Ianculescu AG, Giacomini KM and Scanlan TS (2009) Identification and characterization of 3-iodothyronamine intracellular transport. *Endocrinology* **150**(4):1991-1999.
Iida A, Saito S, Sekine A, Mishima C, Kondo K, Kitamura Y, Harigae S, Osawa S and Nakamura Y (2001) Catalog of 258 single-nucleotide polymorphisms (SNPs) in genes encoding three organic anion transporters, three organic anion-transporting polypeptides, and three NADH:ubiquinone oxidoreductase flavoproteins. *Journal of human genetics* 46(11):668-683.
Inoue M, Kinne R, Tran T and Arias IM (1984) Taurocholate transport by rat liver canalicular membrane vesicles. Evidence for the presence of an Na+-independent transport system. *J Clin Invest* **73**(3):659-663.
Ito K, Suzuki H, Horie T and Sugiyama Y (2005) Apical/basolateral surface expression of drug transporters and its role in vectorial drug transport. *Pharm Res* 22(10):1559-1577.
Iwai M, Suzuki H, Ieiri I, Otsubo K and Sugiyama Y (2004) Functional analysis of single nucleotide polymorphisms of hepatic organic anion transporter OATP1B1 (OATP-C). *Pharmacogenetics* 14(11):749-757.
Jacquemin E, Hagenbuch B, Stieger B, Wolkoff AW and Meier PJ (1994) Expression cloning of a rat liver Na(+)-independent organic anion transporter. *Proc Natl Acad Sci U S A* 91(1):133-137.
Jones G, Willett P and Glen RC (1995) A genetic algorithm for flexible molecular overlay and pharmacophore elucidation. *J Comput Aided Mol Des* 9(6):532-549.
Kameyama Y, Yamashita K, Kobayashi K, Hosokawa M and Chiba K (2005) Functional characterization of SLCO1B1 (OATP-C) variants, SLCO1B1*5, SLCO1B1*15 and SLCO1B1*15+C1007G, by using transient expression systems of HeLa and HEK293 cells. *Pharmacogenetics and genomics* 15(7):513-522.
Kanai N, Lu R, Bao Y, Wolkoff AW, Vore M and Schuster VL (1996) Estradiol 17 beta-D-glucuronide is a high-affinity substrate for oatp organic anion transporter. *Am J Physiol* **270**(2 Pt 2):F326-331.
Karwatsky JM and Georges E (2004) Drug binding domains of MRP1 (ABCC1) as revealed by photoaffinity labeling. *Current medicinal chemistry* **4**(1):19-30.
Kassem NA, Deane R, Segal MB, Chen R and Preston JE (2007) Thyroxine (T4) transfer from CSF to choroid plexus and ventricular brain regions in rabbit: contributory role of P-glycoprotein and organic anion transporting polypeptides. *Brain research* 1181:44-50.
Kast C and Gros P (1997) Topology mapping of the amino-terminal half of multidrug resistance-associated protein by epitope insertion and immunofluorescence. *The Journal of biological chemistry* **272**(42):26479-26487.
Kennedy JM and van Rij AM (2006) Drug absorption from the small intestine in immediate postoperative patients. *Br J Anaesth* **97**(2):171-180.
Kilic F and Rudnick G (2000) Oligomerization of serotonin transporter and its functional consequences. *Proceedings of the National Academy of Sciences of the United States of America* **97**(7):3106-3111.

Kim RB (2003) Organic anion-transporting polypeptide (OATP) transporter family and drug disposition. *European journal of clinical investigation* **33 Suppl 2**:1-5.
Kniesel U and Wolburg H (2000) Tight junctions of the blood-brain barrier. *Cell Mol Neurobiol* 20(1):57-76.
Koch-Weser J and Sellers EM (1976) Drug therapy. Binding of drugs to serum albumin (second of two parts). *N Engl J Med* 294(10):526-531.
Kocher O, Comella N, Gilchrist A, Pal R, Tognazzi K, Brown LF and Knoll JH (1999) PDZK1, a novel PDZ domain-containing protein up-regulated in carcinomas and mapped to chromosome 1q21, interacts with cMOAT (MRP2), the multidrug resistance-associated protein. *Laboratory investigation; a journal of technical methods and pathology* **79**(9):1161-1170.
Konig J, Cui Y, Nies AT and Keppler D (2000a) Localization and genomic organization of a new hepatocellular organic anion transporting polypeptide. *The Journal of biological chemistry* 275(30):23161-23168.
Konig J, Cui Y, Nies AT and Keppler D (2000b) A novel human organic anion transporting polypeptide localized to the basolateral hepatocyte membrane. *American journal of physiology* 278(1):G156-164.
Konig J, Seithel A, Gradhand U and Fromm MF (2006) Pharmacogenomics of human OATP transporters. *Naunyn-Schmiedeberg's archives of pharmacology* 372(6):432-443.
Konig J, Seithel A, Gradhand U and Fromm MF (2006) Pharmacogenomics of human OATP transporters. *Naunyn-Schmiedeberg's archives of pharmacology* **372**(6):432-443.
Kullak-Ublick GA, Hagenbuch B, Stieger B, Schteingart CD, Hofmann AF, Wolkoff AW and Meier PJ (1995) Molecular and functional characterization of an organic anion transporting polypeptide cloned from human liver. *Gastroenterology* 109(4):1274-1282.
Kusuhara H and Sugiyama Y (2004) Efflux transport systems for organic anions and cations at the blood-CSF barrier. *Adv Drug Deliv Rev* 56(12):1741-1763.
Kusuhara H and Sugiyama Y (2005) Active efflux across the blood-brain barrier: role of the solute carrier family. *NeuroRx* 2(1):73-85.
Lai CS, Korytowski W, Niu CH and Cheng SY (1985) Transverse motion of spin-labeled 3,3',5-triiodo-L-thyronine in phospholipid bilayers. *Biochemical and biophysical research communications* 131(1):408-412.
Lee TK, Koh AS, Cui Z, Pierce RH and Ballatori N (2003) N-glycosylation controls functional activity of Oatp1, an organic anion transporter. *American journal of physiology* **285**(2):G371-381.
Lee W, Glaeser H, Smith LH, Roberts RL, Moeckel GW, Gervasini G, Leake BF and Kim RB (2005) Polymorphisms in human organic anion-transporting polypeptide 1A2 (OATP1A2): implications for altered drug disposition and central nervous system drug entry. *The Journal of biological chemistry* 280(10):9610-9617.
Lei J, Nowbar S, Mariash CN and Ingbar DH (2003) Thyroid hormone stimulates Na-K-ATPase activity and its plasma membrane insertion in rat alveolar epithelial cells. *American journal of physiology* 285(3):L762-772.

Leuthold S, Hagenbuch B, Mohebbi N, Wagner CA, Meier PJ and Stieger B (2009) Mechanisms of pH-gradient driven transport mediated by organic anion polypeptide transporters. *Am J Physiol Cell Physiol* 296(3):C570-582.

Li JY, Boado RJ and Pardridge WM (2001) Differential kinetics of transport of 2',3'-dideoxyinosine and adenosine via concentrative Na+ nucleoside transporter CNT2 cloned from rat blood-brain barrier. *The Journal of pharmacology and experimental therapeutics* **299**(2):735-740.

Li L, Lee TK, Meier PJ and Ballatori N (1998) Identification of glutathione as a driving force and leukotriene C4 as a substrate for oatp1, the hepatic sinusoidal organic solute transporter. *J Biol Chem* 273(26):16184-16191.

Li L, Meier PJ and Ballatori N (2000) Oatp2 mediates bidirectional organic solute transport: a role for intracellular glutathione. *Molecular pharmacology* 58(2):335-340.

Lim CF, Loidl NM, Kennedy JA, Topliss DJ and Stockigt JR (1996) Drug effects on triiodothyronine uptake by rat anterior pituitary cells in vitro. *Exp Clin Endocrinol Diabetes* **104**(2):151-157.

Mahagita C, Grassl SM, Piyachaturawat P and Ballatori N (2007) Human organic anion transporter 1B1 and 1B3 function as bidirectional carriers and do not mediate GSH-bile acid cotransport. *Am J Physiol Gastrointest Liver Physiol* 293(1):G271-278.

Martin C, Berridge G, Higgins CF, Mistry P, Charlton P and Callaghan R (2000) Communication between multiple drug binding sites on P-glycoprotein. *Molecular pharmacology* **58**(3):624-632.

Marzolini C, Tirona RG and Kim RB (2004) Pharmacogenomics of the OATP and OAT families. *Pharmacogenomics* 5(3):273-282.

McGeer PL (2000) Cyclo-oxygenase-2 inhibitors: rationale and therapeutic potential for Alzheimer's disease. *Drugs Aging* **17**(1):1-11.

McGeer PL, Schulzer M and McGeer EG (1996) Arthritis and anti-inflammatory agents as possible protective factors for Alzheimer's disease: a review of 17 epidemiologic studies. *Neurology* **47**(2):425-432.

Meier-Abt F, Mokrab Y and Mizuguchi K (2005) Organic anion transporting polypeptides of the OATP/SLCO superfamily: identification of new members in nonmammalian species, comparative modeling and a potential transport mode. *J Membr Biol* 208(3):213-227.

Meyer MC, Straughn AB, Mhatre RM, Shah VP, Chen ML, Williams RL and Lesko LJ (2001) Variability in the bioavailability of phenytoin capsules in males and females. *Pharm Res* **18**(3):394-397.

Mikkaichi T, Suzuki T, Onogawa T, Tanemoto M, Mizutamari H, Okada M, Chaki T, Masuda S, Tokui T, Eto N, Abe M, Satoh F, Unno M, Hishinuma T, Inui K, Ito S, Goto J and Abe T (2004) Isolation and characterization of a digoxin transporter and its rat homologue expressed in the kidney. *Proceedings of the National Academy of Sciences of the United States of America* **101**(10):3569-3574.

Mikkaichi T, Suzuki T, Tanemoto M, Ito S and Abe T (2004b) The organic anion transporter (OATP) family. *Drug Metab Pharmacokinet* 19(3):171-179.

Mitchell AM, Tom M and Mortimer RH (2005) Thyroid hormone export from cells: contribution of P-glycoprotein. *The Journal of endocrinology* 185(1):93-98.

Miyagawa M, Maeda K, Aoyama A and Sugiyama Y (2009) The eighth and ninth transmembrane domains in organic anion transporting polypeptide 1B1 affect the transport kinetics of estrone-3-sulfate and estradiol-17beta-D-glucuronide. *The Journal of pharmacology and experimental therapeutics* **329**(2):551-557.

Morrison JH, Brinton RD, Schmidt PJ and Gore AC (2006) Estrogen, menopause, and the aging brain: how basic neuroscience can inform hormone therapy in women. *J Neurosci* **26**(41):10332-10348.

Moss AA, Lin SK, Margules ER, Motson RW and Riegelman S (1979) Pharmacokinetics of iopanoic acid in the rhesus monkey: biliary excretion, plasma protein binding and biotransformation. *Invest Radiol* **14**(2):171-176.

Mostov KE, Verges M and Altschuler Y (2000) Membrane traffic in polarized epithelial cells. *Curr Opin Cell Biol* 12(4):483-490.

Nakao N, Takagi T, Iigo M, Tsukamoto T, Yasuo S, Masuda T, Yanagisawa T, Ebihara S and Yoshimura T (2006) Possible involvement of organic anion transporting polypeptide 1c1 in the photoperiodic response of gonads in birds. *Endocrinology* 147(3):1067-1073.

Neuvonen PJ, Kantola T and Kivisto KT (1998) Simvastatin but not pravastatin is very susceptible to interaction with the CYP3A4 inhibitor itraconazole. *Clinical pharmacology and therapeutics* 63(3):332-341.

Niemi M, Backman JT, Kajosaari LI, Leathart JB, Neuvonen M, Daly AK, Eichelbaum M, Kivisto KT and Neuvonen PJ (2005a) Polymorphic organic anion transporting polypeptide 1B1 is a major determinant of repaglinide pharmacokinetics. *Clinical pharmacology and therapeutics* 77(6):468-478.

Niemi M, Neuvonen PJ, Hofmann U, Backman JT, Schwab M, Lutjohann D, von Bergmann K, Eichelbaum M and Kivisto KT (2005b) Acute effects of pravastatin on cholesterol synthesis are associated with SLCO1B1 (encoding OATP1B1) haplotype *17. *Pharmacogenetics and genomics* 15(5):303-309.

Niemi M, Schaeffeler E, Lang T, Fromm MF, Neuvonen M, Kyrklund C, Backman JT, Kerb R, Schwab M, Neuvonen PJ, Eichelbaum M and Kivisto KT (2004) High plasma pravastatin concentrations are associated with single nucleotide polymorphisms and haplotypes of organic anion transporting polypeptide-C (OATP-C, SLCO1B1). *Pharmacogenetics* 14(7):429-440.

Nishizato Y, Ieiri I, Suzuki H, Kimura M, Kawabata K, Hirota T, Takane H, Irie S, Kusuhara H, Urasaki Y, Urae A, Higuchi S, Otsubo K and Sugiyama Y (2003) Polymorphisms of OATP-C (SLC21A6) and OAT3 (SLC22A8) genes: consequences for pravastatin pharmacokinetics. *Clinical pharmacology and therapeutics* 73(6):554-565.

Noe B, Hagenbuch B, Stieger B and Meier PJ (1997) Isolation of a multispecific organic anion and cardiac glycoside transporter from rat brain. *Proc Natl Acad Sci U S A* **94**(19):10346-10350.

Noe J, Portmann R, Brun ME and Funk C (2007) Substrate-dependent drug-drug interactions between gemfibrozil, fluvastatin and other organic anion-transporting

peptide (OATP) substrates on OATP1B1, OATP2B1, and OATP1B3. *Drug metabolism and disposition: the biological fate of chemicals* **35**(8):1308-1314.
Nozawa T, Imai K, Nezu J, Tsuji A and Tamai I (2004) Functional characterization of pH-sensitive organic anion transporting polypeptide OATP-B in human. *The Journal of pharmacology and experimental therapeutics* 308(2):438-445.
Nozawa T, Nakajima M, Tamai I, Noda K, Nezu J, Sai Y, Tsuji A and Yokoi T (2002) Genetic polymorphisms of human organic anion transporters OATP-C (SLC21A6) and OATP-B (SLC21A9): allele frequencies in the Japanese population and functional analysis. *The Journal of pharmacology and experimental therapeutics* **302**(2):804-813.
O'Banion MK (1999) COX-2 and Alzheimer's disease: potential roles in inflammation and neurodegeneration. *Expert Opin Investig Drugs* **8**(10):1521-1536.
Ohtsuki S, Takizawa T, Takanaga H, Hori S, Hosoya K and Terasaki T (2004) Localization of organic anion transporting polypeptide 3 (oatp3) in mouse brain parenchymal and capillary endothelial cells. *J Neurochem* 90(3):743-749.
Oppenheimer JH and Schwartz HL (1997) Molecular basis of thyroid hormone-dependent brain development. *Endocrine reviews* 18(4):462-475.
Oppenheimer JH, Surks MI and Schwartz HL (1969) The metabolic significance of exchangeable cellular thyroxine. *Recent Prog Horm Res* 25:381-422.
Palha JA, Fernandes R, de Escobar GM, Episkopou V, Gottesman M and Saraiva MJ (2000) Transthyretin regulates thyroid hormone levels in the choroid plexus, but not in the brain parenchyma: study in a transthyretin-null mouse model. *Endocrinology* 141(9):3267-3272.
Pardridge WM (2003) Molecular Biology of the blood-brain barrier. *Methods Mol Med* 89: 385-399
Pardridge WM and Landaw EM (1984) Tracer kinetic model of blood-brain barrier transport of plasma protein-bound ligands. Empiric testing of the free hormone hypothesis. *J Clin Invest* 74(3):745-752.
Parepally JM, Mandula H and Smith QR (2006) Brain uptake of nonsteroidal anti-inflammatory drugs: Ibuprofen, flurbiprofen, and indomethacin. *Pharm Res* **23**(5):873-881.
Parfenova H, Eidson TH and Leffler CW (1997) Upregulation of COX-2 in cerebral microvascular endothelial cells by smooth muscle cell signals. *Am J Physiol* **273**(1 Pt 1):C277-288.
Parfenova H, Levine V, Gunther WM, Pourcyrous M and Leffler CW (2002) COX-1 and COX-2 contributions to basal and IL-1 beta-stimulated prostanoid synthesis in human neonatal cerebral microvascular endothelial cells. *Pediatr Res* **52**(3):342-348.
Parfenova H, Parfenov VN, Shlopov BV, Levine V, Falkos S, Pourcyrous M and Leffler CW (2001) Dynamics of nuclear localization sites for COX-2 in vascular endothelial cells. *Am J Physiol Cell Physiol* **281**(1):C166-178.
Pasinetti GM (2001) Cyclooxygenase and Alzheimer's disease: implications for preventive initiatives to slow the progression of clinical dementia. *Arch Gerontol Geriatr* **33**(1):13-28.

Pizzagalli F, Hagenbuch B, Stieger B, Klenk U, Folkers G and Meier PJ (2002) Identification of a novel human organic anion transporting polypeptide as a high affinity thyroxine transporter. *Mol Endocrinol* 16(10):2283-2296.

Potschka H and Loscher W (2001) In vivo evidence for P-glycoprotein-mediated transport of phenytoin at the blood-brain barrier of rats. *Epilepsia* 42(10):1231-1240.

Rao GS, Eckel J, Rao ML and Breuer H (1976) Uptake of thyroid hormone by isolated rat liver cells. *Biochemical and biophysical research communications* 73(1):98-104.

Roberts LM, Woodford K, Zhou M, Black DS, Haggerty JE, Tate EH, Grindstaff KK, Mengesha W, Raman C and Zerangue N (2008) Expression of the thyroid hormone transporters monocarboxylate transporter-8 (SLC16A2) and organic ion transporter-14 (SLCO1C1) at the blood-brain barrier. *Endocrinology* 149(12):6251-6261.

Rohrbacher M, Kirchhof A, Skarke C, Geisslinger G and Lotsch J (2006) Rapid identification of three functionally relevant polymorphisms in the OATP1B1 transporter gene using Pyrosequencing. *Pharmacogenomics* 7(2):167-176.

Sali A and Blundell TL (1993) Comparative protein modelling by satisfaction of spatial restraints. *J Mol Biol* 234(3):779-815.

Scanlan TS, Suchland KL, Hart ME, Chiellini G, Huang Y, Kruzich PJ, Frascarelli S, Crossley DA, Bunzow JR, Ronca-Testoni S, Lin ET, Hatton D, Zucchi R and Grandy DK (2004) 3-Iodothyronamine is an endogenous and rapid-acting derivative of thyroid hormone. *Nature medicine* **10**(6):638-642.

Schussler GC (2000) The thyroxine-binding proteins. *Thyroid* 10(2):141-149.

Schuster VL (1998) Molecular mechanisms of prostaglandin transport. *Annu Rev Physiol* **60**:221-242.

Schwartz CE, May MM, Carpenter NJ, Rogers RC, Martin J, Bialer MG, Ward J, Sanabria J, Marsa S, Lewis JA, Echeverri R, Lubs HA, Voeller K, Simensen RJ and Stevenson RE (2005) Allan-Herndon-Dudley syndrome and the monocarboxylate transporter 8 (MCT8) gene. *American journal of human genetics* **77**(1):41-53.

Sedlakova R, Shivers RR and Del Maestro RF (1999) Ultrastructure of the blood-brain barrier in the rabbit. *J Submicrosc Cytol Pathol* 31(1):149-161.

Segal MB (2000) The choroid plexuses and the barriers between the blood and the cerebrospinal fluid. *Cell Mol Neurobiol* **20**(2):183-196.

Shapiro AB, Fox K, Lam P and Ling V (1999) Stimulation of P-glycoprotein-mediated drug transport by prazosin and progesterone. Evidence for a third drug-binding site. *European journal of biochemistry / FEBS* **259**(3):841-850.

Shitara Y, Hirano M, Sato H and Sugiyama Y (2004) Gemfibrozil and its glucuronide inhibit the organic anion transporting polypeptide 2 (OATP2/OATP1B1:SLC21A6)-mediated hepatic uptake and CYP2C8-mediated metabolism of cerivastatin: analysis of the mechanism of the clinically relevant drug-drug interaction between cerivastatin and gemfibrozil. *The Journal of pharmacology and experimental therapeutics* **311**(1):228-236.

Shitara Y, Sugiyama D, Kusuhara H, Kato Y, Abe T, Meier PJ, Itoh T and Sugiyama Y (2002) Comparative inhibitory effects of different compounds on rat oatpl (slc21a1)- and Oatp2 (Slc21a5)-mediated transport. *Pharm Res* **19**(2):147-153.

Shou M, Lin Y, Lu P, Tang C, Mei Q, Cui D, Tang W, Ngui JS, Lin CC, Singh R, Wong BK, Yergey JA, Lin JH, Pearson PG, Baillie TA, Rodrigues AD and Rushmore TH (2001) Enzyme kinetics of cytochrome P450-mediated reactions. *Current drug metabolism* **2**(1):17-36.

Sidney Jones KT, Grant Anderson (2005) The role of thyroid hormone in fetal and neonatal brain development. *Current Opinion in Endocrinology and Diabetes* **12**:10-16.

Smith JP and Drewes LR (2006) Modulation of monocarboxylic acid transporter-1 kinetic function by the cAMP signaling pathway in rat brain endothelial cells. *The Journal of biological chemistry* 281(4):2053-2060.

Smith NF, Acharya MR, Desai N, Figg WD and Sparreboom A (2005) Identification of OATP1B3 as a high-affinity hepatocellular transporter of paclitaxel. *Cancer biology & therapy* 4(8):815-818.

Smith PJ and Surks MI (1984) Multiple effects of 5,5'-diphenylhydantoin on the thyroid hormone system. *Endocr Rev* **5**(4):514-524.

Snead AN, Santos MS, Seal RP, Miyakawa M, Edwards RH and Scanlan TS (2007) Thyronamines inhibit plasma membrane and vesicular monoamine transport. *ACS chemical biology* **2**(6):390-398.

Southwell BR, Duan W, Alcorn D, Brack C, Richardson SJ, Kohrle J and Schreiber G (1993) Thyroxine transport to the brain: role of protein synthesis by the choroid plexus. *Endocrinology* 133(5):2116-2126.

Stitzer LK and Jacquez JA (1975) Neutral amino acid transport pathways in uptake of L-thyroxine by Ehrlich ascites cells. *The American journal of physiology* 229(1):172-177.

Strazielle N and Ghersi-Egea JF (2000) Choroid plexus in the central nervous system: biology and physiopathology. *J Neuropathol Exp Neurol* 59(7):561-574.

Strazielle N and Preston JE (2003) Transport across the choroid plexuses in vivo and in vitro. *Methods Mol Med* 89:291-304.

Strazielle N, Khuth ST and Ghersi-Egea JF (2004) Detoxification systems, passive and specific transport for drugs at the blood-CSF barrier in normal and pathological situations. *Adv Drug Deliv Rev* **56**(12):1717-1740.

Sugiyama D, Kusuhara H, Shitara Y, Abe T and Sugiyama Y (2002) Effect of 17 beta-estradiol-D-17 beta-glucuronide on the rat organic anion transporting polypeptide 2-mediated transport differs depending on substrates. *Drug metabolism and disposition: the biological fate of chemicals* **30**(2):220-223.

Sugiyama D, Kusuhara H, Shitara Y, Abe T, Meier PJ, Sekine T, Endou H, Suzuki H and Sugiyama Y (2001) Characterization of the efflux transport of 17beta-estradiol-D-17beta-glucuronide from the brain across the blood-brain barrier. *J Pharmacol Exp Ther* 298(1):316-322.

Sugiyama D, Kusuhara H, Taniguchi H, Ishikawa S, Nozaki Y, Aburatani H and Sugiyama Y (2003) Functional characterization of rat brain-specific organic anion

transporter (Oatp14) at the blood-brain barrier: high affinity transporter for thyroxine. *J Biol Chem* 278(44):43489-43495.
Suzuki T and Abe T (2008) Thyroid hormone transporters in the brain. *Cerebellum (London, England)* **7**(1):75-83.
Takano T, Tian GF, Peng W, Lou N, Libionka W, Han X and Nedergaard M (2006) Astrocyte-mediated control of cerebral blood flow. *Nat Neurosci* 9(2):260-267.
Tamai I and Tsuji A (2000) Transporter-mediated permeation of drugs across the blood-brain barrier. *J Pharm Sci* 89(11):1371-1388.
Tamai I, Nozawa T, Koshida M, Nezu J, Sai Y and Tsuji A (2001) Functional characterization of human organic anion transporting polypeptide B (OATP-B) in comparison with liver-specific OATP-C. *Pharmaceutical research* 18(9):1262-1269.
Tanaka H and Mizojiri K (1999) Drug-protein binding and blood-brain barrier permeability. *J Pharmacol Exp Ther* 288(3):912-918.
Tate CG, Kunji ER, Lebendiker M and Schuldiner S (2001) The projection structure of EmrE, a proton-linked multidrug transporter from Escherichia coli, at 7 A resolution. *The EMBO journal* **20**(1-2):77-81.
Tirona RG and Kim RB (2002) Pharmacogenomics of organic anion-transporting polypeptides (OATP). *Advanced drug delivery reviews* **54**(10):1343-1352.
Tirona RG, Leake BF, Merino G and Kim RB (2001) Polymorphisms in OATP-C: identification of multiple allelic variants associated with altered transport activity among European- and African-Americans. *The Journal of biological chemistry* 276(38):35669-35675.
Tohyama K, Kusuhara H and Sugiyama Y (2004) Involvement of multispecific organic anion transporter, Oatp14 (Slc21a14), in the transport of thyroxine across the blood-brain barrier. *Endocrinology* **145**(9):4384-4391.
Topliss DJ, Kolliniatis E, Barlow JW, Lim CF and Stockigt JR (1989) Uptake of 3,5,3'-triiodothyronine by cultured rat hepatoma cells is inhibitable by nonbile acid cholephils, diphenylhydantoin, and nonsteroidal antiinflammatory drugs. *Endocrinology* **124**(2):980-986.
Tracy TS (2003) Atypical enzyme kinetics: their effect on in vitro-in vivo pharmacokinetic predictions and drug interactions. *Current drug metabolism* **4**(5):341-346.
Tracy TS (2006) Atypical cytochrome p450 kinetics: implications for drug discovery. *Drugs in R&D* **7**(6):349-363.
Tracy TS, Hutzler JM, Haining RL, Rettie AE, Hummel MA and Dickmann LJ (2002) Polymorphic variants (CYP2C9*3 and CYP2C9*5) and the F114L active site mutation of CYP2C9: effect on atypical kinetic metabolism profiles. *Drug metabolism and disposition: the biological fate of chemicals* **30**(4):385-390.
Tsujimoto M, Hirata S, Dan Y, Ohtani H and Sawada Y (2006) Polymorphisms and linkage disequilibrium of the OATP8 (OATP1B3) gene in Japanese subjects. *Drug metabolism and pharmacokinetics* 21(2):165-169.
Uchino H, Kanai Y, Kim DK, Wempe MF, Chairoungdua A, Morimoto E, Anders MW and Endou H (2002) Transport of amino acid-related compounds mediated by L-

type amino acid transporter 1 (LAT1): insights into the mechanisms of substrate recognition. *Molecular pharmacology* **61**(4):729-737.

van der Deure WM, Appelhof BC, Peeters RP, Wiersinga WM, Wekking EM, Huyser J, Schene AH, Tijssen JG, Hoogendijk WJ, Visser TJ and Fliers E (2008) Polymorphisms in the brain-specific thyroid hormone transporter OATP1C1 are associated with fatigue and depression in hypothyroid patients. *Clinical endocrinology*.

Vane SJ (2000) Aspirin and other anti-inflammatory drugs. *Thorax* **55 Suppl 2**:S3-9.

Voltaren (2003) Product Information. *Norvartis Pharmaceuticals Corporation, East Hanover NJ*.

Wang P, Hata S, Xiao Y, Murray JW and Wolkoff AW (2008) Topological assessment of oatp1a1: a 12-transmembrane domain integral membrane protein with three N-linked carbohydrate chains. *American journal of physiology* **294**(4):G1052-1059.

Wang P, Wang JJ, Xiao Y, Murray JW, Novikoff PM, Angeletti RH, Orr GA, Lan D, Silver DL and Wolkoff AW (2005) Interaction with PDZK1 is required for expression of organic anion transporting protein 1A1 on the hepatocyte surface. *The Journal of biological chemistry* **280**(34):30143-30149.

Westholm DE, Rumbley JN, Salo DR, Rich TP and Anderson GW (2008) Organic anion-transporting polypeptides at the blood-brain and blood-cerebrospinal fluid barriers. *Curr Top Dev Biol* **80**:135-170.

Westholm DE, Stenehjem DD, Rumbley JN, Drewes LR and Anderson GW (2009) Competitive inhibition of organic anion transporting polypeptide 1c1-mediated thyroxine transport by the fenamate class of nonsteroidal antiinflammatory drugs. *Endocrinology* **150**(2):1025-1032.

Winiwarter S and Hilgendorf C (2008) Modeling of drug-transporter interactions using structural information. *Current opinion in drug discovery & development* **11**(1):95-103.

Wolka AM, Huber JD and Davis TP (2003) Pain and the blood-brain barrier: obstacles to drug delivery. *Adv Drug Deliv Rev* 55(8):987-1006.

Yarim M, Moro S, Huber R, Meier PJ, Kaseda C, Kashima T, Hagenbuch B and Folkers G (2005) Application of QSAR analysis to organic anion transporting polypeptide 1a5 (Oatp1a5) substrates. *Bioorg Med Chem* 13(2):463-471.

Yin Y, He X, Szewczyk P, Nguyen T and Chang G (2006) Structure of the multidrug transporter EmrD from Escherichia coli. *Science (New York, NY* **312**(5774):741-744.